

POLITECNICO DI TORINO

SCUOLA DI DOTTORATO

PhD Course in Physics – XXVII cycle

PhD Dissertation

**Microscopic modeling of energy
dissipation and decoherence in
nanoscale materials and devices**



Roberto Rosati

Tutor

Prof. Fausto Rossi

Coordinatore del corso di dottorato

Prof.sa Arianna Montorsi

October 2014

Alle Giraffe

A Luca,
che ora prepara
la migliore trippa del paradiso

Summary

Primary goal of this thesis work is to develop and implement microscopic modeling strategies able to describe semiconductor-based nanomaterials and nanodevices, overcoming both the intrinsic limits of the semiclassical transport theory and the huge computational costs of non Markovian approaches.

The progressive reduction of modern optoelectronic devices space-scales, triggered by the evolution on semiconductor heterostructures at the nanoscale, heavily exploits the principles of band-gap engineering, achieved by confining charge carriers in spatial regions comparable to their de Broglie wavelengths. This, together with the decrease of the typical time-scales involved, pushes device miniaturization toward limits where the application of the traditional Boltzmann transport theory becomes questionable, and a comparison with more rigorous quantum transport approaches is imperative. In spite of the quantum-mechanical nature of electron and photon dynamics in the core region of typical solid-state nanodevices the overall behavior of such quantum systems is often governed by a highly non-trivial interplay between phase coherence and dissipation/dephasing. To this aim, the crucial step is to adopt a quantum mechanical description of the carrier subsystem; this can be performed at different levels, ranging from phenomenological dissipation/decoherence models to quantum-kinetic treatments. However, due to their high computational cost, non-Markovian Green' s-function as well as density-matrix approaches like quantum Monte Carlo techniques or quantum-kinetics are currently unsuitable for the design and optimization of new-generation nanodevices. On the other end, the Wigner-function technique is a widely used approach which, in principle, is well suited to describe an interplay between coherence and dissipation: in fact it can be regarded both as a phase space formulation of the electronic density matrix, and a

quantum equivalent of the classical distribution function. The evolution of this quasi-distribution function is governed by the Wigner-equation, which is usually solved by applying local spatial boundary conditions. However, such a scheme has recently showed some intrinsic limits.

Part I provides a brief introduction on the theoretical tools needed for modeling the interplay between dissipation and decoherence. In particular, based on either the conventional or the recently proposed [1] Markov Approximations, two different descriptions for the scattering-induced dynamics of the many-body density matrix are given; however, it will be shown that only the novel Markov limit provides a Lindblad dynamics.

In part II we introduce one of the most-known approaches used to model charge transport in semiconductor nanodevices, the Wigner-function. In particular, we present a detailed analysis of the strengths and limits of the U boundary condition scheme applied to the Wigner Transport Equation. As already stressed and recently showed [2], such a scheme may provide highly unphysical solutions such as negative stationary spatial charge densities. In part II we analyze both the reasons for these unphysical features –pointing out the need of different and purely quantum approaches– and the limits in which they should not appear, thus justifying why these problems had not been encountered in the numerous quantum-transport simulations based on this procedure.

Based on the novel Markov approximation previously recalled, in part III we present a novel single-particle simulation strategy able to describe the interplay between coherence and dissipation/dephasing. In Chap. 12 we show how this model is, contrary to the one obtainable from the conventional Markov approximation, able to guarantee the positivity of the evolution; in addition, as shown in Chap. 13 its semiclassical limit provides the local Boltzmann collision term. However, as shown in Chap. 14 in the low-density limit, the more the system goes deep into the quantum regime, the more this model provides a scattering-induced charge-density variation (unaffordable through semiclassical treatments). This genuine quantum effect may be predicted also by other simplified treatments of the dissipation/decoherence like e.g. the Relaxation Time Approximation: the latter however turns out to be totally nonlocal and unable to recover the Boltzmann results in the semiclassical limit. As shown in Chap. 15, these quantum scattering-induced effects produce a speedup of the diffusion and, in

superlattice structures, a suppression of the coherent oscillations.

Acknowledgements

Il mio primo ringraziamento va alla mia famiglia, per avermi sorretto quando necessario, trasmesso la tenacia che ha mosso le mie azioni e fornito la serenità necessaria per sostenerle.

Ringrazio il Prof. Fausto Rossi, poiché non solo mi ha dato l'opportunità di continuare a coltivare il sogno di essere un fisico, ma ha anche costantemente dimostrato di volere condividere le sue enormi conoscenze con me. Lo ringrazio per ciò che mi ha insegnato (praticamente tutto ciò che so), per avermi aiutato a colmare le mie lacune e sopportato le mie bizzarrie. Ringrazio tutti i membri del gruppo Nanophysics and Quantum Systems, poiché ognuno di loro mi ha fornito un mattone necessario per completare la torre del mio Dottorato. Ringrazio inoltre tutti i miei colleghi d'ufficio, per avermi concesso di condividere le mie passioni.

Ringrazio i miei amici perché, nonostante le mie assenze, non mi hanno mai fatto mancare supporto, sorrisi e consolazioni. In questi ultimi anni starmi a fianco è stato ancor più difficile del solito, eppure la loro presenza si è sempre fatta sentire.

Ringrazio la Croce Verde per avermi fatto sentire parte di qualcosa di grande e perché qualcosa di grande è ciò che ci consente di fare; ringrazio i pazienti per avermi insegnato che “sarebbe stato meglio essere sani, ma se dobbiamo ammalarci tanto vale restare positivi”[cit.].

Ringrazio tutte quelle voci, il cui eco vibrante mi ha permesso di portare i miei sogni nella vita quotidiana; e ringrazio chi ai sogni di una vita ha dato un volto.

Contents

Summary	III
Acknowledgements	VI
I Fundamentals of Nanodevice modeling	1
1 Introduction	3
1.1 Quantum Confinement and Envelope Function Formalism . . .	6
1.2 Overview of the principals scattering mechanisms	7
1.3 Semiclassical Descriptions	9
2 The density-matrix formalism	13
2.1 The Liouville-von Neumann Equation	14
2.2 The Markov Approximation	15
3 A Novel Lindblad description for dissipation/decoherence	19
3.1 The complete-positivity requirement	19
3.2 The Lindblad Superoperator	21
3.2.1 Lindblad-like scattering-induced dynamics	23
3.3 An alternative Markov limit	24
II The failure of the Wigner function in describing nano- metric spatially open systems	27
4 Introduction	29

5	The Wigner Function formalism	33
6	The Coherent Wigner Equation	37
6.1	The Wigner transport equation	37
6.2	The Semiclassical Limit of the Coherent Wigner Equation . .	43
7	The Inflow or U-boundary condition	45
7.1	Physical vs. Mathematical solutions	46
7.2	Nonuniqueness of the solution	49
8	Dissipation and decoherence	57
8.1	Scattering-induced current	58
9	The delta-like potential as a toy model	63
9.1	Analytical Evaluation of the Wigner function	64
9.2	Unphysical and non-unique solutions	68
9.3	Analytical Wigner-function boundary value vs Fermi-Dirac distribution	74
9.4	The anomalous behaviour of the coherent current	76
9.5	Negative charge densities in the presence of dissipation/decoherence	78
10	Summary and conclusions	83
 III Scattering-induced quantum phenomena in semicon- ductor nanodevices: a positive-definite density matrix de- scription		85
11	The Single-particle description	87
11.1	Introduction	87
11.2	The many-electron density matrix	90
11.3	The single-particle density matrix	93
11.4	Scattering-induced single-particle dynamics	95
11.4.1	Carrier-phonon mechanism in the mean-field approx- imation	95
11.4.2	The Carrier-Carrier mechanism in the mean-field ap- proximation	99
11.4.3	In- vs Out-Scattering contributions	101

11.5 Single-particle description of Spatially Open System	102
12 Study of the positivity	107
13 The Semiclassical limit	115
14 Quantum nonlocality	121
14.1 Physical model and simulation strategy	122
14.2 Scattering nonlocality in homogeneous GaN systems	125
15 Dissipation-induced quantum diffusion	131
15.1 Quantum diffusion in homogeneous GaN systems	131
15.2 Scattering-induced suppression of the coherent oscillations in superlattices	136
16 Summary and Conclusion	141
Bibliography	145

List of Figures

4.1	Spatially Open Systems	30
7.1	U boundary conditions	46
9.1	Non-unique solutions	70
9.2	Charge Density from dissipative Wigner Equation	71
9.3	Charge Current from dissipative Wigner Equation	73
9.4	Boundary Wigner function: pure state	75
9.5	Boundary Wigner function: mixed state	80
9.6	Unphysical charge density	81
12.1	Physical vs. unphysical evolutions	111
14.1	Quantum nonlocality from Lindblad models	126
14.2	Quantum nonlocality from Lindblad models: In vs Out contributions	127
14.3	Quantum nonlocality from Lindblad models: In and Out contributions vs. initial-localization	128
14.4	Quantum nonlocality from Relaxation Time Approximation .	130
15.1	Diffusion in 1-D homogeneous GaN systems: models in comparison	132
15.2	Evolution in 1-D homogeneous GaN systems of the effective spatial distribution: models in comparison	134
15.3	Evolution in 1-D homogeneous GaN systems of the effective spatial distribution in the quasi-elastic limit: models in comparison	136
15.4	Diffusion in GaN-based superlattices: models in comparison .	137
15.5	Coherent vs. dissipative evolutions in GaN-based superlattices	138
15.6	Evolution of the effective spatial distribution in GaN-based superlattices: models in comparison	139

Part I

**Fundamentals of Nanodevice
modeling**

Chapter 1

Introduction

In the late 1959, Richard Feynman held a lecture titled “There’s Plenty of Room at the Bottom” [3], a seminal paper which is often considered as the inspirational beginning of the nanotechnologies, a term which was introduced almost fifteen years later by Norio Taniguchi [4]. Nano-technologies are defined as those fields of science concerning devices whose size range from 1 to 100 nanometers; the topics included in this definition range from molecular-manipulation to nanomedicine and nanobiology, passing obviously through the study of electronic devices, which is the subject of this thesis.

In 1948, at the Bell Telephon Laboratories, John Bardeen and Walter H. Brattain obtained the first transistor [5]; few months later, their-group chief William B. Shockley suggested that the (useful) emitter current could flow through the bulk rather than over the surface, opening the way for the bipolar-junction diode [6]; for this achievement they all won the Nobel prize in Physics in 1956. However, it took few years for the realization of commercial transistor, as the first transistors showed a leakage current between emitter and collector and stopped working above 70/80 Celsius degree. These issues were solved by going from the Germanium to the Silicon [7], the latter having a wider energy-gap than the former: finally, in 1954 Teal [8] astonished the audience of the IRE conference by presenting the first practical realization of a Silicon-based transistor working at high temperature. Since then, the sizes of the transistors have been shrinking

by following the well-known Moore’s Law [9], e.g. by doubling-up the number of transistors per square-centimeter every 24 months. As the sizes of the transistor decrease, semiclassical physics may no longer be applicable [10] – during an interview September 18, 2007, Gordon Moore himself stated “another decade, a decade and a half I think we will hit something fairly fundamental”. In fact, reducing the distance between source and drain (the analogous of emitter and collector in modern Field Effect Transistor like, e.g., the MOSFET) a spontaneous current occurs due to quantum tunneling effect, a somehow similar problem to that of leakage current: if the latter issue has been solved using Silicon, the possible ways of handling the former one range from leaving the electronic degrees of freedom, as in modern spintronics approaches, to using it as an ally as in Tunnel Field Effect Transistor [11]. In either cases, Quantum Mechanics has to be taken into account.

In parallel, nanotechnologies had a tremendous impact in the LASER science. The first lasers, obtained in 1962 by Robert Hall at the General Electric Laboratories [12], were based on a GaAs p-n homojunction – developing a theoretical idea originated by John von Neumann in 1953 [13]. The first breakthrough in the laser technology was the advent of heterostructures, e.g. materials made-up of layers of different compositions stuck together by a perfect matching of the respective lattices at the interfaces (called “ideal” heterojunction): in 1964, Alferov [14] and Kroemer [15] independently formulated the concept of double heterostructures lasers, for which they won the Nobel prize in Physics in 2000. The heterostructures employed in the early ’60s were still, however, in the micrometric scale, with the light emission being concentrated entirely in the middle layer. It is with the seminal paper by Leo Esaki and Raphael Tsu that the *superlattices* made their debut: these are periodic structures of different-in-composition layers with thickness of few nanometers. In the superlattices a crucial role is, once-again, played by the tunnel effect, which the same Esaki showed [16] in the tunnel diodes (also called Esaki-diode) and for which he won the Nobel Prize in Physics in 1973¹. The tunnel effect allows for the (in principle)

¹In his Nobel lecture [17], which is mainly dedicated to the tunnel effect in Semiconductors, Esaki opens the section dedicated to superlattices with the sentence “The natural

infinite periodicity of superlattices, given by an alternation of *barriers* and *wells* (see below): thanks to Quantum Mechanics laws, as the formers may be “tunneled”, the so-called quantum wells may show discretized states. Due to the different underlying physical mechanisms, Alferov himself in his Nobel lecture [18] distinguishes between classical (e.g. micrometric) heterostructures and heterostructures quantum wells. Finally, the concept of stimulated emission in superlattices, set forth by Kazarinov and Suris in the early '70s [19], found a real implementation thanks to Capasso et coworkers [20] in 1994: this is the birth of Quantum Cascade Lasers, operating in the mid-IR range.

Although this section was intended as an overview over the topic of electronic nanodevices, it may be viewed as an introduction to my thesis, as many of the concepts, models and devices here discussed has been analyzed in my thesis work. By studying the interplay between decoherence and dissipation we explored that regime in which additional genuine quantum phenomena arise beyond a genuine Boltzmann-like (e.g., semiclassical) description. In part III we show, by employing a positive-definite model, some of these peculiar quantum effects like the speedup of the semiclassical diffusion of an electronic spatial distribution or the suppression of the coherent oscillatory motion between adjacent quantum wells in superlattices. We will make a large use of the envelope function formalism, which is based on the concept of confinement over spatial scales which are neither as big as to be considered classical (e.g., micrometric in the meaning of Alferov) nor as small as to be of the order of the (quantum-threshold of the) De Broglie length. We will face semiclassical models, like the U-boundary condition scheme applied to the Wigner function formalism, which, despite their success in describing electronic devices, may provide unphysical results when approaching the quantum regime, as shown in part II. Finally, the search for a proper description of spatially open systems will be one of the leitmotiv of this thesis work.

extension of double barriers will be to construct a series of tunnel junctions by a periodic variation of alloy composition”

1.1 Quantum Confinement and Envelope Function Formalism

The spectrum of a semiconductor shows the typical *band structure*, where the gap between the (top of the full) valence and the (bottom of the empty) conduction is called *bandgap*. In a heterostructure, two (or more) semiconducting materials with different band gaps are joint together, thus producing abrupt modification of the band profile; depending on the shape of the misalignment, one talks about

- (i) *type I* or *straddling materials*, if both the top of the valence band and the bottom of the conduction one in the smallest gap material fall in the gap of the larger one;
- (ii) *type II* or *staggered alignment*, if either the top of the valence or the bottom of the conduction of one material falls within the band gap of the other;
- (iii) *type III* or *broken-gap alignment*, if the band gaps do not overlap at all.

The different materials involved in the interface or heterojunction should have perfect lattice matching; typical superlattices are AlGaAs/GaAs or AlGaN/GaN, where in example AlGaAs stands for every alloy $\text{Al}_x\text{Ga}_{1-x}\text{As}$ (as an example, in his Nobel lecture [17] Esaki described a $x = 0.75$ alloy). Nowadays technologies permit the creation of layers so thin as to allow a mechanical manipulation which, by straining one of the materials involved in the heterostructure, permits to overcome the lattice-matching problem: these materials are called *strained layers*.

The dimensionality of a nanostructure D is defined as the number of interface-free directions ($0 \leq D \leq 3$): low-dimensional structures are called quantum-wells ($D = 2$), wires ($D = 1$) and dots ($D = 0$). In this work we will focus on type-I heterostructures and carrier degrees of freedom. The energetic difference between the bottom of the conduction bands of the materials involved in the heterojunction gives rise to a potential along the direction(s) orthogonal to the interfaces, where the largest bandgap material behaves like a barrier. Depending on the height of the barrier and

on the spatial widths of both barriers and wells, the carrier wave function may be confined in the smallest gap material or communicate with the next smallest-bandgap-material layer thanks to tunnel-effect as in superlattices. The eigenfunctions of the whole system are usually assumed to be given by the product of the bulk wave-functions times the so-called envelope-function $\psi(\mathbf{r})$, which fulfills the Schrödinger Equation

$$\left(-\frac{\hbar^2}{2m^*} \nabla_{\mathbf{r}}^2 + V(\mathbf{r}) \right) \psi(\mathbf{r}) = \epsilon \psi(\mathbf{r}) \quad , \quad (1.1)$$

where a parabolic band has been considered and $V(\mathbf{r})$ is a potential term induced by the bands misalignment. The states $|\alpha\rangle$ whose associated wave function $\psi_{\alpha}(\mathbf{r}) = \langle \mathbf{r} | \alpha \rangle$ fulfills Eq. (1.1) are hence eigenstates of the single-particle Hamiltonian

$$\hat{H}^{\text{sp}} = \sum_{\alpha} \epsilon_{\alpha} \hat{c}_{\alpha}^{\dagger} \hat{c}_{\alpha} \quad , \quad (1.2)$$

where $\hat{c}_{\alpha}^{\dagger}$ and \hat{c}_{α} are the usual fermionic creation and annihilation operators.

1.2 Overview of the principals scattering mechanisms

The Bloch theorem is defined on static periodic lattices; however, ions are not static neither from a semiclassical point of view (at finite temperatures they should vibrate) nor from a quantum one (they must fulfill the Heisenberg uncertainty principle) [21]. As a consequence, one must consider the ionic vibrations which, going from classical to quantum mechanics, give raise to the *phonons*. We will consider both acoustic and optical phonons in the long-wavelength (e.g., small wave vector) limit, where the frequency $\omega_{\mathbf{q}}$ of the acoustic and optical phonons may be considered respectively as linear and constant in the wave-vector \mathbf{q} . The phonons contribute to the global Hamiltonian \hat{H} both via a free-phonon Hamiltonian \hat{H}^{ph} , which is typically in the form

$$\hat{H}^{\text{ph}} = \sum_{\mathbf{q}} \hbar \omega_{\mathbf{q}} \hat{b}_{\mathbf{q}}^{\dagger} \hat{b}_{\mathbf{q}} \quad , \quad (1.3)$$

where $\hat{b}_{\mathbf{q}}^\dagger$ and $\hat{b}_{\mathbf{q}}$ denote the creation and annihilation operators of a phononic state with wave-vector \mathbf{q} and energy $\hbar\omega_{\mathbf{q}}$, and via² a carrier-phonon Hamiltonian \hat{H}^{cph} in the form

$$\hat{H}^{\text{cph}} = \sum_{\alpha, \alpha', \mathbf{q}} \left(g_{\alpha\alpha'}^{\mathbf{q}+} \hat{c}_\alpha^\dagger \hat{c}_{\alpha'} \hat{b}_{\mathbf{q}}^\dagger + g_{\alpha'\alpha}^{\mathbf{q}-} \hat{c}_\alpha^\dagger \hat{c}_{\alpha'} \hat{b}_{\mathbf{q}} \right) . \quad (1.4)$$

The coefficients $g_{\alpha\alpha'}^{\mathbf{q}\pm}$ must fulfill

$$g_{\alpha\alpha'}^{\mathbf{q}\pm} = g_{\alpha\alpha'}^{\mathbf{q}\mp*} \quad (1.5)$$

in order for \hat{H}^{cph} to be Hermitian and can always be written as the product

$$g_{\alpha\alpha'}^{\mathbf{q}\pm} = \bar{g}^{\mathbf{q}\pm} \mathcal{F}_{\alpha\alpha'}^{\mathbf{q}} , \quad (1.6)$$

where $\mathcal{F}_{\alpha\alpha'}^{\mathbf{q}}$ evaluates the overlapping of the eigenfunctions $\psi_\alpha(\mathbf{r}) = \langle \mathbf{r} | \alpha \rangle$ and $\psi_{\alpha'}^*(\mathbf{r})$,

$$\mathcal{F}_{\alpha\alpha'}^{\mathbf{q}} = \int d\mathbf{r} \psi_\alpha(\mathbf{r}) \psi_{\alpha'}^*(\mathbf{r}) e^{i\mathbf{q}\cdot\mathbf{r}} , \quad (1.7)$$

while $\bar{g}^{\mathbf{q}\pm}$, which strongly depends on the nature of phonon and material, may be naively interpreted as the phonon-induced variation $\delta E_{\mathbf{k}\nu}$ of the static-lattice electronic dispersion $E_{\mathbf{k}\nu}$. In particular, the variation $\delta E_{\mathbf{k}\nu}$ may be induced by

- (i) spatial (e.g. volume or bond-length) variations, such as

$$\delta E_{\mathbf{k}\nu} \propto a_{\mathbf{k}\nu} \frac{\delta V}{V} \quad (1.8)$$

for acoustic phonons (V is the volume of the primitive cell and δV its variation) or

$$\delta E_{\mathbf{k}\nu} \propto D_{\mathbf{k}\nu} \frac{\delta a_0}{a_0} \quad (1.9)$$

for optical phonons, where a_0 is the distance of the two atoms in the center of the cell and δa_0 their relative displacement; $a_{\mathbf{k}\nu}$ and $D_{\mathbf{k}\nu}$ are respectively the so-called acoustic *volume* and optical-phonon *deformation potentials*;

²Any interaction involving more than one phonon will not be considered in this work.

- (ii) an Electric field variation $\delta\mathbf{E}$ generated by piezo-electric effect (for acoustic phonon) or by relative displacement of the electrical charges within the cell for optical phonons; the carrier-Optical phonon scattering is also called Frölich interaction

The piezoelectric effect is stronger in more-ionic wurtzite semiconductors such as ZnO or CSe [22], which however will not be considered in this thesis work, while the effects of acoustic phonons in GaAs have been considered in [23]. In polar semiconductors (like, e.g., the Gallium-nitride (GaN)) at room temperatures the dominant scattering mechanism is the Frölich interaction: as a consequence, in Chaps. 14 and 15, where a detailed study of phonon-induced nonlocality and diffusion speedup in GaN at $T = 300$ K is presented, the LO-optical phonons only are considered.

The carrier-carrier mechanism is governed by the Coulomb Hamiltonian \hat{H}^{cc}

$$\hat{H}^{\text{cc}} = \frac{1}{2} \sum_{\alpha, \alpha', \bar{\alpha}, \bar{\alpha}'} g_{\alpha\alpha'\bar{\alpha}\bar{\alpha}'} \hat{c}_{\alpha}^{\dagger} \hat{c}_{\alpha'}^{\dagger} \hat{c}_{\bar{\alpha}} \hat{c}_{\bar{\alpha}'} \quad , \quad (1.10)$$

where the coefficients are proportional to the matrix element induced by the Coulomb potential $V^{\text{cc}}(\mathbf{r})$,

$$g_{\alpha\alpha'\bar{\alpha}\bar{\alpha}'} \propto \int d\mathbf{r} d\mathbf{r}' \psi_{\alpha}(\mathbf{r}) \psi_{\alpha'}(\mathbf{r}') V^{\text{cc}}(\mathbf{r} - \mathbf{r}') \psi_{\bar{\alpha}}^*(\mathbf{r}) \psi_{\bar{\alpha}'}^*(\mathbf{r}') \quad . \quad (1.11)$$

Others scattering mechanisms, like e.g. carrier-impurity, carrier-photon or carrier-plasmon interactions, will not be discussed in this thesis.

1.3 Semiclassical Descriptions

In the 19th century, Ludwig Boltzmann [24] introduced the probability distribution function $f(\mathbf{r}, \mathbf{p})$ in order to describe a classical gas made of N particles with position \mathbf{r} and momentum \mathbf{p} ; extending this concept to the case of an electron gas in a crystal, where $\mathbf{p} = \hbar\mathbf{k}$ and \mathbf{k} is the wave vector, the resulting *Boltzmann Equation* for parabolic bands is

$$\left[\frac{\partial}{\partial t} + \frac{\hbar\mathbf{k}}{m^*} \nabla_{\mathbf{r}} - \frac{1}{\hbar} (\nabla_{\mathbf{r}} V(\mathbf{r})) \nabla_{\mathbf{k}} \right] f(\mathbf{r}, \mathbf{k}, t) = \left. \frac{\partial f(\mathbf{r}, \mathbf{k}, t)}{\partial t} \right|_{\text{scat}} \quad , \quad (1.12)$$

where the distribution is normalized by the number of particles \bar{N}

$$\frac{1}{(2\pi)^3} \int d\mathbf{k} d\mathbf{r} f(\mathbf{r}, \mathbf{k}) = \bar{N} \quad ; \quad (1.13)$$

the r.h.s. of Eq. (1.12) provides the scattering-induced dynamics of $f(\mathbf{r}, \mathbf{k}, t)$ and, assuming instantaneous and local interactions, is given by

$$\left. \frac{\partial f(\mathbf{r}, \mathbf{k}, t)}{\partial t} \right|_{\text{scat}} = \hbar^3 \int d\mathbf{k}' (P(\mathbf{k}, \mathbf{k}') f(\mathbf{r}, \mathbf{k}') - P(\mathbf{k}', \mathbf{k}) f(\mathbf{r}, \mathbf{k})) \quad , \quad (1.14)$$

where $P(\mathbf{k}, \mathbf{k}')$ are the so-called *scattering rates* and provide the probability per unit time that an electron goes from a state labelled by \mathbf{k}' to one with \mathbf{k} . The integral in Eq. (1.14) is called Boltzmann collision term, which shows the typical *in-* versus *out-scattering* contributions. Since the electrons fulfill the Pauli exclusion principle, at high carrier concentration Eq. (1.14) must be replaced by

$$\begin{aligned} \left. \frac{\partial f(\mathbf{r}, \mathbf{k}, t)}{\partial t} \right|_{\text{scat}} = \hbar^3 \int d\mathbf{k}' [(1 - f(\mathbf{r}, \mathbf{k})) P(\mathbf{k}, \mathbf{k}') f(\mathbf{r}, \mathbf{k}') \\ - (1 - f(\mathbf{r}, \mathbf{k}')) P(\mathbf{k}', \mathbf{k}) f(\mathbf{r}, \mathbf{k})] \quad . \end{aligned} \quad (1.15)$$

The spatial charge density is given by

$$n(\mathbf{r}) = \frac{1}{(2\pi)^3} \int d\mathbf{k} f(\mathbf{r}, \mathbf{k}) \quad , \quad (1.16)$$

and its scattering-induced time variation coming from Eq. (1.14) is null, in fact

$$\begin{aligned} \left. \frac{\partial n(\mathbf{r})}{\partial t} \right|_{\text{scat}} &= \frac{1}{(2\pi)^3} \int d\mathbf{k} \left. \frac{\partial f(\mathbf{r}, \mathbf{k}, t)}{\partial t} \right|_{\text{scat}} \\ &= \frac{\hbar^3}{(2\pi)^3} \int d\mathbf{k} d\mathbf{k}' [P(\mathbf{k}, \mathbf{k}') f(\mathbf{r}, \mathbf{k}') - P(\mathbf{k}', \mathbf{k}) f(\mathbf{r}, \mathbf{k})] = 0, \end{aligned} \quad (1.17)$$

where the last equality comes trivially after exchanging the dummy variables \mathbf{k}, \mathbf{k}' in the out term. Since the same null result for charge density variation would have been obtained at high carrier densities (e.g., using Eq. (1.15)), the scattering-induced dynamics provided by the Boltzmann Equation (see Eqs. (1.14) and (1.15)) is said to be local in space.

When applied to Quantum Mechanics, the scattering-induced term of the Boltzmann Equation may be interpreted, through the scattering rates $P(\mathbf{k}, \mathbf{k}')$, as the study (of the effects) of transition from states $|\mathbf{k}'\rangle$ to $|\mathbf{k}\rangle$; this concept may be generalized to transitions between states $|\phi_a\rangle$, with $a = 1, \dots, N'$, belonging to a N' -dimensional Hilbert space \mathcal{H}' . If a system has a probability f_a of being in the state $|\phi_a\rangle$ then, a somehow discretized and space-independent generalization of Eqs. (1.14) and (1.15) is given by

$$\left. \frac{\partial f_a}{\partial t} \right|_{\text{scat}} = \sum_{a'=1}^{N'} (P_{aa'} f_{a'} - P_{a'a} f_a) \quad (1.18)$$

and

$$\left. \frac{\partial f_a}{\partial t} \right|_{\text{scat}} = \sum_{a'=1}^{N'} ((1 - f_a) P_{aa'} f_{a'} - (1 - f_{a'}) P_{a'a} f_a) \quad (1.19)$$

respectively, where $P_{aa'}$ furnishes the probability per unit time of a transition from state $|\phi_{a'}\rangle$ to $|\phi_a\rangle$. The Equation (1.18), which is usually stated in term of (diagonal) density-matrix operator (which will be introduced in Chap. 2), is also called *Pauli-Master Equation*.

Chapter 2

The density-matrix formalism

A statistical mixture of generic (pure) quantum-states¹ $|\phi_i\rangle$, with $i = 1, \dots, N$, where N is the dimensionality of the underlying Hilbert space of the system \mathcal{H}_S , is usually described by the density-matrix operator $\hat{\rho}$,

$$\hat{\rho} = \sum_{i,j=1}^N \rho_{ij} |\phi_i\rangle \langle \phi_j| \quad , \quad (2.1)$$

from which it follows that, if states $|\phi_i\rangle$ are orthonormalized,

$$\langle \phi_i | \phi_j \rangle = \delta_{ij} \quad , \quad (2.2)$$

then

$$\rho_{ij} = \langle \phi_i | \hat{\rho} | \phi_j \rangle \quad . \quad (2.3)$$

The diagonal elements $f_i = \rho_{ii}$ are the so-called *populations*, e.g. the average occupation number of states $|\phi_i\rangle$, while the off-diagonal terms express the correlation between different states in the mixture. The expectation value of a generic operator \hat{A} in the mixed-state described by $\hat{\rho}$ is given by

$$\langle \hat{A} \rangle = \text{Tr} \{ \hat{A} \hat{\rho} \} = \sum_{i,j} A_{ij} \rho_{ji} \quad , \quad (2.4)$$

¹Unless differently specified, the states are in general composed by many electrons and many quasiparticles.

where

$$A_{ij} = \langle \phi_i | \hat{A} | \phi_j \rangle \quad . \quad (2.5)$$

2.1 The Liouville-von Neumann Equation

In the Schrödinger picture, given the (generic) Hamiltonian \hat{H} , the states $|\phi_i\rangle \in \mathcal{H}_S$ fulfill the equation

$$i\hbar \frac{\partial |\phi_i\rangle}{\partial t} = \hat{H} |\phi_i\rangle \quad , \quad (2.6)$$

hence the time evolution of the density-matrix operator defined in Eq. (2.1) is given by

$$\begin{aligned} i\hbar \frac{\partial \hat{\rho}}{\partial t} &= i\hbar \sum_{ij} \rho_{ij} \left[\left(\frac{\partial |\phi_i\rangle}{\partial t} \right) \langle \phi_j | + |\phi_i\rangle \left(\frac{\partial \langle \phi_j |}{\partial t} \right) \right] \\ &= [\hat{H}, \hat{\rho}] \quad : \end{aligned} \quad (2.7)$$

this is the well-known *Liouville-von Neumann Equation*. Although in principle very simple, the equation of motion in (2.7) is complicated by the fact that the total Hamiltonian \hat{H} is given by the sum

$$\hat{H} = \hat{H}^\circ + \hat{H}' \quad , \quad (2.8)$$

where the first term \hat{H}° is a free Hamiltonian of the form

$$\hat{H}^\circ = \hat{H}^c + \hat{H}^{\text{ph}} \quad , \quad (2.9)$$

where \hat{H}^c and \hat{H}^{ph} are respectively the single-particle and free-phonon Hamiltonian of Eq. (1.2) and (1.3), and of an additional term \hat{H}' describing some scattering-mechanisms, i.e. the carrier-phonon or carrier-carrier Hamiltonian of Eqs. (1.4) and (1.10). This suggests to rewrite the density-matrix operator $\hat{\rho}$ at generic time t in Eq. (2.1) in the interaction-picture as $\hat{\rho}^i(t)$,

$$\hat{\rho}^i = \hat{U}^{\circ\dagger}(t - t_0) \hat{\rho} \hat{U}^\circ(t - t_0) \quad , \quad (2.10)$$

where t_0 is the initial time of the evolution, $t_0 \leq t$, and the operator $\hat{U}^\circ(t - t_0)$ fulfills

$$i\hbar \frac{\partial \hat{U}^\circ(t - t_0)}{\partial t} = \hat{H}^\circ \hat{U}^\circ(t - t_0) \quad : \quad (2.11)$$

since \hat{H}° is often time-independent, the solution of Eq. (2.11) (given the boundary condition $\hat{U}^\circ(t_0, t_0) = \hat{\mathcal{I}}$, where $\hat{\mathcal{I}}$ is the N -dimensional identity operator) is

$$\hat{U}^\circ(t - t_0) = e^{-\frac{i}{\hbar}\hat{H}^\circ(t-t_0)} \quad . \quad (2.12)$$

By left- and right-multiplying the Liouville-von Neumann Equation (2.7), where \hat{H} is given in Eq. (2.8), for respectively $\hat{U}^{\circ\dagger}$ and \hat{U}° , one obtains the equation of motion of $\hat{\rho}^i$

$$i\frac{\partial\hat{\rho}^i}{\partial t} = [\hat{\mathcal{H}}', \hat{\rho}^i] \quad , \quad (2.13)$$

where

$$\hat{\mathcal{H}}^s \equiv \hat{\mathcal{H}}'(t) = \frac{1}{\hbar}\hat{U}^{\circ\dagger}(t - t_0)\hat{H}'\hat{U}^\circ(t - t_0) \quad . \quad (2.14)$$

The evaluation of the r.h.s of Eq. (2.13) is one the most difficult and important tasks faced when modeling (nano-) electronic devices. In particular, thanks to their numerical feasibility, the models based on the conventional Markov approximation, briefly recalled in Sec. 2.2, are widely employed; however, as will be explained in Chap. 12 by employing the single-particle density matrix, they fail in guaranteeing the positivity of the evolution: for this reason, a novel Markov approximation, recalled in Section (3.3), has been introduced in [1], the latter being able to provide a complete-positive (see Sec. 3.1) dynamics.

Usually the operator Equation (2.13) is expressed in terms of the eigenbasis $|\lambda_i\rangle$ with eigenvalues ϵ_i° of \hat{H}° ; typically, the matrix elements of $\hat{\mathcal{H}}'$ are much smaller than the corresponding difference of the free-energies,

$$|\hbar\langle\phi_i|\hat{\mathcal{H}}'|\phi_j\rangle| \ll |\epsilon_i^\circ - \epsilon_j^\circ| \quad : \quad (2.15)$$

in these cases, the interacting Hamiltonians \hat{H}^s may be considered as small perturbations of the free Hamiltonian \hat{H}° .

2.2 The Markov Approximation

Since [25]

$$\hat{\rho}^i(t) = \hat{\rho}^i(t_0) - i \sum_s \int_{t_0}^t [\hat{\mathcal{H}}^s(t'), \hat{\rho}^i(t')] \quad , \quad (2.16)$$

the dynamics in Eq. (2.13) may be rewritten as

$$\frac{\partial \hat{\rho}^i(t)}{\partial t} = -\imath \left[\hat{\mathcal{H}}'(t), \hat{\rho}^i(t_0) \right] - \left[\hat{\mathcal{H}}'(t), \int_{t_0}^t dt' \left[\hat{\mathcal{H}}'(t'), \hat{\rho}^i(t') \right] \right] \quad . \quad (2.17)$$

Assuming, as is usually possible for typical electronic nanodevices, the validity of Eq. (2.15), the time variation of $\hat{\rho}^i(t')$ should be considered adiabatically slow compared to that of $\hat{\mathcal{H}}'(t')$, hence the integral in Eq. (2.17) may be rewritten as

$$\int_{t_0}^t dt' \left[\hat{\mathcal{H}}'(t'), \hat{\rho}^i(t') \right] \approx \left[\hat{\mathcal{K}}'(t), \hat{\rho}^i(t) \right] \quad , \quad (2.18)$$

where [25]

$$\hat{\mathcal{K}}'(t) = \int_{t_0}^t dt' \hat{\mathcal{H}}'(t') \quad : \quad (2.19)$$

Equation (2.18) furnishes the so-called *adiabatic* or *Markov approximation*, which, going back to the original Schrödinger picture, furnishes the closed and local-in-time Equation of motion²

$$\frac{\partial \hat{\rho}}{\partial t} = -\frac{\imath}{\hbar} \left[\hat{H}^\circ, \hat{\rho} \right] + \hat{\mathcal{C}} - \left[\hat{\mathcal{H}}', \left[\hat{\mathcal{K}}', \hat{\rho} \right] \right] \quad , \quad (2.20)$$

with

$$\hat{\mathcal{C}}(t) = -\imath \left[\hat{\mathcal{H}}', e^{-\frac{\imath}{\hbar} \hat{H}^\circ (t-t_0)} \hat{\rho}(t_0) e^{\frac{\imath}{\hbar} \hat{H}^\circ (t-t_0)} \right] \quad . \quad (2.21)$$

Here as in the following, we write that the Equation of motion of the global density matrix $\hat{\rho}$ in the form

$$\frac{\partial \hat{\rho}}{\partial t} = \left. \frac{\partial \hat{\rho}}{\partial t} \right|_{\text{free}} + \hat{\mathcal{C}} + \left. \frac{\partial \hat{\rho}}{\partial t} \right|_{\text{scat}} \quad , \quad (2.22)$$

where

- (i) $\left. \frac{\partial \hat{\rho}}{\partial t} \right|_{\text{free}}$ describes the free-like evolution dictated by the free Hamiltonian \hat{H}° plus eventual energy renormalization contribution;

²From now on, unless contrary specified, when we write $\hat{\rho}$ we mean $\hat{\rho} \equiv \hat{\rho}(t)$.

- (ii) $\hat{\mathcal{C}}$ acts as a source term and describes the evolution induced by \hat{U}° of the initial quantum correlations: $\hat{\mathcal{C}}$ is responsible for several quantum mechanical phenomena like the ones coming from coherent phonons;
- (iii) $\left. \frac{\partial \hat{\rho}}{\partial t} \right|_{\text{scat}}$ indicates the scattering-induced contribution to the dynamics and for models neglecting memory effects is usually given by a super-operator acting on $\hat{\rho}$; in particular, for conventional Markov Approximations it is given by

$$\left. \frac{\partial \hat{\rho}}{\partial t} \right|_{\text{scat}} = - \left[\hat{\mathcal{H}}', \left[\hat{\mathcal{K}}', \hat{\rho} \right] \right] . \quad (2.23)$$

In this thesis work we will consider global density matrices describing systems without initial correlation ($\hat{\mathcal{C}} = 0$), hence

$$\frac{\partial \hat{\rho}}{\partial t} = \left. \frac{\partial \hat{\rho}}{\partial t} \right|_{\text{free}} + \left. \frac{\partial \hat{\rho}}{\partial t} \right|_{\text{scat}} . \quad (2.24)$$

Chapter 3

A Novel Lindblad description for dissipation/decoherence

3.1 The complete-positivity requirement

The Equation of motion (2.20) is, apart from the source term, the sum of a single-commutator term plus a double-commutator contribution: in the absence of any scattering mechanism, e.g. $\hat{H}' = 0$, the system undergoes a reversible unitary transformation induced by the single-commutator term, thus preserving the trace and the positive character of our density-matrix operator $\hat{\rho}$. In contrast, the perturbation Hamiltonian \hat{H}' within the Markov limit previously introduced will induce an evolution which is not, in general, reversible, as expected from a contribution which must provide energy dissipation. As a consequence, the many-body scattering-induced evolution is not, in general, unitary, hence additional requirements are necessary in order to establish the validity of the dynamics. In particular, any model able to properly describe the energetic exchanges should:

- (i) preserve the hermiticity of $\hat{\rho}$, otherwise there would be complex probabilities of finding the system in a given state;
- (ii) preserve the trace of $\hat{\rho}$ in spatially closed systems, otherwise there would be particle exchange - up to now, we are not discussing the

problem of spatially open systems, which will be treated later on;

- (iii) preserve the positivity of $\hat{\rho}$, otherwise there would be negative probabilities of finding the system in a given state.

The condition (iii) is often replaced by the stronger

- (iv) the model should be *complete positive*.

Given a density matrix operator $\hat{\rho}$, which acts over the N dimensional Hilbert space of the system \mathcal{H}_s , the superoperator $\mathcal{L} \equiv \mathcal{L}(\hat{\rho})$ which provides the scattering-induced dynamics (for example, in the Markov Approximation, $\mathcal{L}(\hat{\rho})$ coincide with the r.h.s. of Eq. (2.23)) is said to be positive iff [26], for every $|\psi\rangle \in \mathcal{H}_s$, one has

$$\langle \psi | \mathcal{L}(\hat{\rho}) | \psi \rangle \geq 0 \quad . \quad (3.1)$$

We consider a second m -dimensional Hilbert space \mathcal{H}'_m , the identity and generic operators, respectively $\hat{\mathcal{I}}_m$ and \hat{G}'_m , acting on \mathcal{H}'_m , and a superoperator \mathcal{L}'_m such that

$$\mathcal{L}'_m(\hat{\rho} \otimes \hat{\mathcal{I}}_m) = \mathcal{L}(\hat{\rho}) \otimes \hat{\mathcal{I}}_m \quad , \quad \mathcal{L}'_m(\hat{\mathcal{I}}_S \otimes \hat{G}'_m) = \hat{\mathcal{I}}_S \otimes \hat{G}'_m \quad , \quad (3.2)$$

where $\hat{\mathcal{I}}_S$ is the identity operator acting on \mathcal{H}_S . If this second superoperator \mathcal{L}'_m is positive (in the sense of Eq. (3.1) for every $|\psi'\rangle \in \mathcal{H}_S \otimes \mathcal{H}'_m$), then [27] the former one $\mathcal{L}(\hat{\rho})$ is said to be *m-positive*; if $\mathcal{L}(\hat{\rho})$ is *m-positive* for every positive integer m , then $\mathcal{L}(\hat{\rho})$ is *completely positive*. As we stressed, the completely-positive requirement is stronger or (at least) as strong as the positivity one; every unitary operator or element of a Quantum Dynamical Semigroup [28] is automatically complete-positive, the latter being the reason for which complete-positivity has gained so much popularity. In Sec. (3.2) we present the most general form (as usually found in literature) of Lindblad superoperator, while in Sec. (3.3) we present a recently proposed [1] Markov approximation which provides a Lindblad (e.g., completely positive) dynamics.

3.2 The Lindblad Superoperator

Every operator \hat{A} acting on a N -dimensional Hilbert space \mathcal{H}_S and such that $\text{tr}[\hat{A}^\dagger \hat{A}]_{\mathcal{H}_S}$ is finite may be written as

$$\hat{A} = \sum_{i=1}^{N^2} c_i \hat{\sigma}_i \quad , \quad (3.3)$$

where

$$c_i = \text{tr} \left[\hat{\sigma}_i^\dagger \hat{A} \right]_{\mathcal{H}_S} \quad (3.4)$$

and the operators $\hat{\sigma}_i$, with $i = 1, \dots, N^2$, are operators acting on \mathcal{H}_S and fulfilling¹,

$$\text{tr} \left[\hat{\sigma}_i^\dagger \hat{\sigma}_j \right]_{\mathcal{H}_S} = \delta_{ij} \quad ; \quad (3.6)$$

the condition in Eq. (3.6) is analogous to say that operators $\hat{\sigma}_i$ are orthonormal according to the inner product defined as

$$\left(\hat{B}, \hat{C} \right) := \text{tr} \left[\hat{B}^\dagger \hat{C} \right]_{\mathcal{H}_S} \quad (3.7)$$

for every couple of operators \hat{B} and \hat{C} acting on \mathcal{H}_S . For a given Hilbert space \mathcal{H}_S there are infinite possible sets of operators $\hat{\sigma}_i$ fulfilling Eq. (3.6); a widely employed choice, which will be used here as well, is to set $\hat{\sigma}_{N^2}$ as proportional to the identity operator²,

$$\hat{\sigma}_{N^2} = \frac{1}{\sqrt{N}} \hat{\mathcal{I}}_{N \times N} \quad . \quad (3.9)$$

¹The most direct example comes from matrix representation: if \hat{A} is represented by the $N \times N$ matrix A , the latter may be written as $A = \sum_i c_i \sigma^i$, where σ^i are N^2 different $N \times N$ matrix whose elements $(\sigma^i)_{ab}$ for $a, b = 1, \dots, N$ are given by

$$(\sigma^i)_{ab} = \delta_{i, (N-1)a+b} \quad (3.5)$$

e.g. by all possible different N^2 matrices of dimension N with only one non-null element equal to one.

²This assumption complicates the writing of the matrices σ^i representing $\hat{\sigma}_i$, as they must be (apart from σ^{N^2}) traceless: as an example, when $N = 2$ a possible choice of

The operators $\hat{\sigma}_i$ are typically used [26, 28] in order to write two alternatives and standard versions of completely-positive dynamics $\mathcal{L}(\hat{\rho})$ (see Sec. (3.1)) acting on a finite dimensional Hilbert space: the first one is the so-called *first standard form*,

$$\mathcal{L}(\hat{\rho}) = -\frac{i}{\hbar} [\hat{H}, \hat{\rho}] + \sum_{i,j=1}^{N^2-1} g_{ij} \left(\hat{\sigma}_i \hat{\rho} \hat{\sigma}_j^\dagger - \frac{1}{2} \{ \hat{\rho}, \hat{\sigma}_j^\dagger \hat{\sigma}_i \} \right) \quad , \quad (3.10)$$

where \hat{H} is an Hamiltonian typically given by the sum of the free Hamiltonian \hat{H}° of Eq. (2.9) plus some energy-renormalization contributions (see below) and the coefficients g_{ij} must be such that the matrix g with matrix elements $(g)_{ij} := g_{ij}$ is positive. The matrix g may be diagonalized by means of a unitary $(N^2 - 1) \times (N^2 - 1)$ matrix u ,

$$\gamma = ugu^\dagger \quad , \quad \text{with} \quad uu^\dagger = u^\dagger u = \hat{\mathcal{I}}_{(N^2-1) \times (N^2-1)} \quad , \quad (3.11)$$

with $\gamma = \text{diag}(\gamma_1, \dots, \gamma_{N^2-1})$; since g is positive, then $\gamma_l \geq 0$ for every $l=1, \dots, N^2 - 1$. As a consequence, the dynamics in Eq. (3.10) may be rewritten in the second standard version of completely-positive dynamics, the so-called *diagonal form*, which is given by

$$\mathcal{L}(\hat{\rho}) = -\frac{i}{\hbar} [\hat{H}, \hat{\rho}] + \sum_{l=1}^{N^2-1} \gamma_l \left(\hat{A}_l \hat{\rho} \hat{A}_l^\dagger - \frac{1}{2} \{ \hat{\rho}, \hat{A}_l^\dagger \hat{A}_l \} \right) \quad . \quad (3.12)$$

where the operators \hat{A}_l are defined by

$$\hat{A}_l = \sum_{m=1}^{N^2-1} \hat{\sigma}_m u_{lm}^* \quad ; \quad (3.13)$$

matrices σ^i fulfilling both Eq. (3.6) and (3.9) is given by

$$\begin{aligned} \sigma^1 &= \frac{1}{\sqrt{2}} \begin{pmatrix} 1 & 0 \\ 0 & -1 \end{pmatrix} \quad , \quad \sigma^2 = \frac{1}{\sqrt{2}} \begin{pmatrix} 0 & 1 \\ -1 & 0 \end{pmatrix} \quad , \\ \sigma^3 &= \frac{1}{\sqrt{2}} \begin{pmatrix} 0 & 1 \\ 1 & 0 \end{pmatrix} \quad , \quad \sigma^4 = \frac{1}{\sqrt{2}} \begin{pmatrix} 1 & 0 \\ 0 & 1 \end{pmatrix} \quad . \end{aligned} \quad (3.8)$$

from the definition in Eq. (3.13), it comes that the operators \hat{A}_l are orthonormal in the sense of Eqs. (3.6) and (3.7), in fact

$$\begin{aligned}
 (\hat{A}_l, \hat{A}_{l'}) &= \text{tr} \left[\hat{A}_l^\dagger \hat{A}_{l'} \right]_{\mathcal{H}_S} \\
 &= \sum_{m, m'=1}^{N^2-1} u_{lm} u_{l'm'}^* \text{tr} \left[\hat{\sigma}_m^\dagger \hat{\sigma}_{m'} \right]_{\mathcal{H}_S} \\
 &= \sum_{m=1}^{N^2-1} u_{lm} u_{l'm}^* \equiv (uu^\dagger)_{ll'} = \delta_{ll'} \quad .
 \end{aligned} \tag{3.14}$$

The two Eqs (3.10) and (3.12) are perfectly equivalent and have been found independently [28] by V. Gorini, A. Kossakowski and E. C. G. Sudarshan [29] and G. Lindblad [27]. The Equation (3.12) is sometimes called *Lindblad equation* and its second term (the one involving sum over orthonormal operators) *Lindblad superoperator*.

3.2.1 Lindblad-like scattering-induced dynamics

In this thesis work, we will often employ scattering-induced superoperator (see Eq. (2.22)) in the form

$$\left. \frac{\partial \hat{\rho}}{\partial t} \right|_{\text{scat}} = \sum_s \hat{\mathcal{A}}^s \hat{\rho} \hat{\mathcal{A}}^{s\dagger} - \frac{1}{2} \left\{ \hat{\rho}, \hat{\mathcal{A}}^{s\dagger} \hat{\mathcal{A}}^s \right\} \quad , \tag{3.15}$$

where the operators $\hat{\mathcal{A}}^s$ and $\hat{\rho}$ will be different in nature (e.g. many-particle, many-electron or single-electron) depending on the problem considered and the sum will be over a scattering index s . In any case, the operators $\hat{\mathcal{A}}^s$ will be derived microscopically from the interacting Hamiltonians and are hence not, in general, orthonormal in the sense of Eq. (3.6); however, using Eq. (3.3), we may decompose every $\hat{\mathcal{A}}^s$ on the basis of orthonormalized trace-class operators $\{\hat{\sigma}_i\}$,

$$\hat{\mathcal{A}}^s = \sum_{i=1}^N c_i^s \hat{\sigma}_i \quad : \tag{3.16}$$

inserting Eq. (3.16) into Eq. (3.15), the latter may be rewritten as

$$\begin{aligned} \left. \frac{\partial \hat{\rho}}{\partial t} \right|_{\text{scat}} &= \sum_{i,j=1}^{N-1} g_{ij} \left(\hat{\sigma}_i \hat{\rho} \hat{\sigma}_j^\dagger - \frac{1}{2} \{ \hat{\rho}, \hat{\sigma}_j^\dagger \hat{\sigma}_i \} \right) \\ &+ \frac{1}{2N} \sum_s \sum_{i=1, N-1} \text{Tr}^*[\hat{\mathcal{A}}^s]_{\mathcal{H}_S} c_i^s [\hat{\sigma}_i, \hat{\rho}] + \text{H.c.} \quad , \end{aligned} \quad (3.17)$$

where we made use (see Eqs. (3.9) and (3.4)) of the equalities $\sigma_{N^2} = \frac{1}{\sqrt{N}} \hat{\mathcal{L}}$, $c_{N^2} = \frac{1}{\sqrt{N}} \text{Tr}[\hat{\mathcal{A}}^s]_{\mathcal{H}_S}$ and

$$g_{ij} = \sum_s c_i^s c_j^{s*} \quad . \quad (3.18)$$

The matrix g with elements $(g)_{ij} = g_{ij}$ is positive: in fact for every vector $\mathbf{z} = \sum_{l=1}^{N^2-1} z_l \mathbf{e}_l \in \mathbb{C}^{N^2-1}$, where $\{\mathbf{e}_l, l = 1, \dots, N^2 - 1\}$ is an orthonormal basis of \mathbb{C}^{N^2} , (e.g. $\mathbf{e}_l^* \mathbf{e}_m = \delta_{lm}$), one has

$$\sum_{i,j=1}^{N^2-1} g_{ij} z_i z_j^* = \sum_s \left(\sum_{i=1}^{N^2-1} c_i^s z_i \right) \left(\sum_{j=1}^{N^2-1} c_j^s z_j \right)^* \geq 0 \quad . \quad (3.19)$$

As a consequence, the scattering-induced dynamics in Eq. (3.15) is of the Lindblad type in Eq. (3.17) (see also Eq. (3.12)), which is the sum of a Lindblad superoperator (the term with two sums) plus some other terms which, due to their commutative forms, may be absorbed in the free-like term of Eq. (3.12).

3.3 An alternative Markov limit

In [1] a novel Markov limit has been proposed, the latter being able to provide a scattering-induced dynamics of the global density matrix $\hat{\rho}$ in the form

$$\left. \frac{\partial \hat{\rho}}{\partial t} \right|_{\text{scat}} = \hat{\mathcal{A}}' \hat{\rho} \hat{\mathcal{A}}'^\dagger - \frac{1}{2} \{ \hat{\rho}, \hat{\mathcal{A}}'^\dagger \hat{\mathcal{A}}' \} \quad , \quad (3.20)$$

where the operators $\hat{\mathcal{A}}'$ are microscopically determined from the scattering Hamiltonian \hat{H}' as

$$\hat{\mathcal{A}}' = \left(\frac{2}{\pi t^2} \right)^{\frac{1}{4}} \int dt' \hat{\mathcal{H}}'(t') e^{-\left(\frac{t'}{t} \right)^2} \quad . \quad (3.21)$$

In the following we will restrict to two of the main interactions, the carrier-phonon of Eq. (1.4) and the carrier-carrier mechanism in Eq. (1.10), which thanks to Eq. (3.21) give raise to the operators

$$\begin{aligned}
 \hat{\mathcal{A}}^{\text{cph}} &= \left(\frac{2}{\pi \bar{t}^2} \right)^{\frac{1}{4}} \int_{-\infty}^{\infty} dt' \hat{\mathcal{H}}^{\text{cph}}(t') e^{-\left(\frac{t'}{\bar{t}}\right)^2} \\
 &= \sum_{\alpha\alpha', \mathbf{q}} \left(\mathbf{A}_{\alpha\alpha'}^{\mathbf{q}+} \hat{c}_{\alpha}^{\dagger} \hat{c}_{\alpha'} \hat{b}_{\mathbf{q}}^{\dagger} + \mathbf{A}_{\alpha\alpha'}^{\mathbf{q}-} \hat{c}_{\alpha'}^{\dagger} \hat{c}_{\alpha} \hat{b}_{\mathbf{q}} \right) , \\
 \hat{\mathcal{A}}^{\text{cc}} &= \left(\frac{2}{\pi \bar{t}^2} \right)^{\frac{1}{4}} \int_{-\infty}^{\infty} dt' \hat{\mathcal{H}}^{\text{cc}}(t') e^{-\left(\frac{t'}{\bar{t}}\right)^2} \\
 &= \frac{1}{2} \sum_{\alpha\alpha'\bar{\alpha}\bar{\alpha}'} A_{\alpha\bar{\alpha}\alpha'\bar{\alpha}'} \hat{c}_{\alpha}^{\dagger} \hat{c}_{\bar{\alpha}}^{\dagger} \hat{c}_{\alpha'} \hat{c}_{\bar{\alpha}'} \\
 &\equiv \frac{1}{2} \sum_{\alpha\alpha'\bar{\alpha}\bar{\alpha}'} \mathcal{A}_{\alpha\bar{\alpha}\alpha'\bar{\alpha}'}^{\text{cc}} \hat{c}_{\alpha}^{\dagger} \hat{c}_{\bar{\alpha}}^{\dagger} \hat{c}_{\alpha'} \hat{c}_{\bar{\alpha}'} ,
 \end{aligned} \tag{3.22}$$

where

$$\begin{aligned}
 \mathbf{A}_{\alpha\alpha'}^{\mathbf{q}\pm} &= \left(\frac{2}{\pi \bar{t}^2} \right)^{\frac{1}{4}} \frac{1}{\hbar} g_{\alpha\alpha'}^{\mathbf{q}\pm} \int_{-\infty}^{\infty} dt' e^{-i \frac{\epsilon_{\alpha} - \epsilon_{\alpha'} \pm \epsilon_{\mathbf{q}}}{\hbar} t'} e^{-\left(\frac{t'}{\bar{t}}\right)^2} \\
 &= \sqrt{\frac{2\pi}{\hbar}} g_{\alpha\alpha'}^{\mathbf{q}\pm} \left(\frac{1}{2\pi \bar{\epsilon}^2} \right)^{\frac{1}{4}} e^{-\left(\frac{\epsilon_{\alpha} - \epsilon_{\alpha'} \pm \epsilon_{\mathbf{q}}}{2\bar{\epsilon}}\right)^2} , \\
 A_{\alpha\bar{\alpha}\alpha'\bar{\alpha}'} &= \left(\frac{2}{\pi \bar{t}^2} \right)^{\frac{1}{4}} g_{\alpha\bar{\alpha}\alpha'\bar{\alpha}'} \int_{-\infty}^{\infty} dt' e^{-i \frac{\epsilon_{\alpha} + \epsilon_{\bar{\alpha}} - \epsilon_{\alpha'} - \epsilon_{\bar{\alpha}'}}{\hbar} t'} e^{-\left(\frac{t'}{\bar{t}}\right)^2} \\
 &= \sqrt{\frac{2\pi}{\hbar}} g_{\alpha\bar{\alpha}\alpha'\bar{\alpha}'} \left(\frac{1}{2\pi \bar{\epsilon}^2} \right)^{\frac{1}{4}} e^{-\left(\frac{\epsilon_{\alpha} + \epsilon_{\bar{\alpha}} - \epsilon_{\alpha'} - \epsilon_{\bar{\alpha}'}}{2\bar{\epsilon}}\right)^2} ,
 \end{aligned} \tag{3.23}$$

where $g_{\alpha\alpha'}^{\mathbf{q}\pm}$ and $g_{\alpha\bar{\alpha}\alpha'\bar{\alpha}'}$ are the coefficients of the respective Hamiltonians of Eqs. (1.4) and (1.10), $\bar{\epsilon} = \frac{\hbar}{\bar{t}}$ is a measure of the energy uncertainty in the interaction process induced by the temporal coarse graining and, due to the well-know fermionic algebra, the coefficients $\mathcal{A}_{\alpha\bar{\alpha},\alpha'\bar{\alpha}'}^{\text{cc}}$,

$$\mathcal{A}_{\alpha\bar{\alpha},\alpha'\bar{\alpha}'}^{\text{cc}} = \frac{1}{4} \left(A_{\alpha\bar{\alpha},\alpha'\bar{\alpha}'} - A_{\bar{\alpha}\alpha,\alpha'\bar{\alpha}'} - A_{\alpha\bar{\alpha},\bar{\alpha}'\alpha'} + A_{\bar{\alpha}\alpha,\bar{\alpha}'\alpha'} \right) , \tag{3.24}$$

denote the totally antisymmetric parts of the two-body coefficients $A_{\alpha\bar{\alpha},\alpha'\bar{\alpha}'}$ in (3.23).

Part II

The failure of the Wigner function in describing nanometric spatially open systems

Chapter 4

Introduction

The aim of part II is to point out and explain the intrinsic limitations of the conventional quantum-device modeling based on the Wigner-function paradigm. In particular, we provide a definite answer to open questions related to the application of the conventional spatial boundary-condition scheme for the solution of the Wigner transport equation, explaining why and when this scheme exhibits some intrinsic limitations which lead to totally unphysical results, especially in the coherent-transport regime, like e.g. negative spatial charge densities. In order to illustrate this aspect, we shall mainly discuss a simple but physically relevant one-dimensional system, namely a delta-like potential profile. Our detailed analysis will show that (i) in the absence of energy dissipation (coherent limit) the solution of the Wigner equation (compatible with given boundary conditions) is not unique, and (ii) also when decoherence/dissipation phenomena are taken into account (via a relaxation-time approximation) and the solution is unique, the latter is not necessarily a Wigner function, i.e., a Weyl-Wigner transform of a single-particle density matrix.

A typical nanodevice [25] is a “localized system”, i.e., a portion of material characterized by a well defined volume and by spatial boundaries acting as electric contacts to external charge reservoirs, as sketched in Fig. 4.1. Here, z denotes the transport direction, l is the longitudinal length of the device, the electric contacts being located at $z = -l/2$ and $z = +l/2$. The

modeling of a nanostructure device thus represents an intrinsically space-dependent problem, so that a real-space quantum treatment accounting for the presence of quite different spatial regions becomes mandatory. To this purpose, the Wigner-function formalism [30, 31] is a widely adopted framework. Within this formalism, the statistical quantum state of the electronic subsystem is fully described in terms of the Wigner function $f(\mathbf{r}, \mathbf{k})$, defined over the conventional phase-space (\mathbf{r}, \mathbf{k}) as the Weyl-Wigner transform of the single-particle density-matrix operator $\hat{\rho}$ [32], which is a single particle operator (see Eq. (5.17)) obtainable from the global density matrix operator $\hat{\rho}$ by a procedure extensively described in Chap. 11.

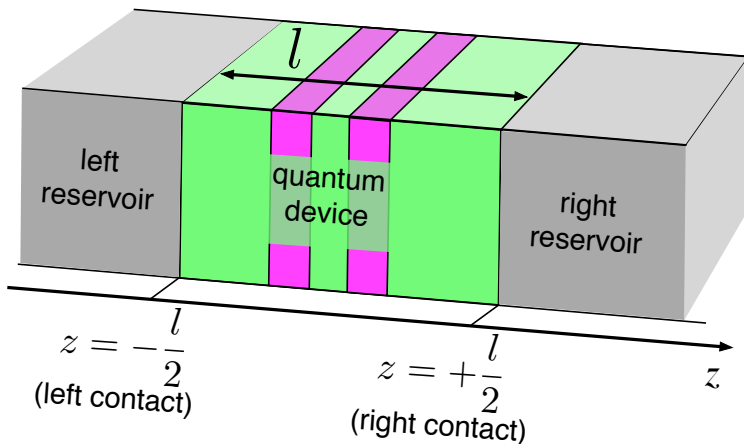


Figure 4.1. Schematic representation of a typical semiconductor-based quantum device as an open system connected to two external charge reservoirs. Here, the distance between the interfaces is l , and z is the longitudinal transport direction.

Based on the Wigner-function formalism, various approaches for the study of quantum-transport phenomena in semiconductor nanomaterials and nanodevices have been proposed. [33–52] On the one end, starting from the pioneering work by Frensley, [33] quantum-transport simulations based on a direct numerical solution of the Wigner equation have been performed via finite-difference approaches [36], by imposing on the Wigner function the standard U boundary condition scheme (see Fig. 7.1 in Chap. 7). On

the other end, a generalization to systems with open boundaries of the semiconductor Bloch equations has also been proposed. [53, 54] In addition to these two alternative simulation strategies –both based on effective treatments of relevant interaction mechanisms– Jacoboni and co-workers have proposed a fully quantum-mechanical simulation scheme for the study of electron-phonon interaction based on the “Wigner paths”; [55] this approach is intrinsically able to overcome the standard approximations of conventional quantum-transport models, namely the Markov approximation and the completed-collision limit; [56] however, due to the huge amount of computation required, its applicability is often limited to short time-scales and extremely simplified situations.

Motivated by a few unphysical results [54] obtained via the generalized semiconductor Bloch equations mentioned above, a recent study [2] has shown that the application of the conventional space boundary condition scheme to the Wigner transport equation may lead to partially negative charge probability densities, unambiguous proof of the failure of such classical-like Wigner-function treatment.

As already stressed, the main goal of this part is a detailed analysis of the strengths and limits of the Wigner function formalism. In order to complete this task. we will follow the already published paper [57], from which the numerical results here reported come.

Before moving on to the description it is useful to spend a few words about the phase-space description of Quantum Mechanics. In Classical Mechanics, a large ensemble of states, each one occupying a point in the phase space, gives naturally rise to the definition of a probability distribution $f_{cl}(\mathbf{r}, \mathbf{p})$ depending on the spatial- and momentum-vector coordinates \mathbf{r} and \mathbf{p} - see Sec. 1.3 for an example. Given a generic function of position and velocity $A(\mathbf{r}, \mathbf{p})$, its statistical average is given by

$$\langle A \rangle_{cl} = \int d\mathbf{r}d\mathbf{p} A(\mathbf{r}, \mathbf{p}) f_{cl}(\mathbf{r}, \mathbf{p}) \quad . \quad (4.1)$$

In contrast, in Quantum Mechanics the expectation value of a generic single-particle operator \hat{B} is given by

$$\langle \hat{B} \rangle_q = \text{Tr} [\hat{B} \hat{\rho}] \quad , \quad (4.2)$$

where $\hat{\rho}$ is the single-particle density matrix. In analogy to the classical average (see Eq. (4.1)), a phase-space approach to Quantum Mechanics would like to evaluate the quantum expectation value in Eq. (4.2) as an integral over the phase space,

$$\langle \hat{B} \rangle_q = \int d\mathbf{r}d\mathbf{p} B(\mathbf{r}, \mathbf{p}) f_q(\mathbf{r}, \mathbf{p}) \quad , \quad (4.3)$$

where $B(\mathbf{r}, \mathbf{p})$ is a function associated to the quantum operator \hat{B} and $f_q(\mathbf{r}, \mathbf{p})$ should be a quantum-mechanical analogous to the classical probability distribution $f_{cl}(\mathbf{r}, \mathbf{p})$. However, a unique recipe for obtaining $B(\mathbf{r}, \mathbf{p})$ and $f_q(\mathbf{r}, \mathbf{p})$ does not exist, in fact several different approaches have been proposed, most of them sharing few rules: one common feature is the non-positive character of $f_q(\mathbf{r}, \mathbf{p})$ ¹, from which the function $f_q(\mathbf{r}, \mathbf{p})$ is defined as a *quasi*-probability distribution. Apart from the Wigner function, some popular quasi-probability distribution are the P representation, both in the original [59, 60] and generalized version [61]; we also cite the Husimi distribution [62] which, however, is nonnegative and, as a consequence, does not represent the probability of mutually exclusive states.

¹In fact, a positive definite $f_q(\mathbf{r}, \mathbf{p})$ would not be able to describe orthogonal states [58].

Chapter 5

The Wigner Function formalism

In order to account for the space-dependent character of a quantum device, a widely employed strategy is the Wigner-function treatment of the problem. [30] The Wigner function $f(\mathbf{r}, \mathbf{k})$ associated to a single-particle density-matrix operator $\hat{\rho}$ (which will be defined in terms of the global density matrix operator $\hat{\rho}$ in Chap 11) is defined as its Weyl-Wigner transform [32]

$$\begin{aligned} f(\mathbf{r}, \mathbf{k}) &= \int d\mathbf{r}' e^{-i\mathbf{k}\cdot\mathbf{r}'} \left\langle \mathbf{r} + \frac{\mathbf{r}'}{2} \left| \hat{\rho} \right| \mathbf{r} - \frac{\mathbf{r}'}{2} \right\rangle \\ &= \text{tr}\{\hat{W}(\mathbf{r}, \mathbf{k})\hat{\rho}\} , \end{aligned} \quad (5.1)$$

corresponding to the quantum-plus-statistical average of the Wigner operator [25]

$$\hat{W}(\mathbf{r}, \mathbf{k}) = \int d\mathbf{r}' \left| \mathbf{r} - \frac{\mathbf{r}'}{2} \right\rangle e^{-i\mathbf{k}\cdot\mathbf{r}'} \left\langle \mathbf{r} + \frac{\mathbf{r}'}{2} \right|. \quad (5.2)$$

In particular, for a pure state $|\beta\rangle$ the Wigner function reduces to the expectation value of the Weyl-Wigner operator

$$f_{\beta}(\mathbf{r}, \mathbf{k}) = \langle \beta | \hat{W}(\mathbf{r}, \mathbf{k}) | \beta \rangle . \quad (5.3)$$

The Weyl-Wigner transform in Eq. (5.1) relates the quantum-mechanical operator $\hat{\rho}$ to its associated function $f(\mathbf{r}, \mathbf{k})$; the same mechanism could be

applied to a generic operator \hat{A} in order to establish a link between the latter and a function defined over the phase-space,

$$\hat{A} \leftrightarrow A(\mathbf{r}, \mathbf{k}), \text{ with } A(\mathbf{r}, \mathbf{k}) = \text{tr}\{\hat{W}(\mathbf{r}, \mathbf{k})\hat{A}\} \quad , \quad (5.4)$$

such that the expectation value of \hat{A} can be rewritten according to the Wigner picture as

$$\langle \hat{A} \rangle = (2\pi)^{-3} \int d\mathbf{r}d\mathbf{k}A(\mathbf{r}, \mathbf{k})f(\mathbf{r}, \mathbf{k}) \quad . \quad (5.5)$$

Within such Wigner-function representation the average values of charge and current densities at location \mathbf{r} are given by

$$n(\mathbf{r}) = \int \frac{d\mathbf{k}}{(2\pi)^3} f(\mathbf{r}, \mathbf{k}) \quad (5.6)$$

and

$$\mathbf{J}(\mathbf{r}) = \int \frac{d\mathbf{k}}{(2\pi)^3} \mathbf{v}(\mathbf{k}) f(\mathbf{r}, \mathbf{k}) \quad , \quad (5.7)$$

where $\mathbf{v}(\mathbf{k}) = \hbar\mathbf{k}/m^*$ is the velocity of a conduction electron with effective mass m^* .

The time evolution for the Wigner function can be derived from the equation of motion for the density-matrix operator: the latter will be extensively discussed in part III, but for the moment we may write it in the following generic form valid in the low-density limit: [25]

$$\frac{d\hat{\rho}}{dt} = \frac{1}{i\hbar} \left[\hat{H}^{\text{sp}}, \hat{\rho} \right] + \Gamma(\hat{\rho}) \quad . \quad (5.8)$$

Here, the first contribution on the r.h.s. describes the coherent dynamics dictated by the non-interacting Hamiltonian \hat{H}^{sp} of Eq. (1.2), including energy renormalizations or elastic single-electron scattering processes, while the second term is a linear superoperator Γ encoding the energy-dissipative/decoherent scattering mechanisms that electrons experience within the host material.

In particular, by choosing as basis states $|\alpha\rangle$ the eigenstates of \hat{H}^{sp} ,

$$\hat{H}^{\text{sp}} = \sum_{\alpha} |\alpha\rangle \epsilon_{\alpha} \langle \alpha| \quad , \quad (5.9)$$

the density-matrix equation (5.8) may be rewritten as

$$\frac{d\rho_{\alpha_1\alpha_2}}{dt} = \frac{\epsilon_{\alpha_1} - \epsilon_{\alpha_2}}{i\hbar} \rho_{\alpha_1\alpha_2} + \sum_{\alpha'_1\alpha'_2} \Gamma_{\alpha_1\alpha_2,\alpha'_1\alpha'_2} \rho_{\alpha'_1\alpha'_2}. \quad (5.10)$$

Such set of coupled equations of motion for the density-matrix elements $\rho_{\alpha_1\alpha_2}$ are usually referred to as the semiconductor Bloch equations. [25]

By applying the Weyl-Wigner transform (5.1), together with its inverse

$$\hat{\rho} = \frac{1}{(2\pi)^3} \int d\mathbf{r} \int d\mathbf{k} \hat{W}(\mathbf{r}, \mathbf{k}) f(\mathbf{r}, \mathbf{k}), \quad (5.11)$$

to the density-matrix equation (5.8), one obtains the equation of motion for the Wigner function

$$\frac{\partial f(\mathbf{r}, \mathbf{k})}{\partial t} = \left. \frac{\partial f(\mathbf{r}, \mathbf{k})}{\partial t} \right|_{\text{sp}} + \left. \frac{\partial f(\mathbf{r}, \mathbf{k})}{\partial t} \right|_{\text{scat}} \quad (5.12)$$

with

$$\left. \frac{\partial f(\mathbf{r}, \mathbf{k})}{\partial t} \right|_{\text{sp}} = \int d\mathbf{r}' d\mathbf{k}' \epsilon(\mathbf{r}, \mathbf{k}; \mathbf{r}', \mathbf{k}') f(\mathbf{r}', \mathbf{k}') \quad (5.13)$$

and

$$\left. \frac{\partial f(\mathbf{r}, \mathbf{k})}{\partial t} \right|_{\text{scat}} = \int d\mathbf{r}' d\mathbf{k}' \Gamma(\mathbf{r}, \mathbf{k}; \mathbf{r}', \mathbf{k}') f(\mathbf{r}', \mathbf{k}') , \quad (5.14)$$

where

$$\epsilon(\mathbf{r}, \mathbf{k}; \mathbf{r}', \mathbf{k}') = -\frac{i}{(2\pi)^3 \hbar} \text{tr} \left\{ \hat{W}(\mathbf{r}, \mathbf{k}) \left[\hat{H}^{\text{sp}}, \hat{W}(\mathbf{r}', \mathbf{k}') \right] \right\} \quad (5.15)$$

and

$$\Gamma(\mathbf{r}, \mathbf{k}; \mathbf{r}', \mathbf{k}') = \frac{1}{(2\pi)^3} \text{tr} \left\{ \hat{W}(\mathbf{r}, \mathbf{k}) \Gamma \left(\hat{W}(\mathbf{r}', \mathbf{k}') \right) \right\} \quad (5.16)$$

are the single-particle and the scattering superoperators written in the (\mathbf{r}, \mathbf{k}) Wigner picture, respectively.

Given the states $|\alpha\rangle$, the single-particle density-matrix operator can be expressed in terms of entries $\rho_{\alpha_1\alpha_2}$ as

$$\hat{\rho} = \sum_{\alpha_1\alpha_2} |\alpha_1\rangle \rho_{\alpha_1\alpha_2} \langle \alpha_2| , \quad (5.17)$$

whereas the Wigner function in (5.1) can be written as

$$f(\mathbf{r}, \mathbf{k}) = \sum_{\alpha_1 \alpha_2} W_{\alpha_2 \alpha_1}(\mathbf{r}, \mathbf{k}) \rho_{\alpha_1 \alpha_2} \quad (5.18)$$

with

$$W_{\alpha_2 \alpha_1}(\mathbf{r}, \mathbf{k}) = \int d\mathbf{r}' \psi_{\alpha_1} \left(\mathbf{r} + \frac{\mathbf{r}'}{2} \right) e^{-i\mathbf{k} \cdot \mathbf{r}'} \psi_{\alpha_2}^* \left(\mathbf{r} - \frac{\mathbf{r}'}{2} \right). \quad (5.19)$$

We emphasize that in general the Wigner equation (5.12) is non-local in both \mathbf{r} and in \mathbf{k} . As a consequence, the conventional boundary-condition scheme adopted to solve the semiclassical Boltzmann equation cannot be applied. [25] However, in order to simplify the problem, the rigorous expressions of the single-particle and scattering superoperators in Eqs. (5.13) and (5.14) are often replaced by effective/phenomenological models. In particular, as we shall discuss in detail in Sec. 6.1, within the conventional effective-mass and envelope-function approximations, the single-particle superoperator (5.13) turns out to be local. Furthermore, adopting a generalized relaxation-time approximation (see also Chap. 8), the fully quantum-mechanical scattering superoperator (5.14) is replaced by the local form [30]

$$\left. \frac{\partial f(\mathbf{r}, \mathbf{k})}{\partial t} \right|_{\text{scat}} = - \frac{f(\mathbf{r}, \mathbf{k}) - f^\circ(\mathbf{r}, \mathbf{k})}{\tau}, \quad (5.20)$$

describing the effect of dissipation/decoherence (induced by the host material) toward the equilibrium Wigner function $f^\circ(\mathbf{r}, \mathbf{k})$ in terms of a relaxation time τ .

Chapter 6

The Coherent Wigner Equation

In order to investigate the intrinsic limitations of the boundary-condition scheme pointed out above, we shall first focus on a fully coherent system/device, where energy-dissipation/decoherence processes occur over timescales that are much longer than the typical timescales induced by \hat{H}^{sp} . In this regime, the density-matrix equation (5.8) reduces to the Liouville-von Neumann equation

$$\frac{d\hat{\rho}}{dt} = \frac{1}{i\hbar} [\hat{H}^{\text{sp}}, \hat{\rho}] . \quad (6.1)$$

6.1 The Wigner transport equation

For the purpose of the present thesis work, it is enough to consider a one-dimensional system ($\mathbf{r}, \mathbf{k} \rightarrow z, k$) described by the envelope-function Hamiltonian [25] (see also Sec. 1.1)

$$\hat{H}^{\text{sp}} = K(\hat{k}) + V(\hat{z}) , \quad (6.2)$$

where \hat{z} and \hat{k} denote, respectively, the quantum-mechanical operators associated to the electronic coordinate (z) and to the electronic momentum/wavevector (k); generalizations to a fully three-dimensional problem are straightforward. According to the usual prescription of the envelope-function theory, the function K in Eq. (6.2) describes the bulk electronic

band, while V describes the nanostructure potential profile. The Hamiltonian (6.2) leads Eq. (6.1) to acquire the form

$$\frac{d\hat{\rho}}{dt} = \frac{d\hat{\rho}}{dt}\Big|_K + \frac{d\hat{\rho}}{dt}\Big|_V, \quad (6.3)$$

with

$$\frac{d\hat{\rho}}{dt}\Big|_K = \frac{1}{i\hbar} \left[K(\hat{k}), \hat{\rho} \right] \quad (6.4)$$

and

$$\frac{d\hat{\rho}}{dt}\Big|_V = \frac{1}{i\hbar} \left[V(\hat{z}), \hat{\rho} \right]. \quad (6.5)$$

Applying the Weyl-Wigner transform to the density-matrix equation (6.3), one gets the (one-dimensional version of the) single-particle contribution $\frac{\partial f(z,k)}{\partial t}\Big|_{\text{sp}}$ in Eq. (5.13) of Wigner-function equation for $f(z, k)$ as a sum of a free-evolution (also named *drift*) term and a potential-induced one,

$$\frac{\partial f(z, k)}{\partial t}\Big|_{\text{sp}} = \frac{\partial f(z, k)}{\partial t}\Big|_K + \frac{\partial f(z, k)}{\partial t}\Big|_V. \quad (6.6)$$

In doing that, the Wigner function (5.1) can be expressed in two different and equivalent ways, corresponding to the momentum (k) and coordinate (z) representations, respectively. By setting $\alpha = k$ as well as $\alpha = z$ in Eq. (5.18) one obtains

$$f(z, k) = \int dk' e^{izk'} \rho\left(k + \frac{k'}{2}, k - \frac{k'}{2}\right) \quad (6.7)$$

$$= \int dz' e^{-ikz'} \rho\left(z + \frac{z'}{2}, z - \frac{z'}{2}\right). \quad (6.8)$$

These two expressions turn out to be both useful because the kinetic and potential contributions (6.4) and (6.5) are diagonal in the momentum (k) and coordinate (z) representations, respectively, i.e.

$$\frac{d\rho(k_1, k_2)}{dt}\Big|_K = \frac{K(k_1) - K(k_2)}{i\hbar} \rho(k_1, k_2) \quad (6.9)$$

and

$$\frac{d\rho(z_1, z_2)}{dt}\Big|_V = \frac{V(z_1) - V(z_2)}{i\hbar} \rho(z_1, z_2). \quad (6.10)$$

- (i) By applying the Weyl-Wigner transform (6.7), as well as its inverse (given by Eq. (5.11) written in the k -representation),

$$\rho\left(k + \frac{k'}{2}, k - \frac{k'}{2}\right) = \int dz \frac{e^{-ik'z}}{2\pi} f(z, k), \quad (6.11)$$

to the kinetic contribution (6.9), one gets

$$\left. \frac{\partial f(z, k)}{\partial t} \right|_K = - \int dz' \mathcal{K}(z - z', k) f(z', k) \quad (6.12)$$

with

$$\mathcal{K}(z'', k) = \frac{i}{\hbar} \int dk' \frac{e^{iz''k'}}{2\pi} \left[K\left(k + \frac{k'}{2}\right) - K\left(k - \frac{k'}{2}\right) \right]. \quad (6.13)$$

The kinetic operator in the Wigner picture, appearing on the r.h.s. of Eq. (6.12), is always local in k and, in general, is non-local in z . In particular, by adopting the usual effective-mass approximation,

$$K(k) = \frac{\hbar^2 k^2}{2m^*}, \quad (6.14)$$

the non-local kinetic operator (6.12) reduces to

$$\left. \frac{\partial f(z, k)}{\partial t} \right|_K = -v(k) \frac{\partial f(z, k)}{\partial z}, \quad (6.15)$$

where $v(k) = \hbar k/m^*$ denotes the effective-mass carrier group velocity. Notably, within the effective-mass approximation (6.14) the kinetic contribution coincides with its semiclassical counterpart, i.e., it reduces to the standard diffusion term of the Boltzmann equation (see also the three-dimensional Equation in (1.12)).

- (ii) By applying the Weyl-Wigner transform (6.8), as well as its inverse (given by Eq. (5.11) written in the z -representation),

$$\rho\left(z + \frac{z'}{2}, z - \frac{z'}{2}\right) = \int dk \frac{e^{iz'k}}{2\pi} f(z, k), \quad (6.16)$$

to the potential contribution in (6.10), one gets

$$\left. \frac{\partial f(z, k)}{\partial t} \right|_V = - \int dk' \mathcal{V}(z, k - k') f(z, k') \quad (6.17)$$

with

$$\mathcal{V}(z, k'') = \frac{i}{\hbar} \int dz' \frac{e^{-ik''z'}}{2\pi} \left[V \left(z + \frac{z'}{2} \right) - V \left(z - \frac{z'}{2} \right) \right]. \quad (6.18)$$

In contrast with the kinetic one, the potential operator appearing on the r.h.s. of Eq.(6.17) is always local in z and, in general, is non-local in k . For the particular case of a quadratic potential

$$V(z) = \frac{1}{2}az^2 + bz + c \quad , \quad (6.19)$$

corresponding to the classical force

$$F(z) = - \frac{dV(z)}{dz} = -(az + b), \quad (6.20)$$

the non-local potential operator (6.17) simply reduces to

$$\left. \frac{\partial f(z, k)}{\partial t} \right|_V = - \frac{F(z)}{\hbar} \frac{\partial f(z, k)}{\partial k}. \quad (6.21)$$

Thus, for the particular case of the quadratic potential profile (6.19), the potential contribution coincides with its semiclassical counterpart, i.e., it reduces to the standard scattering-free term of the Boltzmann equation (see also the three-dimensional Equation in (1.12) with null r.h.s.); it follows that the non-local character of the generic potential superoperator in (6.17) vanishes in the presence of a parabolic potential only.

The analysis performed so far has shown a strongly symmetric role between real-space (z) and momentum (k) coordinates; this is confirmed by the fact that the corresponding equations of motion (each one written within the related representation) display the very same mathematical structure [see Eqs. (6.9) and (6.10)]. Moreover, for a physical system characterized by an effective Hamiltonian quadratic in both the coordinate and the momentum, the equation of motion of the Wigner function coincides with its

semiclassical (Boltzmann) counterpart, thus showing the intimate link between the Wigner function and the semiclassical distribution. This can also be regarded as a formal proof of the fact that, for a particle subjected to a quadratic potential, its classical and quantum equations of motion coincide, a fundamental result originally pointed out by Richard P. Feynman via his “path integral” formulation of quantum mechanics. [63]

For the microscopic modeling of semiconductor quantum devices, the effective-mass approximation (6.14) is widely employed, and constitutes a good starting point for the description of the bulk band structure. In contrast, for a generic optoelectronic device, the effective potential profile $V(z)$ is usually far from the quadratic form in (6.19). As a consequence, within this approximation scheme the single-particle superoperator ϵ in (5.13) is always local in z , and the total (i.e., kinetic plus potential) equation of motion for $f(z, k)$ –obtained combining Eqs. (6.15) and (6.17)– contains a non-local term in k induced by the potential profile:

$$\frac{\partial f(z, k)}{\partial t} + v(k) \frac{\partial f(z, k)}{\partial z} + \int dk' \mathcal{V}(z, k - k') f(z, k') = 0 . \quad (6.22)$$

Equation (6.22), also referred to as the *Wigner transport equation*, describes the time evolution of the one-dimensional Wigner function in the absence of energy-dissipation/decoherence processes. In steady-state conditions ($\partial f(z, k)/\partial t = 0$) it reduces to

$$v(k) \frac{\partial f(z, k)}{\partial z} = - \int dk' \mathcal{V}(z, k - k') f(z, k') . \quad (6.23)$$

In terms of the variable z the above equation is a first-order differential equation. In this respect, it is thus similar to the (steady-state) semiclassical Boltzmann equation [25] in the absence of scattering-interactions (see also the three-dimensional Equation in (1.12) with a null r.h.s.)

$$v(k) \frac{\partial f(z, k)}{\partial z} = - \frac{F(z)}{\hbar} \frac{\partial f(z, k)}{\partial k} . \quad (6.24)$$

Based on this analogy, outlined in the pioneering work by Frensley, [33] several quantum-transport problems have been treated by following a semiclassical approach, i.e. by applying to the Wigner transport equation (6.23)

the strategy commonly adopted for the Boltzmann Equation (6.24). Indeed most of these studies [30] are based on a numerical solution of Eq. (6.23), often supplemented by an additional relaxation-time term (see Chap. 8), where one imposes on $f(z, k)$ the U spatial boundary condition scheme described in Chap. 7. The latter, depicted in Fig. 7.1, consists in requiring that the inflowing Wigner function acquires some fixed values at the two contacts $z = \pm l/2$, and that these values are determined by the distribution of carriers incoming from the two reservoirs. Explicitly, the values $f(-l/2, k)$ are specified for carriers incoming from the left reservoir ($k > 0$) and the values $f(+l/2, k)$ are specified for electrons incoming from the right reservoir ($k < 0$). In a compact notation, introducing $z^b(k) = \text{sign}(k)l/2$ (where sign denotes the sign function), the Wigner transport equation (6.23) is thus equipped with the k -dependent spatial boundary condition

$$f^b(k) \equiv f(z^b(k), k). \quad (6.25)$$

Within such boundary-condition paradigm, it is also possible to rewrite the Wigner problem (6.23)-(6.25) in an equivalent integral form [2]

$$v(k) f(z, k) = v(k) f^b(k) - \int_{z^b(k)}^z dz' \int_{-\infty}^{+\infty} dk' \mathcal{V}(z', k - k') f(z, k'). \quad (6.26)$$

This integral equation is the starting point of the Neumann-series solution employed in Ref. [2], i.e., a numerical treatment based on an iterative expansion of the solution $f(z, k)$ in powers of the potential superoperator \mathcal{V} .

We wish to point out that, in spite of the (classical versus quantum) analogies mentioned above, an important difference emerges between the Wigner equation (6.23) and the semiclassical Boltzmann equation (6.24). While the latter is local in k , the former is not. Indeed, because of the non-local character (in k) of the potential superoperator \mathcal{V} appearing in (6.23), the differential equation for one value of k is in fact coupled to the differential equations for all other k values. The non-locality of \mathcal{V} therefore makes the Wigner problem intrinsically different from the Boltzmann one. Indeed, as will be shown in Sec. 7.2 while the solution of the Boltzmann equation (compatible with given boundary values) is always unique, the same does not apply to the Wigner equation (see below).

6.2 The Semiclassical Limit of the Coherent Wigner Equation

The aim of this section is to provide the semiclassical limit of the coherent (e.g., scattering-free) Wigner Equation (6.22). In order to complete this task, we have to introduce the notion of Moyal brackets: given two generic functions $a(z, p)$, $b(z, p)$, the Moyal brackets [64] of the two functions $\{a(z, p), b(z, p)\}_M$ are defined as

$$\{a(z, p), b(z, p)\}_M = \sin \left[i\hbar \left(\frac{\partial}{\partial z} \frac{\partial}{\partial p'} - \frac{\partial}{\partial z'} \frac{\partial}{\partial p} \right) \right] a(z, p) b(z', p') \Big|_{z'=z, p'=p} . \quad (6.27)$$

Exploiting the latter definition, an alternative form for the potential contribution $\frac{\partial f(z, k)}{\partial t} \Big|_V$ in Eq. (6.22) for a parabolic band is

$$\frac{df(z, p)}{dt} \Big|_V = -\frac{1}{i\hbar} \{f(z, p), V(z)\}_M , \quad (6.28)$$

where $V(z)$ is the spatial-representation of the operator $V(\hat{z})$ of Eq. (6.2) and we wrote $f(z, p)$ in terms of $p = \hbar k$ rather than k in order to make easier the comparisons with the Boltzmann Equation (see Eq. (1.12) with null r.h.s.).

Before moving to the semiclassical limit, a few comments on Eq. (6.28) are mandatory. As already stressed by Frenslley [30], although Eq. (6.28) and (6.17) are equivalent, the latter is preferred (especially) in simulative experiments due to the fact that the former would need an infinite expansion in \hbar . The Eq. (6.28) may be obtained exploiting the *Groenewold relation* [65], which relates the phase-space function (see Eq. (5.4)) $F(z, p) = \text{Tr}[\hat{W}(z, p)\hat{F}]$, where \hat{F} is given by the product of two generic operators \hat{A} and \hat{B} , with the functions $A(z, p) = \text{Tr}[\hat{W}(z, p)\hat{A}]$ and $B(z, p) = \text{Tr}[\hat{W}(z, p)\hat{B}]$,

$$\begin{aligned} \hat{F} &= \hat{A}\hat{B} \quad \leftrightarrow \\ F(z, p) &= \sin \left[i\hbar \left(\frac{\partial}{\partial z} \frac{\partial}{\partial p'} - \frac{\partial}{\partial z'} \frac{\partial}{\partial p} \right) \right] A(z, p) B(z', p') \Big|_{z'=z, p'=p} . \end{aligned} \quad (6.29)$$

Applying Eq. (6.29) to the Liouville-von Neumann Equation (6.1) for a parabolic conduction band, the Eq. (6.28) comes trivially after noting that

the functions $K(p) = \text{Tr}[\hat{W}(z, p)K(\hat{p})]$ and $V(z) = \text{Tr}[\hat{W}(z, p)V(\hat{z})]$ coincide with the (respectively) momentum and coordinate representation of the operators in the r.h.s. of Eq. (6.2); the function $H^{\text{sp}}(z, p)$ is given by the sum $H^{\text{sp}}(z, p) = K(p) + V(z)$.

In order to obtain the semiclassical limit of Eq. (6.27), we consider the (formal) limit of $\hbar \rightarrow 0$, which gives

$$\lim_{\hbar \rightarrow 0} \left. \frac{df(z, p)}{dt} \right|_V = - \frac{\partial V}{\partial z} \frac{\partial f(z, p)}{\partial p} \quad , \quad (6.30)$$

hence, recalling the diffusive term in Eq. (6.15), the scattering-free equation of motion of the Wigner function in the Semiclassical limit is given by

$$\begin{aligned} \lim_{\hbar \rightarrow 0} \frac{df(z, p)}{dt} &= \left. \frac{df(z, p)}{dt} \right|_K + \left. \frac{df(z, p)}{dt} \right|_V \\ &= \frac{\partial f(z, p)}{\partial z} \frac{\partial H^{\text{sp}}(z, p)}{\partial p} - \frac{\partial f(z, p)}{\partial p} \frac{\partial H^{\text{sp}}(z, p)}{\partial z} \\ &\equiv \{f(z, p), H^{\text{sp}}(z, p)\}_P \quad , \end{aligned} \quad (6.31)$$

where $\{a(z, p), b(z, p)\}_P$ indicates the Poisson brackets [66] of the functions $a(z, p)$ and $b(z, p)$; as expected, the r.h.s. of Eq. (6.31) coincides with the scattering-free Boltzmann Equation (see also the three-dimensional Eq. (1.12)). Summarizing, the *semiclassical limit* of the coherent Wigner transport equation provides the scattering-free semiclassical equation of motion.

As a final remark, we refer to Chap. (13) for the semiclassical limit of the dissipation/decoherence contribution to the dynamics of the Wigner function: as will be discussed there, for a particular choice of the quantum scattering superoperator, the former reduces to the Boltzmann collision term of Eq. (1.14).

Chapter 7

The Inflow or U-boundary condition

The density-matrix formalism recalled so far as well as its Weyl-Wigner representation apply to “extended systems”, i.e., systems extending over the whole coordinate space. Indeed, given the state of the system at the initial time t_0 , its time evolution is fully dictated by the density-matrix equation (5.8) or, equivalently, via the corresponding Wigner-function equation (5.12) defined over the whole coordinate space \mathbf{r} . However, such approach cannot be straightforwardly applied to a nanostructured device, since the latter is a “localized system”, i.e., a portion of material characterized by a well defined volume and by spatial boundaries acting as electric contacts to external charge reservoirs (see Fig. 4.1). It follows that, in addition to the initial condition previously mentioned, one is forced to impose on the Wigner-function equation (5.12) spatial boundary conditions as well.

The Wigner Transport Equation (6.22) presents a first order derivative in the spatial coordinate; for this reason, starting from the pioneering work by Frensky [33], a number of quantum-transport simulations have been performed imposing the standard inflow boundary condition on the Wigner Equation. When applied to one-dimensional problem, the inflow boundary condition may be schematically pictured as in Fig. 7.1, where the left and right vertical bold lines represent the contacts at $z = \pm l/2$, while the horizontal one figures the starting Wigner function in the whole space: as

a consequence, this prescription is often called U boundary condition. Finally, when combined with finite-difference scheme, the inflowing boundary conditions are also called upwind BC.

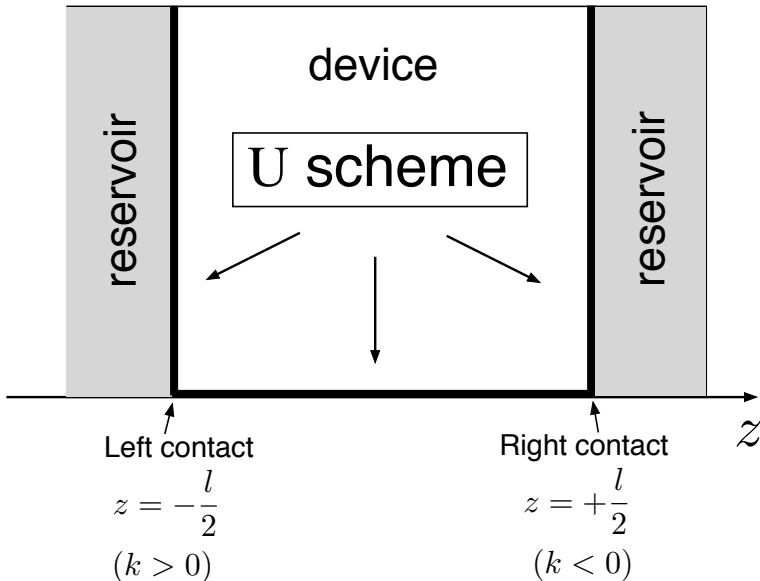


Figure 7.1. The conventional inflow or U boundary condition scheme adopted in semiclassical device modeling, [25] for a one-dimensional problem. The value of the Wigner function $f(z, k)$ is specified at the boundaries $z^b(k)$ of the active region, i.e., $f(-l/2, k > 0)$ and $f(+l/2, k < 0)$ are fixed by the incoming/inflowing carrier distribution function.

7.1 Physical vs. Mathematical solutions

While such boundary-condition scheme is fully compatible with the conventional semiclassical transport theory (mainly due to the local character of the Boltzmann equation), its application to a quantum-mechanical problem is in general not justified. In particular, two crucial issues need to be investigated: i) does such classical-like boundary-condition scheme applied to the Wigner-function equation (5.12) provide a physically acceptable solution, i.e., a Weyl-Wigner transform of a single-particle density matrix ? ii) is the uniqueness of such solution guaranteed?

The aim of this section is to provide a definite answer to the first question, while the second issue will be addressed in Sect. 7.2.

In order to gain more insight about physical versus unphysical solutions, let us focus on the steady-state version of Eq. (5.12), namely

$$\int d\mathbf{r}' d\mathbf{k}' L(\mathbf{r}, \mathbf{k}; \mathbf{r}', \mathbf{k}') f(\mathbf{r}', \mathbf{k}') = 0 \quad (7.1)$$

with

$$L(\mathbf{r}, \mathbf{k}; \mathbf{r}', \mathbf{k}') = \epsilon(\mathbf{r}, \mathbf{k}; \mathbf{r}', \mathbf{k}') + \Gamma(\mathbf{r}, \mathbf{k}; \mathbf{r}', \mathbf{k}') . \quad (7.2)$$

Generally speaking, it is a matter of fact that the set of solutions of a given differential equation is usually larger than the physically acceptable ones. Indeed, in view of the linear character of Eq. (7.1), given two physical solutions $f_a(\mathbf{r}, \mathbf{k})$ and $f_b(\mathbf{r}, \mathbf{k})$, the linear combination

$$f(\mathbf{r}, \mathbf{k}) = c_a f_a(\mathbf{r}, \mathbf{k}) + c_b f_b(\mathbf{r}, \mathbf{k}) \quad (7.3)$$

is also a mathematical solution of the same equation, leading to a spatial carrier density [see Eq. (5.6)] of the form

$$n(\mathbf{r}) = c_a n_a(\mathbf{r}) + c_b n_b(\mathbf{r}) . \quad (7.4)$$

In spite of the positive-definite character of the spatial charge densities n_a and n_b , an inappropriate choice of the coefficients c_a and c_b may give rise to a partially negative charge distribution, which corresponds to an unphysical solution. On the other end, the presence of given spatial boundary conditions is expected to impose additional constraints on the two coefficients c_a and c_b , thus reducing the set of available solutions.

In order to better understand the link among the system density matrix $\hat{\rho}$, the Wigner function $f(\mathbf{r}, \mathbf{k})$, and the corresponding boundary function $f^b(\mathbf{k})$, let us examine in more detail the Weyl-Wigner transform in (5.1). Because the density-matrix operator $\hat{\rho}$ is always Hermitian and positive-definite, its spectral decomposition

$$\hat{\rho} = \sum_{\beta} p_{\beta} |\beta\rangle \langle \beta| \quad (7.5)$$

involves *non-negative* eigenvalues $p_{\beta} \geq 0$. Inserting Eq.(7.5) into (5.1) and employing the pure-state result (5.3), the Wigner function turns out to be

$$f(\mathbf{r}, \mathbf{k}) = \sum_{\beta} p_{\beta} f_{\beta}(\mathbf{r}, \mathbf{k}) , \quad p_{\beta} \geq 0 \quad (7.6)$$

The above linear combination can be regarded as a statistical average (i.e., a mixed state) of the Wigner functions $f_\beta(\mathbf{r}, \mathbf{k})$ corresponding to the pure states $|\beta\rangle$. As a consequence the spatial carrier density corresponding to the Wigner function in (7.6) reads

$$n(\mathbf{r}) = \sum_{\beta} p_{\beta} n_{\beta}(\mathbf{r}) \quad (7.7)$$

and is always positive, being a linear combination of the positive-definite functions $n_{\beta}(\mathbf{r}) \propto \int d\mathbf{k} f(\mathbf{r}, \mathbf{k})$ with positive-definite coefficients p_{β} . Such physical result thus originates from the positive-definite character of the density-matrix operator.

On the other end, in the conventional boundary-condition scheme (see Fig. 7.1) employed for the simulation of quantum devices with open spatial boundaries, one arbitrarily fixes the value of the Wigner function entering the device from the spatial boundary \mathbf{r}^b . The crucial question is whether, for any given (real and positive-definite) boundary function $f^b(\mathbf{k}) \equiv f(\mathbf{r}^b, \mathbf{k})$, any mathematical solution of Eq. (7.1) is also a physically acceptable one. Let us consider a generic solution $f(\mathbf{r}, \mathbf{k})$ of our Wigner equation. Exploiting the completeness relation of the Wigner operators, namely

$$(2\pi)^{-3} \text{tr} \left\{ \hat{W}(\mathbf{r}, \mathbf{k}) \hat{W}^\dagger(\mathbf{r}', \mathbf{k}') \right\} = \delta(\mathbf{r} - \mathbf{r}') \delta(\mathbf{k} - \mathbf{k}') , \quad (7.8)$$

the (real) function $f(\mathbf{r}, \mathbf{k})$ defined on the phase space can always be written as

$$f(\mathbf{r}, \mathbf{k}) = \text{tr} \left\{ \hat{W}(\mathbf{r}, \mathbf{k}) \hat{\Phi} \right\} \quad (7.9)$$

where $\hat{\Phi}$ is an *Hermitian* operator, defined as

$$\hat{\Phi} = (2\pi)^{-3} \iint d\mathbf{r} d\mathbf{k} \hat{W}(\mathbf{r}, \mathbf{k}) f(\mathbf{r}, \mathbf{k}) \quad , \quad (7.10)$$

whose spectral decomposition

$$\hat{\Phi} = \sum_{\tilde{\beta}} e_{\tilde{\beta}} |\tilde{\beta}\rangle \langle \tilde{\beta}| \quad (7.11)$$

involves pure states $|\tilde{\beta}\rangle$ and, due to hermiticity, real eigenvalues $e_{\tilde{\beta}}$. However, in contrast to the case of a density-matrix operator $\hat{\rho}$ [see Eq.(7.5)], the

eigenvalues $e_{\tilde{\beta}}$ of $\hat{\Phi}$ are not necessarily positive. Thus, the solution $f(\mathbf{r}, \mathbf{k})$ in (7.9), which can be written as

$$f(\mathbf{r}, \mathbf{k}) = \sum_{\tilde{\beta}} e_{\tilde{\beta}} f_{\tilde{\beta}}(\mathbf{r}, \mathbf{k}) , \quad (7.12)$$

($f_{\tilde{\beta}}(\mathbf{r}, \mathbf{k})$ denoting the Wigner function of the pure state $|\tilde{\beta}\rangle$) is not necessarily a mixed-state Wigner function of the form in (7.6), and therefore may be unphysical. Indeed the corresponding spatial carrier density

$$n(\mathbf{r}) = \sum_{\tilde{\beta}} e_{\tilde{\beta}} n_{\tilde{\beta}}(\mathbf{r}) \quad (7.13)$$

is not necessarily positive-definite due to the possible presence of negative eigenvalues $e_{\tilde{\beta}}$.

This is the mathematical explanation of the unphysical results reported in Ref. [2] as well as in Fig. 9.6. As we shall discuss in Secs. 7.2 and 9.2, from a physical point of view the presence of such unphysical solutions is a clear indication that the non-local character of the Liouville superoperator in (7.2) does not allow one to arbitrarily choose/fix the boundary values of the unknown Wigner function regardless of the specific device under examination, since the Wigner function in \mathbf{r} depends, in general, on the value of the device potential profile in any other point \mathbf{r}' .

To summarize, in view of the completeness property in (7.8), it is always possible to identify a proper linear combination (7.12) of the pure-state Wigner functions fulfilling the desired boundary values $f^b(\mathbf{k})$. However, such linear combination does not necessarily correspond to a physically acceptable solution (see also Sec. 9.2). Moreover, while the existence of such mathematical solution is guaranteed, its uniqueness strongly depends on the particular properties of the effective Liouville superoperator L in (7.2); in particular, as discussed in the following section, in the coherent limit the solution of Eq. (7.1) (compatible with given spatial boundaries) is not unique.

7.2 Nonuniqueness of the solution

In order to show the non-uniqueness of the solution, we start by investigating the general symmetry properties of the Wigner transport equation

(6.23). A closer inspection of the Wigner potential in (6.18) reveals its antisymmetric nature with respect to the momentum coordinate, i.e.,

$$\mathcal{V}(z, k'') = -\mathcal{V}(z, -k'') . \quad (7.14)$$

As a consequence, both $f(z, k)$ and $f(z, -k)$ are solutions of the Wigner equation (6.23). Such property reflects the time-reversal symmetry, i.e., it corresponds to the fact that for any given solution $\phi(z)$ of the time-dependent Schrödinger equation, its complex conjugate $\phi^*(z)$ is also a solution; this is confirmed by recalling that, for a pure state $|\phi\rangle\langle\phi|$ corresponding to a wavefunction $\phi(z)$, the related Wigner function (5.1) is simply given by

$$f(z, k) = \int dz' \phi\left(z + \frac{z'}{2}\right) e^{-ikz'} \phi^*\left(z - \frac{z'}{2}\right) , \quad (7.15)$$

and noticing that the replacement in (7.15) of the two wavefunctions with their complex conjugates is equivalent to changing k in $-k$.

In addition to the antisymmetry (7.14) w.r.t. k , in the presence of a spatially symmetric potential $V(z) = V(-z)$, the Wigner potential (6.18) turns out to be antisymmetric with respect to the spatial coordinate as well,

$$\mathcal{V}(z, k'') = -\mathcal{V}(-z, k'') , \quad (7.16)$$

implying that, for a given solution $f(z, k)$ of the Wigner equation (6.23), also $f(-z, k)$ is a solution of the same equation. Such property corresponds to the fact that, in the presence of a symmetric potential, for any given solution $\phi(z)$, the wavefunction $\phi^*(-z)$ is a solution as well.

For any finite and piece-wise-constant potential $V(z)$, one can easily define a set of doubly degenerate eigenstates called scattering states. [67] For the sake of simplicity, let us assume that $V(z \rightarrow -\infty) = V(z \rightarrow +\infty) = 0$; in this case, for any positive energy value ϵ it is possible to define two degenerate eigenstates, usually referred to as left and right scattering states, corresponding, respectively, to a plane wave incoming from left (+) and right (-), with unit amplitude and wavevector

$$\bar{k} = \pm \frac{\sqrt{2m^*\epsilon}}{\hbar} \quad (7.17)$$

(a typical example will be discussed in Chap. 9). We shall thus label this specific set of eigenfunctions of the effective Hamiltonian (6.2) via the continuous quantum number \bar{k} as $\bar{\phi}(z, \bar{k})$. Recalling the pure-state prescription

in (7.15), the Wigner function corresponding to the generic scattering state is given by

$$\bar{f}(z, k; \bar{k}) = \int dz' \bar{\phi} \left(z + \frac{z'}{2}, \bar{k} \right) e^{-ikz'} \bar{\phi}^* \left(z - \frac{z'}{2}, \bar{k} \right). \quad (7.18)$$

Taking into account that for any value \bar{k} the function $\bar{f}(z, k; \bar{k})$ is a solution of the Wigner equation (6.23), and that the latter is linear and homogeneous, it follows that any function

$$f(z, k) = \int d\bar{k} a(\bar{k}) \bar{f}(z, k; \bar{k}) \quad (7.19)$$

is itself a solution.

In order to verify if the function in (7.19) is a unique solution of the Wigner equation (6.23) compatible with the given spatial boundary condition in (6.25), we impose that the generic solution (7.19) on the spatial boundary $z = z^b(k)$ assumes the required boundary value $f^b(k)$, i.e.,

$$f \left(z^b(k), k \right) = \int d\bar{k} a(\bar{k}) \bar{f} \left(z^b(k), k; \bar{k} \right) = f^b(k). \quad (7.20)$$

This can be regarded to as an infinite set of linear equations for the infinite set of unknowns $a(\bar{k})$:

$$\int d\bar{k} L^a(k, \bar{k}) a(\bar{k}) = f^b(k) \quad (7.21)$$

with

$$L^a(k, \bar{k}) = \bar{f} \left(z^b(k), k; \bar{k} \right). \quad (7.22)$$

Assuming that the linear operator L^a is non-singular, there is always a unique choice of the coefficients $a(\bar{k})$ compatible with the desired boundary conditions (6.25), and therefore a unique solution $f(z, k)$ of the Wigner equation (6.23).

Importantly, the above conclusion is based on the assumption that the function $f(z, k)$ in (7.19) is the most general solution of the Wigner equation; in what follows we shall show that this assumption is wrong. Indeed in view of the time-reversal symmetry $z, k \rightarrow z, -k$ mentioned above, in addition to the set of eigenvalue Wigner functions $\bar{f}(z, k; \bar{k})$ in (7.19), one may consider a second (and linearly independent) set of solutions given by

$\bar{f}(z, -k; \bar{k})$. This allows one to extend the set of possible solutions in (7.19) as

$$f(z, k) = \int d\bar{k} \left(a(\bar{k}) \bar{f}(z, k; \bar{k}) + b(\bar{k}) \bar{f}(z, -k; -\bar{k}) \right) , \quad (7.23)$$

whose spatial charge density is given by

$$n(z) = \int d\bar{k} \left(a(\bar{k}) \bar{n}(z, \bar{k}) + b(\bar{k}) \bar{n}(z, -\bar{k}) \right) \quad (7.24)$$

with $\bar{n}(z, \bar{k}) = |\bar{\phi}(z, \bar{k})|^2$.

By imposing once again the boundary-value prescription (6.25) on the new generic solution in (7.23) one gets

$$\int d\bar{k} \left(L^a(k, \bar{k}) a(\bar{k}) + L^b(k, \bar{k}) b(\bar{k}) \right) = f^b(k) \quad (7.25)$$

with

$$L^b(k, \bar{k}) = \bar{f} \left(z^b(k), -k; -\bar{k} \right) . \quad (7.26)$$

In Eq.(7.25) a second (infinite) set of unknown quantities $b(\bar{k})$ appears, in addition to the (infinite) set of unknown quantities $a(\bar{k})$. It follows that, differently from the linear problem in (7.21), the new global set of coefficients $\{a(\bar{k}), b(\bar{k})\}$ is not uniquely determined by the corresponding linear set of equations in (7.25)¹.

Among all possible choices of the coefficients, it is useful to consider the particular class of solutions

$$b(\bar{k}) = c a(\bar{k}) \quad (7.27)$$

parameterized by the real number c . In this case, the generic solution in (7.23) reduces to

$$f(z, k) = \int d\bar{k} a(\bar{k}) \bar{g}(z, k; \bar{k}) \quad (7.28)$$

¹This is due to the time-reversal symmetry, which, in turn, is intimately related to the energetic double degeneracy of the scattering states. Indeed, the wave function of any quantummechanical state with negative energy ($\epsilon < 0$) is always real, and the time-reversal symmetry just mentioned plays no role; it follows that in the presence of localized states only, e.g., parabolic potentials or quantum wells with infinite-height barriers, the solution of the Wigner transport equation (6.23) is expected to be unique, in agreement with the conclusions of the analysis presented in Ref. [68]

with

$$g(z, k; \bar{k}) = \bar{f}(z, k; \bar{k}) + c\bar{f}(z, -k; -\bar{k}) , \quad (7.29)$$

and the corresponding linear problem in (7.25) reduces to

$$\int d\bar{k} L^c(k, \bar{k}) a(\bar{k}) = f^b(k) \quad (7.30)$$

with

$$L^c(k, \bar{k}) = L^a(k, \bar{k}) + cL^b(k, \bar{k}) , \quad (7.31)$$

thus providing –for any given value of the parameter c – a unique value of the coefficients $a(\bar{k})$ compatible with the desired boundary conditions.

Let us finally discuss the non-uniqueness of the solution in the presence of a spatially symmetric potential: $V(z) = V(-z)$. Indeed, in this case it is possible to show that changing z in $-z$ left-scattering states map into right-scattering ones, and vice versa, i.e., $\bar{\phi}(z, \bar{k}) = \bar{\phi}(-z, -\bar{k})$. In terms of the Wigner-function picture z, k , this symmetry property reduces to

$$\bar{f}(z, -k; -\bar{k}) = \bar{f}(-z, k; \bar{k}) . \quad (7.32)$$

Employing this symmetry property, the generic solution (7.23) comes out to be

$$f(z, k) = \int d\bar{k} \left(a(\bar{k})\bar{f}(z, k; \bar{k}) + b(\bar{k})\bar{f}(-z, k; \bar{k}) \right) , \quad (7.33)$$

and the spatial charge distribution in (7.24) reduces to

$$n(z) = \int d\bar{k} \left(a(\bar{k})\bar{n}(z, \bar{k}) + b(\bar{k})\bar{n}(-z, \bar{k}) \right) . \quad (7.34)$$

Also in the presence of a spatially symmetric potential, the above generic solution compatible with given boundary conditions is definitely not unique; it is then useful to consider the solution set in (7.27) for $c = 1$, i.e., $b(\bar{k}) = a(\bar{k})$; in this particular case, combining the definition in (7.29) with the symmetry property in (7.32), one gets

$$\bar{g}(z, k; \bar{k}) = \bar{f}(z, k; \bar{k}) + \bar{f}(-z, k; \bar{k}) , \quad (7.35)$$

i.e., the functions \bar{g} entering the linear combination (7.28) in this case are always spatially symmetric, and are simply given by twice the symmetric part of the scattering states \bar{f} ; it follows that for the particular case/choice

$c = 1$ the generic solution in (7.28) is always spatially symmetric, and the same applies to the corresponding charge density in (7.34).

Recalling that in the presence of a spatially symmetric potential the analytical and numerical results reported in Ref. [2] (based both on a symmetric finite-difference solution of Eq. (6.23) and on a Neumann-series expansion of Eq. (6.26) (see below)) correspond to spatially symmetric Wigner functions only ($f(z, k) = f(-z, k)$), the natural conclusion is that, among the infinite set of coefficients compatible with the given boundary conditions, such treatments automatically provide/select the symmetric choice $c = 1 \rightarrow b(\bar{k}) = a(\bar{k})$. Moreover, since these treatments show a continuous transition of the solution moving from a symmetric to a non-symmetric potential, one is forced to conclude that also in the presence of non-symmetric potentials the numerical approaches just mentioned are expected to provide/select again the particular solution $b(\bar{k}) = a(\bar{k})$ in (7.23), which in general is spatially non-symmetric. The existence of an infinite set of degenerate solutions, i.e., solutions compatible with the same boundary values, allows also to explain the significant discrepancies between finite-difference treatments based on different (spatially symmetric versus non-symmetric) discretization schemes, already pointed out in Ref. [2]: a change in the spatial discretization scheme may induce significant changes in the numerical results, since, regardless of the actual grid size, it may select a new solution (i.e., a different value of the parameter c in Eq. (7.27)) within the degenerate subspace.

Let us finally discuss the non-uniqueness of the solution in terms of the integral version of the Wigner equation (6.26). To this end, by adopting a compact notation, the latter can be written as

$$\mathcal{A}f = f^b \tag{7.36}$$

with

$$\begin{aligned} \mathcal{A}f(z, k) \doteq & f(z, k) + \\ & + \int_{z^b(k)}^z dz' \int_{-\infty}^{+\infty} dk' \frac{\mathcal{V}(z', k - k')}{v(k)} f(z', k') \end{aligned} \tag{7.37}$$

The non-uniqueness of the solution previously shown tells us that the Wigner

superoperator \mathcal{A} is necessarily not invertible, which implies that the well-known Neumann series/expansion

$$f = \mathcal{A}^{-1} f^b = \sum_{n=0}^{\infty} (1 - \mathcal{A})^n f^b \quad (7.38)$$

in this case provides/selects just one of the infinite solutions; in particular, as shown in Ref. [2], for a symmetric potential the result of the above Neumann expansion is always symmetric, which corresponds to the particular choice $b(\bar{k}) = a(\bar{k})$ previously discussed.

Chapter 8

Dissipation and decoherence

In this section we shall discuss how to extend the coherent-limit treatment considered so far in order to account for energy-dissipation as well as decoherence phenomena induced by non-elastic scattering processes. To this purpose, the simplest model is the well-known relaxation-time approximation; [25] within the single-particle density-matrix formalism of Eq. (5.8), the latter amounts to adopting a scattering superoperator

$$\Gamma(\hat{\rho}) = -\frac{\hat{\rho} - \hat{\rho}^\circ}{\tau}, \quad (8.1)$$

where

$$\hat{\rho}^\circ = \left(\frac{\Omega}{2\pi}\right)^3 \int d\mathbf{k} |\mathbf{k}\rangle f^\circ(\epsilon(\mathbf{k}) - \mu^\circ) \langle \mathbf{k}| \quad (8.2)$$

is the equilibrium density-matrix operator (expressed via the corresponding Fermi-Dirac distribution f°) and τ denotes a phenomenological (or macroscopic) relaxation time, which can be regarded as a sort of effective or average coherence time, and is mainly determined by carrier-phonon as well as carrier-carrier scattering. By applying to the scattering superoperator (8.1) the Weyl-Wigner transform in (5.1), it is easy to obtain the relaxation-time term

$$\left. \frac{\partial f(\mathbf{r}, \mathbf{k})}{\partial t} \right|_{\text{scat}} = \frac{f(\mathbf{r}, \mathbf{k}) - f^\circ(\mathbf{r}, \mathbf{k})}{\tau}, \quad (8.3)$$

where the equilibrium Wigner function coincides with the Fermi-Dirac distribution f° , i.e., $f^\circ(\mathbf{r}, \mathbf{k}) = f^\circ(\epsilon(\mathbf{k}) - \mu^\circ)$. The Eq. (8.1) is sometimes

generalized replacing the parameter τ by a suitable operator $\hat{\tau}$ in order to account for possible space and/or momentum dependence of the relaxation time. However, such a seemingly straightforward generalization may have nontrivial implications. Indeed, due to the nonlocal character of the Weyl-Wigner transform, such a replacement in (8.1) gives rise to a nonlocal contribution in (5.14), which is not simply given by the local term (5.20), where the parameter τ is replaced by a space- and momentum-dependent relaxation time $\tau(\mathbf{r}, \mathbf{k})$. Furthermore, while a constant relaxation time ensures the positive-definite character of the single-particle density matrix, and therefore of the corresponding Wigner function, such positive character does not hold for an arbitrary $\tau(\mathbf{r}, \mathbf{k})$. For these reasons, we shall consider τ as space- and momentum-independent.

For the one-dimensional case considered above, the relaxation-time approximation implies the appearance of an additional contribution to the steady-state Wigner equation (6.23), leading to the generalized Wigner transport equation

$$v(k) \frac{\partial f(z, k)}{\partial z} = - \int dk' \mathcal{V}(z, k - k') f(z, k') - \frac{f(z, k) - f^\circ(z, k)}{\tau}, \quad (8.4)$$

with $f^\circ(z, k) \equiv f^\circ(\epsilon(k) - \mu^\circ)$ denoting the equilibrium Fermi-Dirac distribution induced by the host one-dimensional material.

Opposite to its coherent version in (6.23), the above transport equation does not exhibit the $k \rightarrow -k$ symmetry discussed in Sec. 7.2. From a physical point of view, the inclusion of this relaxation term destroys the time-reversal symmetry ($k \rightarrow -k$) responsible for the non-uniqueness previously discussed; it follows that, regardless of the value of the relaxation time τ , the solution of the generalized Wigner transport equation (8.4) (compatible with given spatial boundary conditions) is always unique.

8.1 Scattering-induced current

In Sec. 1.3 and Eq. (1.17) we showed the local character of the scattering-induced contribution of the Boltzmann semiclassical equation (1.14); contrary, in part III we will show that genuine quantum approaches based on

the single-particle density matrix $\hat{\rho}$ show a scattering-induced nonlocality. Since the Wigner Equation may be seen as a bridge between classical and quantum world, we are here interested to show how nonlocality could raise it up from the generic scattering contribution $\left. \frac{\partial f}{\partial t} \right|_{\text{scat}}$ in Eq. (5.14). In this section, we keep the discussion at a generic level, pointing out how it is the non-local character in both \mathbf{r} and \mathbf{k} (independently of the shape of the $\Gamma(\mathbf{r}, \mathbf{k}; \mathbf{r}', \mathbf{k}')$) of $\left. \frac{\partial f(\mathbf{r}, \mathbf{k})}{\partial t} \right|_{\text{scat}}$ defined in Eq. (5.14), which provides a scattering-induced spatial charge density variation, contrary to the semiclassical scenario of Eq. (1.14). More detailed analysis of specific superoperators Γ will be presented later; in particular, in Chap. 13 we show that the low-density linear superoperator $\Gamma(\hat{\rho})$ of Eq. (11.43) (descending from the global density matrix scattering-induced dynamics of Eq. (3.20)) provides a scattering-induced charge-density variation which becomes local (only) in the semiclassical limit $\hbar \rightarrow 0$. In order to make easier the comparisons with the semiclassical Boltzmann Equation, throughout this whole Section we rewrite the Wigner function as $f^{\text{W}}(\mathbf{r}, \mathbf{p})$, e.g. in terms of $\mathbf{p} = \hbar \mathbf{k}$ rather than \mathbf{k} .

In order to better elucidate the spatial nonlocality of the Wigner-transport theory, it is useful to recall the link between our Wigner function $f^{\text{W}}(\mathbf{r}, \mathbf{p})$ and the corresponding spatial carrier density $n(\mathbf{r})$ (see Eq. (5.6))

$$n(\mathbf{r}) = (2\pi\hbar)^{-3} \int d^3p f^{\text{W}}(\mathbf{r}, \mathbf{p}); \quad (8.5)$$

Combining the above result with the Wigner transport equation (5.12) and employing the single-particle results in (5.13) and (5.14), the time evolution of the spatial carrier density is again given by

$$\frac{\partial n(\mathbf{r})}{\partial t} = \left. \frac{\partial n(\mathbf{r})}{\partial t} \right|_{\text{sp}} + \left. \frac{\partial n(\mathbf{r})}{\partial t} \right|_{\text{scat}} \quad (8.6)$$

with

$$\left. \frac{\partial n(\mathbf{r})}{\partial t} \right|_{\text{sp}} = -(2\pi\hbar)^{-3} \int d\mathbf{r}' d\mathbf{p}' \mathcal{K}(\mathbf{r} - \mathbf{r}', \mathbf{p}') f^{\text{W}}(\mathbf{r}', \mathbf{p}') \quad (8.7)$$

and

$$\left. \frac{\partial n(\mathbf{r})}{\partial t} \right|_{\text{scat}} = (2\pi\hbar)^{-3} \int d\mathbf{r}' d\mathbf{p} d\mathbf{p}' \Gamma(\mathbf{r}, \mathbf{p}; \mathbf{r}', \mathbf{p}') f^{\text{W}}(\mathbf{r}', \mathbf{p}'). \quad (8.8)$$

It is important to stress that, also within the present quantum-mechanical treatment, the time evolution of the spatial carrier density in Eq. (14.2) can be expressed via the usual charge continuity equation, i.e.,

$$\frac{\partial n(\mathbf{r})}{\partial t} + \nabla \cdot \mathbf{J}(\mathbf{r}) = 0 . \quad (8.9)$$

To this end, the carrier current density $\mathbf{J}(\mathbf{r})$ is defined as the average value (see Eqs. (5.5) and (5.4)) of a corresponding quantum-mechanical operator $\hat{\mathbf{J}}(\mathbf{r})$ as

$$\mathbf{J}(\mathbf{r}) = (2\pi\hbar)^{-3} \int d\mathbf{r}' d\mathbf{p}' \mathbf{J}^{\text{W}}(\mathbf{r}; \mathbf{r}', \mathbf{p}') f^{\text{W}}(\mathbf{r}', \mathbf{p}') , \quad (8.10)$$

where

$$\mathbf{J}^{\text{W}}(\mathbf{r}; \mathbf{r}', \mathbf{p}') = \text{tr}\{\hat{W}(\mathbf{r}', \mathbf{p}') \hat{\mathbf{J}}(\mathbf{r})\} \quad (8.11)$$

is the Weyl-Wigner transform of the current-density operator. Combining Eqs. (14.2), (8.9), (8.7), and (8.8), after a straightforward calculation (not reported here) one gets

$$\mathbf{J}^{\text{W}}(\mathbf{r}; \mathbf{r}', \mathbf{p}') = \mathbf{J}_{\text{sp}}^{\text{W}}(\mathbf{r}; \mathbf{r}', \mathbf{p}') + \mathbf{J}_{\text{scat}}^{\text{W}}(\mathbf{r}; \mathbf{r}', \mathbf{p}') \quad (8.12)$$

with

$$\mathbf{J}_{\text{sp}}^{\text{W}}(\mathbf{r}; \mathbf{r}', \mathbf{p}') = (2\pi\hbar)^{-3} \int d\mathbf{r}'' d\mathbf{p}'' \frac{e^{\frac{\mathbf{p}'' \cdot (\mathbf{r}'' - \mathbf{r})}{i\hbar}}}{i\mathbf{p}''} \mathcal{K}(\mathbf{r}'' - \mathbf{r}', \mathbf{p}') \quad (8.13)$$

and

$$\mathbf{J}_{\text{scat}}^{\text{W}}(\mathbf{r}; \mathbf{r}', \mathbf{p}') = -(2\pi\hbar)^{-3} \int d\mathbf{r}'' d\mathbf{p} d\mathbf{p}'' \frac{e^{\frac{\mathbf{p}'' \cdot (\mathbf{r}'' - \mathbf{r})}{i\hbar}}}{i\mathbf{p}''} \Gamma(\mathbf{r}'', \mathbf{p}; \mathbf{r}', \mathbf{p}') . \quad (8.14)$$

It follows that the quantum-mechanical current density in (8.10) is the sum of a single-particle and of a scattering contribution; it is worth stressing that the presence of a scattering-induced current has been clearly pointed out by Gebauer and Car in Ref. [69].

While for the particular case of a parabolic band the kinetic term of the Wigner equation reduces to the diffusion term of the Boltzmann theory (see below) and the single-particle current is simply given by

$$\mathbf{J}_{\text{sp}}(\mathbf{r}) = (2\pi\hbar)^{-3} \int d^3p \mathbf{v}(\mathbf{p}) f^{\text{W}}(\mathbf{r}, \mathbf{p}) , \quad (8.15)$$

for non-parabolic bands the single-particle current density is always described in terms of the spatially non-local superoperator in (8.13). [57,70,71]

As already stressed, the explicit form of the scattering-induced current-density operator in (8.14) will depend strongly on the specific form of the scattering superoperator Γ . In any case, we stress once again that, opposite to the semiclassical scenario, within a fully quantum-mechanical description such scattering-induced current is in general different from zero, which is again a clear fingerprint of the non-local character of our scattering superoperator.

Chapter 9

The delta-like potential as a toy model

As an analytically solvable model, let us consider the case of the delta-like potential barrier

$$V(z) = \Lambda \delta(z) \quad , \quad (9.1)$$

where Λ denotes the barrier-strength parameter. Within the effective-mass approximation (see Eq. (6.14)) the delta-barrier Schrödinger equation (corresponding to the envelope-function Hamiltonian (6.2)) reads

$$\left[-\frac{\hbar^2}{2m^*} \frac{\partial^2}{\partial z^2} + \Lambda \delta(z) \right] \phi(z) = \epsilon \phi(z) . \quad (9.2)$$

As discussed above, the latter exhibits a continuous set of doubly-degenerate scattering eigenstates $\bar{\phi}(z, \bar{k})$ parameterized by the continuous quantum number \bar{k} in (7.17) and describing (for any given energy $\epsilon = \hbar^2 \bar{k}^2 / 2m^*$) injection from the left side (+) onto the barrier (left-scattering state) and injection from the right side (-) onto the barrier (right-scattering state). The explicit form of these scattering states corresponding to the delta-like potential (9.1) can be written in a compact way as

$$\bar{\phi}(z, \bar{k}) = \frac{1}{\sqrt{\Omega}} \begin{cases} e^{i\bar{k}z} + r(\bar{k}) e^{-i\bar{k}z} & \text{for } \bar{k}z < 0 \\ t(\bar{k}) e^{i\bar{k}z} & \text{for } \bar{k}z > 0 \end{cases} , \quad (9.3)$$

Here

$$r(\bar{k}) = -\frac{i\lambda(\bar{k})}{1 + i\lambda(\bar{k})}, \quad t(\bar{k}) = \frac{1}{1 + i\lambda(\bar{k})} \quad (9.4)$$

denote the reflection and transmission amplitudes, respectively,

$$\lambda(\bar{k}) = \frac{m^* \Lambda}{\hbar^2 |\bar{k}|} \quad (9.5)$$

is a dimensionless barrier-strength parameter, and the prefactor $1/\sqrt{\Omega}$ ensures the normalization of the above scattering states over the whole system (device+reservoirs) length Ω ¹.

9.1 Analytical Evaluation of the Wigner function

The goal of this Appendix is twofold: on the one end, we shall discuss the analytical derivation of the Wigner function corresponding to the delta-like potential in (9.1); on the other end, we shall verify that such Wigner function fulfills the corresponding Wigner equation.

We start by introducing the general prescription for the analytical evaluation of the one-dimensional pure-state Wigner function in (7.15). To this end, we shall limit ourselves to quantum-mechanical states whose wavefunctions have different analytical expressions on the left (L) and on the right (R) of the space-coordinate origin ($z = 0$), i.e.,

$$\phi(z) = \begin{cases} \phi_L(z) & \text{for } z < 0 \\ \phi_R(z) & \text{for } z > 0 \end{cases} . \quad (9.6)$$

This applies to any potential profile of the form

$$V(z) = \Lambda\delta(z) + V_o\theta(z) , \quad (9.7)$$

which includes, as particular cases, the delta-like potential in (9.1) as well as the standard step-potential (not considered in this work).

In order to evaluate the explicit form of the Wigner function in (7.15), the key step is to perform the integration over z' ; to this end, for any given

¹Just like for plane waves, one requires that $\int_{-\infty}^{\infty} |\phi^{\pm}(z)|^2 dz = 1$ for $\Omega \rightarrow \infty$.

value z the arguments of the two wavefunctions may assume negative (left) as well as positive (right) values according to the value of z' . In particular one obtains

$$\begin{aligned}
 z' < -2z &\quad \rightarrow \quad z + \frac{z'}{2} < 0 \\
 z' > -2z &\quad \rightarrow \quad z + \frac{z'}{2} > 0 \\
 z' > 2z &\quad \rightarrow \quad z - \frac{z'}{2} < 0 \\
 z' < 2z &\quad \rightarrow \quad z - \frac{z'}{2} > 0 .
 \end{aligned} \tag{9.8}$$

According to the above set of inequalities, the integration domain in (7.15) ($-\infty < z' < +\infty$) needs to be split into three different subdomains. More specifically, for $z > 0$ we have

$$\begin{aligned}
 f(z, k) &= \int_{-\infty}^{+\infty} dz' e^{-ikz'} \phi \left(z + \frac{z'}{2} \right) \phi^* \left(z - \frac{z'}{2} \right) \\
 &= \int_{-\infty}^{-2z} dz' e^{-ikz'} \phi_L \left(z + \frac{z'}{2} \right) \phi_R^* \left(z - \frac{z'}{2} \right) \\
 &+ \int_{-2z}^{+2z} dz' e^{-ikz'} \phi_R \left(z + \frac{z'}{2} \right) \phi_R^* \left(z - \frac{z'}{2} \right) \\
 &+ \int_{+2z}^{+\infty} dz' e^{-ikz'} \phi_R \left(z + \frac{z'}{2} \right) \phi_L^* \left(z - \frac{z'}{2} \right) ,
 \end{aligned} \tag{9.9}$$

while for $z < 0$ we have

$$\begin{aligned}
 f(z, k) &= \int_{-\infty}^{+\infty} dz' e^{-ikz'} \phi \left(z + \frac{z'}{2} \right) \phi^* \left(z - \frac{z'}{2} \right) \\
 &= \int_{-\infty}^{+2z} dz' e^{-ikz'} \phi_L \left(z + \frac{z'}{2} \right) \phi_R^* \left(z - \frac{z'}{2} \right) \\
 &+ \int_{+2z}^{-2z} dz' e^{-ikz'} \phi_L \left(z + \frac{z'}{2} \right) \phi_L^* \left(z - \frac{z'}{2} \right) \\
 &+ \int_{-2z}^{+\infty} dz' e^{-ikz'} \phi_R \left(z + \frac{z'}{2} \right) \phi_L^* \left(z - \frac{z'}{2} \right) .
 \end{aligned} \tag{9.10}$$

Taking into account that for both cases ($z > 0$ and $z < 0$) the last integral is exactly the complex conjugate of the first one, i.e.,

$$\begin{aligned} & \int_{-\infty}^{-2|z|} dz' e^{-ikz'} \phi_L \left(z + \frac{z'}{2} \right) \phi_R^* \left(z - \frac{z'}{2} \right) \\ &= \left(\int_{+2|z|}^{+\infty} dz' e^{-ikz'} \phi_R \left(z + \frac{z'}{2} \right) \phi_L^* \left(z - \frac{z'}{2} \right) \right)^* , \end{aligned} \quad (9.11)$$

and that

$$\int_{2|z|}^{\infty} f(z') dz' = \int_0^{\infty} f(z') dz' - \int_0^{2|z|} f(z') dz' , \quad (9.12)$$

the two results in (9.9) and (9.10) can be combined as:

$$\begin{aligned} f(z, k) &= 2\Re \left(\int_0^{\infty} dz' e^{-ikz'} \phi_R \left(z + \frac{z'}{2} \right) \phi_L^* \left(z - \frac{z'}{2} \right) \right) \\ &\quad - 2\Re \left(\int_0^{2|z|} dz' e^{-ikz'} \phi_R \left(z + \frac{z'}{2} \right) \phi_L^* \left(z - \frac{z'}{2} \right) \right) \\ &\quad + \theta(z) \int_{-2|z|}^{2|z|} dz' e^{-ikz'} \phi_R \left(z + \frac{z'}{2} \right) \phi_R^* \left(z - \frac{z'}{2} \right) \\ &\quad + \theta(-z) \int_{-2|z|}^{2|z|} dz' e^{-ikz'} \phi_L \left(z + \frac{z'}{2} \right) \phi_L^* \left(z - \frac{z'}{2} \right) . \end{aligned} \quad (9.13)$$

We stress that the above prescription can be easily extended to any piecewise-constant potential, like, e.g., multi-step as well as multi-barrier profiles.

For the particular case of the delta-like potential profile (9.1), the explicit form of the left ($z < 0$) and right ($z > 0$) part (ϕ_L and ϕ_R) of the electron wavefunction is provided by the scattering states in (9.3). In particular, by inserting into Eq. (9.13) the explicit form of the left scattering state (i.e., $\bar{k} > 0$), after a lengthy but straightforward calculation one obtains the Wigner function

$$\begin{aligned} \bar{f}(z, k; \bar{k} > 0) &= \frac{2\pi}{\Omega} \left[T(\bar{k}) \delta(k - \bar{k}) + it(\bar{k}) r^*(\bar{k}) \left(\sin(2\bar{k}z) \delta(k) - \frac{2\bar{k} \cos(2(\bar{k} - k)z)}{2\pi k(\bar{k} - k)} \right) \right. \\ &\quad \left. - \frac{\theta(-z) R(\bar{k})}{\pi} \left(\frac{\sin(2(\bar{k} - k)z)}{\bar{k} - k} + \frac{\sin(2(\bar{k} + k)z)}{\bar{k} + k} - \frac{2 \cos(2\bar{k}z) \sin(2kz)}{k} \right) \right] , \end{aligned} \quad (9.14)$$

where $R(\bar{k}) = |r(\bar{k})|^2$ and $T(\bar{k}) = |t(\bar{k})|^2$ are the usual reflection and transmission coefficients. It is possible to show that the Wigner function corresponding to the right scattering state ($\bar{k} < 0$) can simply be obtained from the left-scattering one in (9.14) by replacing z with $-z$ as well as k with $-k$: $\bar{f}(z, k; -\bar{k}) = \bar{f}(-z, -k; \bar{k})$. To this aim, we observe that the application to Eq. (7.15) of the Wigner-space transformation $z, k \rightarrow -z, -k$ is equivalent to replacing $\phi(z)$ with $\phi^*(-z)$, the very same wavefunction transformation linking left and right scattering states.

It is worth noticing that the scattering-state Wigner function (9.14) is spatially non-symmetric, similarly to the charge density ($\bar{n}(z, \bar{k}) = |\bar{\phi}(z, \bar{k})|^2$) corresponding to the generic scattering-state wavefunction in (9.3):

$$\bar{n}(z, \bar{k}) = n_0 \begin{cases} 1 + R(\bar{k}) + 2\Re[r(\bar{k})e^{-2i\bar{k}z}] & \text{for } \bar{k}z < 0 \\ T(\bar{k}) & \text{for } \bar{k}z > 0 \end{cases}. \quad (9.15)$$

This asymmetry has a physically intuitive explanation: since a left/right scattering state describes carrier injection from left/right, the presence of the barrier causes a charge accumulation on the left/right of the barrier with respect to the density of the carriers transmitted on the right/left. Here, as well as throughout the whole part II, n_0 denotes the (space-independent) charge density corresponding to the barrier-free case. For the case we are presently considering –that is, one single scattering state as in Eq. (9.3)– n_0 is simply given by $1/\Omega$.

A lengthy but straightforward calculation, summarized in the Appendix, allows one to verify that the Wigner function (9.14) is a solution of the Wigner transport equation (6.23), where the Wigner potential $\mathcal{V}(z, k)$ induced by the delta-like barrier (9.1) is now given by

$$\mathcal{V}(z, k) = -\frac{4\Lambda}{2\pi\hbar} \sin(2kz) , \quad (9.16)$$

as can be easily verified via its definition in Eq. (6.18).

As a final step, let us verify that the Wigner function (9.14) is a solution of the corresponding Wigner equation. By inserting the potential superoperator (9.16) corresponding to the delta-like barrier profile (9.1)

into Eq.(6.23), the explicit form of the Wigner equation comes out to be

$$v(k) \frac{\partial f(z, k)}{\partial z} = \frac{4\Lambda}{2\pi\hbar} \int dk' \sin(2(k - k')z) f(z, k') . \quad (9.17)$$

In order to verify that the Wigner function (9.14) is indeed a solution of the above Wigner transport equation, let us now evaluate separately its kinetic and potential terms. As far as the kinetic contribution is concerned, after a tedious but straightforward calculation one gets

$$v(k) \frac{\partial f(z, k)}{\partial z} = - \frac{4\lambda\hbar\kappa}{\Omega m^* (1 + \lambda^2)} (\sin(2(\kappa - k)z) - \theta(-z)\lambda (\cos(2(\kappa + k)z) - \cos(2(\kappa - k)z))) . \quad (9.18)$$

Let us now come to the potential contribution in (9.17). By inserting the explicit form of the scattering state Wigner function (9.14), again after a tedious but straightforward calculation one gets

$$\begin{aligned} \frac{4\Lambda}{2\pi\hbar} \int dk' \sin(2(k - k')z) f(z, k') \\ = - \frac{4\Lambda}{\Omega\hbar(1 + \lambda^2)} (\sin(2(\kappa - k)z) - \theta(-z)\lambda (\cos(2(\kappa + k)z) - \cos(2(\kappa - k)z))) . \end{aligned} \quad (9.19)$$

By inserting the explicit forms of the kinetic and potential terms in (9.18) and (9.19) into the Wigner transport equation (9.17), we clearly see that the left-state Wigner function (9.14) is indeed a solution of the Wigner transport equation for $\lambda = m^*\Lambda/\hbar^2\bar{k}$, the very same prescription in (9.5) obtained via a direct solution of the Schrödinger equation.

9.2 Unphysical and non-unique solutions

As shown in Sec. 7.2, the analytical solution in (9.14) –compatible with its boundary values $f^b(k) = \bar{f}(z^b(k), k; \bar{k} > 0)$ – is definitely not unique. Indeed, adopting once again the compact notation introduced in Eqs. (7.17)-(7.18), the generic solution is given by the set in (7.33), where in this case the

coefficients $a(\bar{k})$ and $b(\bar{k})$ should fulfill the following set of linear equations:

$$\begin{aligned} \bar{f}(z^b(k), k; \bar{k}_o) &= \int d\bar{k} a(\bar{k}) \bar{f}(z^b(k), k; \bar{k}) \\ &+ \int d\bar{k} b(\bar{k}) \bar{f}(-z^b(k), k; \bar{k}) . \end{aligned} \quad (9.20)$$

As previously stressed, the choice of the coefficients –and thus of the solution in (7.33)– is not unique, and can be parameterized according to Eq. (7.27). The simplest choice, corresponding to $c = 0$, is

$$a(\bar{k}) = \delta(\bar{k} - \bar{k}_o) , \quad b(\bar{k}) = 0 . \quad (9.21)$$

By inserting such coefficient set into Eq. (7.33) one obtains $f(z, k) = \bar{f}(z, k; \bar{k}_o)$, i.e., the choice $c = 0$ corresponds to the scattering-state solution previously discussed. A second relevant choice, already discussed in Sec. 7.2, is $a(\bar{k}) = b(\bar{k})$, corresponding to $c = 1$. In the presence of a symmetric potential ($V(z) = V(-z)$), this choice always provides a spatially symmetric solution, regardless of the profile of the boundary values.

The non-uniqueness of the solution is illustrated in Fig. 9.1, which shows three carrier-density profiles corresponding to three different solutions of the same Wigner problem, namely of the Wigner transport equation (6.23) applied to the delta-barrier potential (9.1) in the presence of the spatial boundary conditions corresponding to the left-state Wigner function in (9.14). As expected, for $c = 0$ (black solid curve) one obtains the left-state density in (9.15), while for $c = 1$ (red dashed curve) one deals with a spatially symmetric density. Moreover, for the intermediate value $c = 0.05$ (blue dash-dotted curve) we deal with an unphysical solution characterized by negative carrier-density values. As already discussed in Sec. 7.1, the presence of such unphysical solutions is not necessarily ascribed to the non-uniqueness discussed so far; indeed, also in the presence of energy dissipation –for which the solution is always unique (see below)– one may easily obtain unphysical solutions by imposing arbitrary boundary conditions according to the conventional scheme of the semiclassical theory (see Fig. 9.6); this feature, already pointed out in Ref. [2], appears to be the most severe limitation of conventional Wigner-function treatments.

Since in the presence of symmetric potentials any spatially symmetric discretization scheme (applied to the differential equation (6.23) as well as

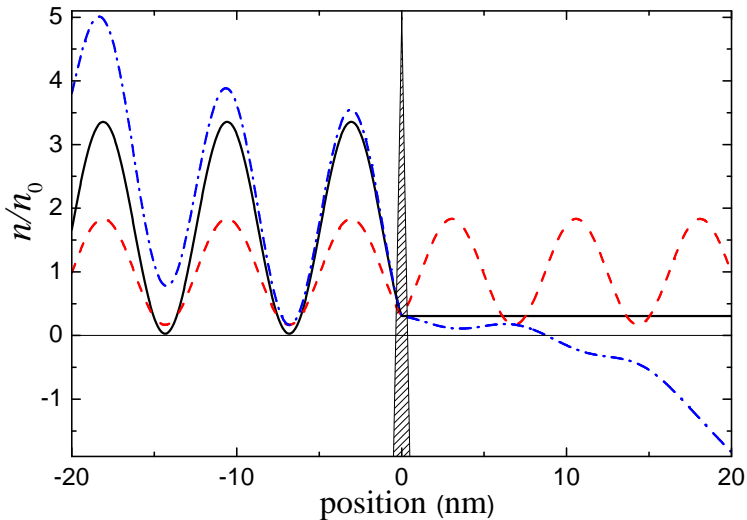


Figure 9.1. Non-uniqueness of the solution of the Wigner problem for the case of the delta-like potential barrier in (9.1). Three different spatial carrier-density profiles (see Eq. (7.34)) corresponding to the solution set in (7.33): the left scattering-state solution in (9.15) corresponding to $c = 0$ (black solid curve), the spatially symmetric solution corresponding to $c = 1$ (red dashed curve), and an unphysical solution (i.e., non-positive-definite) corresponding to $c = 0.05$ (blue dash-dotted curve) (see text). The device parameters are $l = 40$ nm, $\epsilon = 100$ meV, and $\lambda = 1.5$, corresponding to a transmission coefficient $T \simeq 0.3$.

to the Neumann-series expansion of Eq. (6.26)) returns spatially symmetric Wigner functions only, [2] one is forced to conclude that, among the infinite set of coefficients compatible with the given boundary conditions, such treatments automatically provide/select the symmetric choice $c = 1$. This implies that, by applying such numerical treatments to the case of the delta-like potential (9.1) and using as boundary conditions the ones corresponding to the left-state Wigner function (9.14), one is expected to obtain the spatially-symmetric ($c = 1$) carrier density (red dashed curve) reported in Fig. 9.1. In order to validate this conclusion, we have performed a numerical solution of the integral version of the Wigner equation (6.26) via a standard finite-difference technique. As expected, the result of our calculation (not reported here) is symmetric, and –apart from small deviations

due to discretization as well as to phase-space cut-offs– it coincides with the symmetric ($c = 1$) carrier density in Fig. 9.1.

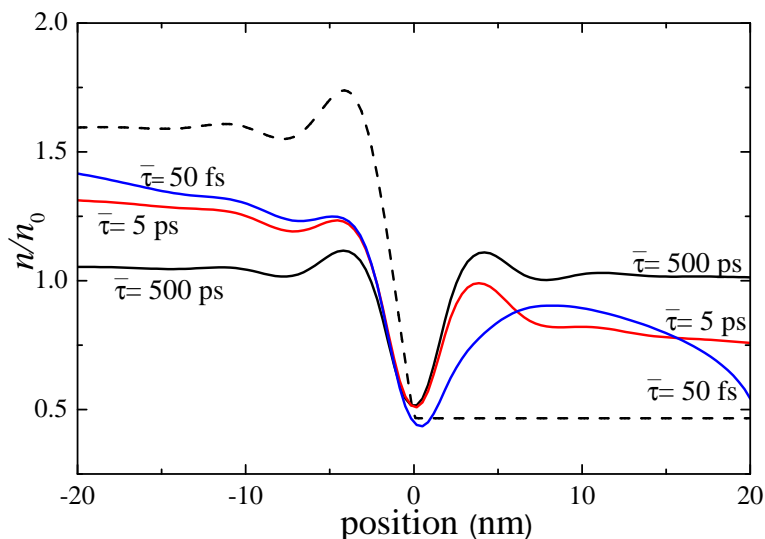


Figure 9.2. Spatial carrier density for the case of the delta-like potential in (9.1). Comparison between the result obtained by an analytical approach to the problem (dashed curve) and via a numerical solution of the generalized Wigner equation (8.4), (based on a standard phase-space discretization scheme in terms of a 120×120 uniform grid) for different values of the relaxation time $\bar{\tau}$ (solid curves), in the presence of a room-temperature carrier injection only from the left ($\mu_R \rightarrow -\infty$) for the same device and simulation parameters considered in Fig. 9.1 and for $\mu_L = 4k_B T$ (see text).

In order to study the interplay between coherence and dissipation/decoherence, we have investigated carrier transport through the delta-barrier potential (9.1) in the presence of a quasiequilibrium thermal injection from the external reservoirs corresponding to the spatial boundaries

$$\begin{aligned}
 f\left(-\frac{l}{2}, k > 0\right) &= f^\circ(\epsilon(k) - \mu_L) \\
 f\left(+\frac{l}{2}, k < 0\right) &= f^\circ(\epsilon(k) - \mu_R), \quad (9.22)
 \end{aligned}$$

where μ_L and μ_R denote the chemical potentials of the left and right reservoirs, and f° the corresponding quasiequilibrium Fermi functions. In particular, we have considered the case of a room-temperature carrier injection from the left reservoir only ($\mu_R \rightarrow -\infty$).

While in the coherent limit ($\bar{\tau} \rightarrow \infty$) such transport problem can be treated analytically via the standard Landauer-Büttiker formalism, [67] a numerical solution of the Wigner equation (8.4) has been performed for different values of the relaxation time $\bar{\tau}$. To this end we have chosen the same device and simulation parameters considered in Fig. 9.1, and we have set $\mu_L = 4k_B T$.

Figure 9.2 shows the obtained spatial carrier density. The dashed curve represents the coherent-transport result provided by a standard scattering-state calculation, and is therefore immune from the unphysical behaviors of the Wigner treatment pointed out above; explicitly, the density is given by the thermal average of the pure-state carrier density in (9.15). In this coherent regime, one recovers the spatial density profile predicted by the Landauer-Büttiker theory: [67] while on the right hand side of the barrier the density is given by the fraction of the carriers injected from the left reservoir that is transmitted across the barrier, on the left hand side the density accumulation is determined by the fraction of carriers reflected back to the left reservoir. Notice that, with respect to the pure-state density profile in Eq. (9.15) (corresponding to a monoenergetic injection), here the thermal average leads to effective transmission and reflection coefficients; besides, the oscillatory contribution in Eq. (9.15) averages out far from $z = 0$.

The solid curves in Fig. 9.2 correspond to three different values of the relaxation time: $\bar{\tau} = 500$ ps, $\bar{\tau} = 5$ ps, and $\bar{\tau} = 50$ fs. These timescales have to be compared to the average transit time, which is given by the ratio between the device length and the dissipation-free carrier drift velocity, and is of the order of 100 fs. Thus, for $\bar{\tau} = 500$ ps the impact of energy relaxation and decoherence is expected to be definitely negligible, and the coherent limit previously considered should be recovered. However, the charge density obtained via a numerical solution of the generalized Wigner equation (8.4) turns out to be significantly different from the dashed-curve one. Here, in spite of the presence of the potential barrier, all injected carriers are transmitted (see below), and no reflection takes place. In contrast,

for smaller values of the relaxation time the impact of dissipation and decoherence becomes significant: a decrease of $\bar{\tau}$ (see solid curves in Fig. 9.2) leads to a progressive decrease of the current, as shown in Fig. 9.3 (solid curve), which corresponds to an effective reflection of the injected carriers back to the left reservoir, induced by the relaxation-time term in (8.4).

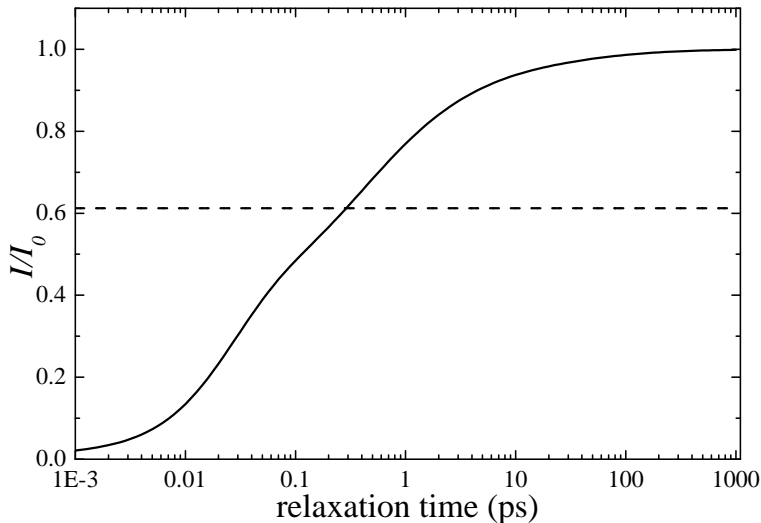


Figure 9.3. Charge current I as a function of the relaxation time $\bar{\tau}$ (in units of its potential- and dissipation-free value I_0) (solid curve) compared to the coherent-limit ($\bar{\tau} \rightarrow \infty$, dashed curve) current corresponding to the analytical charge density predicted by the Landauer-Büttiker theory (see dashed curve in Fig. 9.2) (see text).

The coherence-versus-dissipation scenario described so far is fully confirmed by the electronic-current analysis presented in Fig. 9.3: here, we report the current I as a function of the relaxation time $\bar{\tau}$, in units of its potential- and dissipation-free value I_0 , (solid curve) compared to the dissipation-free current predicted by the Landauer-Büttiker theory (dashed curve) corresponding to the dashed-curve charge-density profile in Fig. 9.2. As anticipated, in the coherent limit ($\bar{\tau} \rightarrow \infty$), while within the Landauer-Büttiker formalism the presence of the potential barrier leads to a significant attenuation of the current ($I/I_0 \simeq 0.6$, dashed curve), the dissipation-free

current obtained via the Wigner equation (8.4) coincides with its potential-free value I_0 (see below). For decreasing values of $\bar{\tau}$ –corresponding to an increased impact of energy-dissipation/decoherence processes– one observes a progressive reduction of the current (see solid curve).

From the numerical analysis reported so far, one concludes that the conventional Wigner-function treatment leads, in general, to an overestimation of tunneling-like phenomena; such overestimation, particularly severe in the coherent-transport limit, may be quantitatively mitigated by the presence of non-elastic scattering processes. It is however important to point out that, from a fundamental point of view, the conventional Wigner-function treatment of coherent transport is intrinsically incompatible with well established results of the Landauer-Büttiker formalism. [67]

9.3 Analytical Wigner-function boundary value vs Fermi-Dirac distribution

Different features of the Wigner-function treatment may induce the anomalous coherent-limit behavior reported in Figs. 9.2 and 9.3. The first issue to be discussed is the validity of the thermal-injection boundary scheme in (9.22). Indeed, as recently pointed out in Refs. [51, 72, 73], such a semiclassical treatment/description of the boundary function $f^b(k)$ seems to be not necessarily compatible with the quantum-mechanical nature of a genuine Wigner function, as confirmed by the highly non-classical (i.e., non positive-definite) shape of the boundary conditions corresponding, e.g., to the scattering state solution (9.14). This is clearly shown in Fig. 9.4, where we report the left ($k > 0$) and right ($k < 0$) quantum-mechanical inflow boundary profile corresponding to the analytical Wigner function in (9.14); as anticipated, opposite to the usual semiclassical treatment, here the boundary function –corresponding to a left-scattering state of incoming wavevector $\bar{k} \simeq 4.2 \text{ nm}^{-1}$ – involves all k values and, more important, is not positive-definite.

We emphasize that, thanks to the presence of external carrier reservoirs in thermal or quasi-thermal equilibrium, the Wigner function of the quantum-device electron is expected to be far from a pure state. For this reason, in order to better compare the rigorous shape of the inflowing

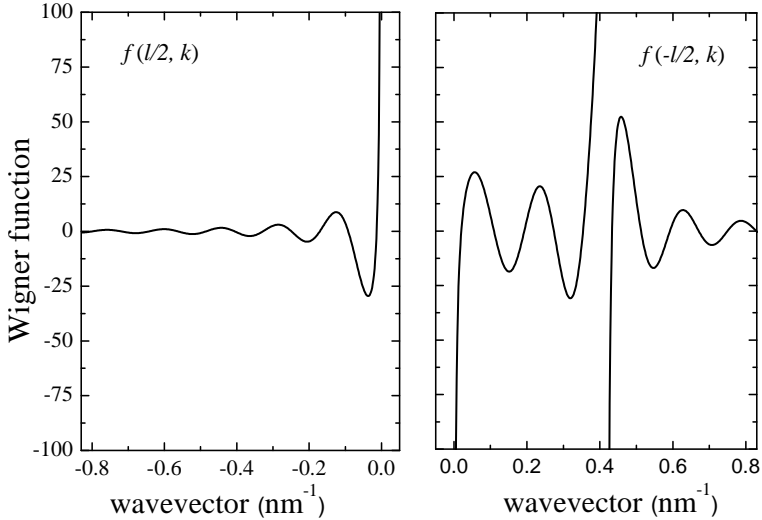


Figure 9.4. The inflow boundary profile determined by the analytical Wigner function (9.14) for a delta-like potential barrier (9.1), namely $f(z = -l/2, k)$ for $k > 0$ (left panel), and $f(z = +l/2, k)$ for $k < 0$ (right panel). The Wigner function is plotted in units of $2\pi/\Omega$, and the device parameters are the same as in Fig. 9.1; in particular, the scattering-state wavevector is $\bar{k} \simeq 4.2 \text{ nm}^{-1}$ (see text).

Wigner function with the usual Fermi-Dirac distribution of the semiclassical theory (employed in the conventional Wigner-function modeling), let us consider the Wigner function corresponding to a mixed state. To this aim, a thermal average is performed as incoherent superposition of the density matrices $|\bar{k}\rangle\langle\bar{k}|$ corresponding to the left- and right-scattering states in (9.3). In more explicit terms, this amounts to assume a density-matrix operator of the form

$$\hat{\rho} = \frac{\Omega}{2\pi} \int d\bar{k} |\bar{k}\rangle f^\circ(\bar{k}) \langle\bar{k}|, \quad (9.23)$$

where the function

$$f^\circ(\bar{k}) = \begin{cases} f^\circ(\epsilon(\bar{k}) - \mu_L) & \text{for } \bar{k} > 0 \\ f^\circ(\epsilon(\bar{k}) - \mu_R) & \text{for } \bar{k} < 0 \end{cases} \quad (9.24)$$

encodes the carrier distribution of the left and right reservoirs according to

the sign of \bar{k} .

By applying to the mixed/thermal-state density matrix (9.23) the one-dimensional version of the Weyl-Wigner transform in (5.1), the corresponding Wigner function comes out to be

$$f(z, k) = \frac{\Omega}{2\pi} \int d\bar{k} \bar{f}(z, k; \bar{k}) f^\circ(\bar{k}) . \quad (9.25)$$

In order to quantify the impact of the above thermal average (with respect to the pure-state result in Fig. 9.4), we have evaluated the inflowing part ($k > 0$) of the Wigner function (9.25) at $z = -l/2$ (left boundary) for the same delta-like potential profile, assuming carrier injection from left only ($\mu_R \rightarrow -\infty$). Figure 9.5 shows a comparison between the left-contact Wigner function in (9.25) (dashed curves) and the corresponding Fermi-Dirac distribution (solid curves) at three different temperatures: $T = 300$ K (a), $T = 30$ K (b), and $T = 3$ K (c); for all three cases we have assumed a chemical potential $\mu_L = 4k_B T$. As one can see, while at room temperature [panel (a)] the two curves coincide over a large range of k values, for low temperatures [panels (b) and (c)] the value of the Wigner function on the left boundary significantly differs from the Fermi-Dirac distribution, unambiguous proof of the failure of a classical-like boundary condition treatment in the low-temperature limit. It is worth stressing that such limitation was already pointed out by Frensley in its original paper; [33] where he noticed that for the case of a resonant-tunneling diode the Wigner-function calculation resembles the experimental results at $T = 300$ K, but at lower temperatures it seriously underestimates the peak-to-valley ratio.

9.4 The anomalous behaviour of the coherent current

From the boundary-condition analysis of Fig. 9.5 it follows that at room temperature the classical-like injection model in (9.22) is definitely appropriate; this seems to suggest that the anomalous coherent-limit results reported in Fig. 9.3 are the hallmark of a more general limitation of the whole Wigner-function transport modeling. Indeed the electric current flowing

through a generic quantum device, expressed in terms of the Wigner function $f(z, k)$ as

$$I(z) \propto \int_{-\infty}^{+\infty} v(k) f(z, k) dk . \quad (9.26)$$

fulfills the charge continuity equation²³. Because in steady-state conditions and in the absence of energy dissipation the current is z -independent [$I(z) = I_0$], it can be computed at any space point. In particular by evaluating Eq. (9.26) at the left boundary $z = -l/2$, and by splitting the integration domain into negative and positive k values, one obtains

$$I_0 \propto \int_{-\infty}^0 v(k) f\left(-\frac{l}{2}, k\right) dk + \int_0^{+\infty} v(k) f\left(-\frac{l}{2}, k\right) dk . \quad (9.31)$$

For the case of a symmetric potential, it is possible to show that the (unique) solution of the generalized Wigner equation (8.4) in the coherent limit $\bar{\tau} \rightarrow \infty$ is always spatially symmetric: $f(z, k) = f(-z, k)$. Recalling that, at

²In order to show that in steady-state conditions the electric current in (9.26) is z -independent, it is enough to show that its space derivative,

$$\frac{dI(z)}{dz} \propto \int dk v(k) \frac{\partial f(z, k)}{\partial z} , \quad (9.27)$$

is always equal to zero. To this end, recalling that in steady state conditions [see Eq. (6.23)]

$$v(k) \frac{\partial f(z, k)}{\partial z} = - \int dk' \mathcal{V}(z, k - k') f(z, k') , \quad (9.28)$$

the space derivative in (9.27) can also be expressed as:

$$\frac{dI(z)}{dz} \propto \int dk \int dk' \mathcal{V}(z, k - k') f(z, k') . \quad (9.29)$$

By setting $k'' = k - k'$ and recalling the antisymmetric character of the potential super-operator ($\mathcal{V}(z, -k'') = -\mathcal{V}(z, k'')$), we finally obtain

$$\frac{dI(z)}{dz} \propto \int dk' f(z, k') \int dk'' \mathcal{V}(z, k'') = 0 . \quad (9.30)$$

³Importantly, within the relaxation-time approximation [see Eq. (8.2)] the charge continuity equation just recalled is not valid anymore, and the steady-state current (see Fig. 9.3) is typically evaluated averaging $I(z)$ over the device active region.

$z = -l/2$ for $k > 0$ and at $z = +l/2$ for $k < 0$, the Wigner function coincides with the inflow boundary function $f^b(k)$, and using the space symmetry of the Wigner function (between $-l/2$ and $+l/2$), Eq. (9.31) can simply be rewritten as:

$$I_o \propto \int_{-\infty}^{+\infty} v(k) f^b(k) dk . \quad (9.32)$$

This equation indicates that for the case of a symmetric potential the coherent-limit electric current is determined by the boundary values only, and is fully independent of the shape of the device potential profile. In particular, this leads to the unphysical result that the value of the current turns out to be the same for a potential-free ballistic device as well as for an infinitely high potential barrier.

9.5 Negative charge densities in the presence of dissipation/decoherence

The coherence-versus-dissipation analysis presented so far may lead to conclude that, while in the coherent limit the Wigner-function modeling is highly problematic, in the presence of a significant energy-dissipation dynamics the results are always physically acceptable. However, this is not the case. Indeed, one can consider the following situation: (i) replace the ideal delta-like barrier in (9.1) with a more realistic rectangular barrier with finite width a and height V_0 , i.e.,

$$v(z) = v_0 \theta \left(\frac{a}{2} - |z| \right) , \quad (9.33)$$

and (ii) replace the thermal injection in (9.22) with a simple monoenergetic carrier injection from left, i.e.,

$$f^b(k) \propto \delta(k - \bar{k}) . \quad (9.34)$$

The resulting spatial carrier-density profiles corresponding to the coherent limit ($\bar{\tau} \rightarrow \infty$) (dashed curve) as well as to two different values of the relaxation time $\bar{\tau}$ (solid curves) are reported in Fig. 9.6. As one can see, while energy dissipation induces once again a spatial asymmetry (see also

Fig. 9.2), in the presence of a monoenergetic injection [see Eq. (9.34)] all three density profiles display negative-value regions. Thus unphysical features also appear in the presence of a strong energy-dissipation dynamics. This result is qualitatively similar to the one reported in [2] for the case of a cosine-like potential, thus confirming the physical limitations of the conventional Wigner-function modeling.

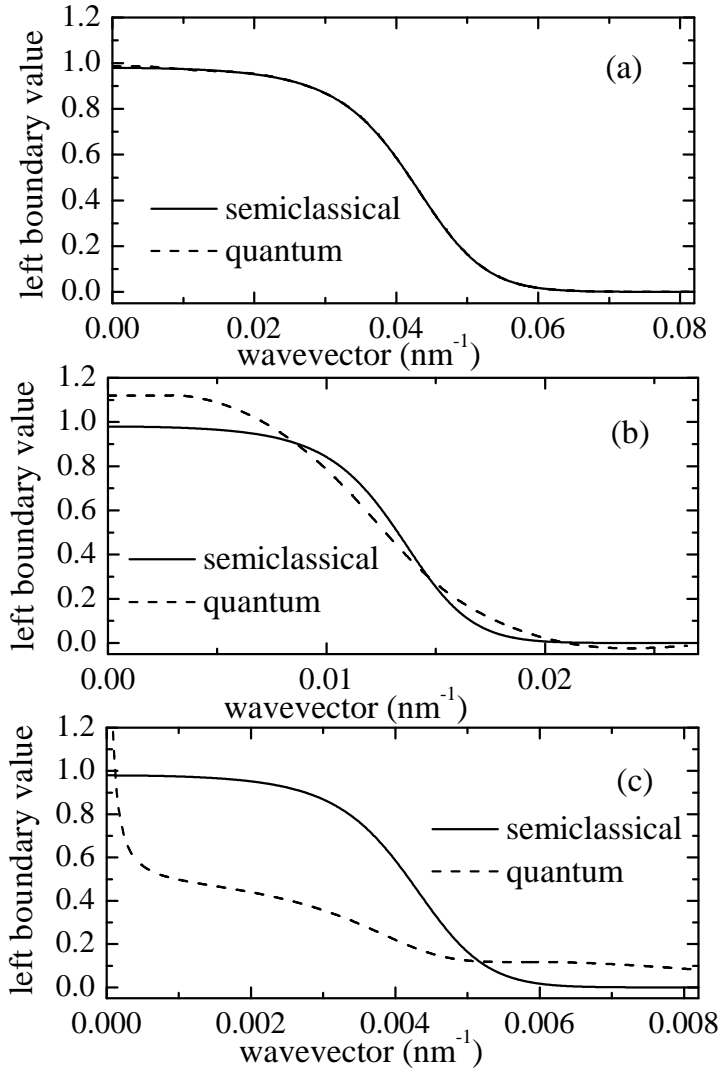


Figure 9.5. Case of the delta-like potential barrier in (9.1). The value of the thermally averaged Wigner function in (9.25) at the left boundary is plotted as a function of the wave vector k (dashed curves) and is compared to the semiclassical assumption of a Fermi-Dirac distribution (solid curves), for three different temperature values: $T = 300 \text{ K}$ (a), $T = 30 \text{ K}$ (b), and $T = 3 \text{ K}$ (c). Here, the device parameters are the same as in Fig. 9.1, and for all three cases we have assumed a chemical potential $\mu_L = 4k_B T$ (see text).

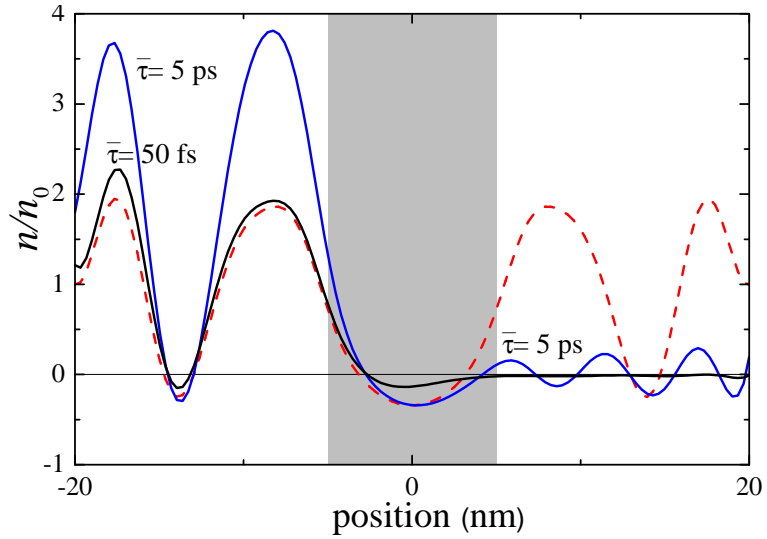


Figure 9.6. Spatial carrier density n (in units of its barrier-free value n_0) corresponding to the rectangular-barrier profile in (9.33) (device length $l = 40$ nm, barrier width $a = 10$ nm, and barrier height $V_0 = 150$ meV) in the presence of a monoenergetic injection from the left ($\epsilon = 50$ meV). Here the coherent-limit ($\bar{\tau} \rightarrow \infty$) density profile (dashed curve) is compared to the results corresponding to two different values of the relaxation time: $\bar{\tau} = 5$ ps and $\bar{\tau} = 50$ fs (solid curves) (see text).

Chapter 10

Summary and conclusions

In part II we have, following the published paper [57], pointed out and explained some intrinsic limitations of the conventional quantum-device modeling strategy based on the well-known Wigner-function formalism. More specifically, we have provided a definite answer to a few open questions related to the application of the conventional space-boundary condition scheme to the Wigner transport equation. By combining analytical and numerical results, our investigation has shown that (i) in the coherent limit the solution of the Wigner equation (compatible with given boundary conditions) is not unique, and (ii) when decoherent/dissipative phenomena are taken into account within the relaxation-time approximation the solution, although unique, may be unphysical. Indeed it is not necessarily a physical Wigner function (see Fig. 9.6), i.e., a Weyl-Wigner transform of a single-particle density matrix.

From a physical point of view, such intrinsic limitations of the standard (i.e., semiclassical) boundary condition scheme applied to the Wigner transport equation can be summarized as follows: The essentially wrong ingredient in the conventional treatment is the artificial space separation between device active region ($|z| < l/2$) and external reservoirs ($|z| > l/2$) (see Fig. 7.1). Indeed, the latter is intrinsically incompatible with the well-known non-local character of quantum mechanics.

Our numerical results show that the above limitations are particularly severe in the coherent limit and/or in the presence of nonequilibrium carrier injection from the external reservoirs (e.g., monoenergetic distributions);

this may explain why such anomalous behaviors are usually not experienced in conventional quantum-device modeling, since the latter is typically based on quasi-thermal injection in the presence of a significant energy-dissipation dynamics. In this respect it is worth stressing that, in principle, some of the limitations discussed in this thesis work may also affect other modeling strategies based, e.g., on the nonequilibrium Green's functions. [74–76] Indeed, in a recent study [73] it has been shown that when the electric contacts are far enough from the device active region, the results of the inflow Wigner-function scheme and of conventional Green's function treatments coincide. Since the anomalous coherent-limit behavior reported in Figs. 9.2 and 9.3 is not related to the boundary location, it seems that such limitation may also affect Green's function treatments; however, in order to provide a definite answer to this point, a specific investigation is imperative.

In order to overcome the basic limitations of the Wigner-function modeling discussed in this part, the crucial step could be to replace the local (i.e., classical-like) boundary condition-scheme treatment of the device-reservoir interaction with a fully non-local approach; to this end, in order to ensure/maintain the positive-definite character of the electronic density matrix, a possible strategy is to describe the system/device-environment/reservoir interaction via a Lindblad-like coupling term: [27] this task, already introduced in [77], will be presented, following the published paper [78], in part III together with a detailed analysis of genuine quantum effects arising from a Lindblad-based description of the scattering-induced decoherence. The model discussed in III is microscopic, contrary to the phenomenological RTA employed in part II, and able to show the scattering-induced current described in Sec. 8.1, contrary to the Boltzmann equation (see Eq. (1.14)).

Part III

Scattering-induced quantum phenomena in semiconductor nanodevices: a positive-definite density matrix description

Chapter 11

The Single-particle description

11.1 Introduction

In Sec. (3.3) we reported the alternative Markov approximation proposed in [1] which provides a Lindblad dynamics (see Eq. (3.20)) for the many-body density matrix $\hat{\rho}$. However, since many physical interesting observables are single particle variables (such as, e.g., charge density, current, momentum distribution or mean kinetic energy), their statistical averages are usually computed exploiting the *single-particle density matrix* $\hat{\rho}$, which can be obtained from the global density matrix $\hat{\rho}$ through a procedure to be introduced below. In other words, given a generic single-particle operator \hat{G} , which may be written in a second-quantized form as

$$\hat{G} = \sum_{\alpha_1 \alpha_2} G_{\alpha_1 \alpha_2} \hat{c}_{\alpha_1}^\dagger \hat{c}_{\alpha_2} , \quad (11.1)$$

a single-particle density matrix $\hat{\rho}$ is introduced,

$$\hat{\rho} = \sum_{\alpha_1 \alpha_2} \rho_{\alpha_1 \alpha_2} \hat{c}_{\alpha_1}^\dagger \hat{c}_{\alpha_2} , \quad (11.2)$$

such that

$$\langle \hat{G} \rangle = \sum_{\alpha_1 \alpha_2} G_{\alpha_1 \alpha_2} \rho_{\alpha_2 \alpha_1} . \quad (11.3)$$

The Equation of motion of $\hat{\rho}$ is always in the form

$$\frac{d\hat{\rho}}{dt} = \frac{d\hat{\rho}}{dt}\Big|_{\text{sp}} + \frac{d\hat{\rho}}{dt}\Big|_{\text{scat}} \quad , \quad (11.4)$$

where (see Eqs. (5.10) and (6.1))

$$\frac{d\hat{\rho}}{dt}\Big|_{\text{sp}} = \frac{1}{i\hbar} [\hat{H}^{\text{sp}}, \hat{\rho}] \quad (11.5)$$

and, neglecting so-called memory effects (see below)

$$\frac{d\hat{\rho}}{dt}\Big|_{\text{scat}} = \bar{\Gamma}(\hat{\rho}) \quad , \quad (11.6)$$

where $\bar{\Gamma}(\hat{\rho})$ is a (in general) nonlinear superoperator.

The above single-particle picture has been applied to a variety of physical problems, [25] ranging from quantum-transport phenomena to ultrafast electro-optical processes; however, it is vital to stress that the degree of accuracy of such density-matrix formalism is intimately related to the choice of the scattering superoperator $\bar{\Gamma}(\hat{\rho})$ in (11.6).

The microscopic derivation of suitable scattering superoperators has been one of the most challenging problems in solid-state physics. Indeed, For purely atomic and/or photonic systems, dissipation and decoherence phenomena may be successfully described via adiabatic-decoupling procedures [79] in terms of extremely simplified models via phenomenological parameters; within such effective treatments, the main goal is to identify a suitable form of the Liouville superoperator, able to ensure the positive-definite character of the corresponding density-matrix operator. [80] This is usually accomplished by identifying proper Lindblad superoperators, [27] expressed in terms of a few crucial system-environment coupling parameters. In contrast, solid-state materials and devices are often characterized by a complex many-electron quantum evolution, resulting in a non-trivial interplay between coherent dynamics and energy-dissipation and decoherence processes; [25, 81] it follows that for a quantitative description of such coherence-versus-dissipation coupling the latter needs to be treated via fully microscopic approaches.

Based on the pioneering works by Van Hove, [82] Kohn and Luttinger, [83] and Zwanzig, [84] a number of adiabatic- or Markov-approximation schemes have been developed and employed for the study of quantum-transport and coherent-optics phenomena in semiconductor materials and devices; the latter may be divided into two general categories: approaches based on semiclassical (i.e., diagonal) scattering superoperators also referred to as Pauli master equations, [69, 85, 86] and fully quantum-mechanical (i.e., non-diagonal) dissipation models. [87–91] Moreover, in order to account for non-markovian or memory effects —relevant in the presence of strong couplings and/or extremely short excitations— a number of quantum-kinetic approaches have been also considered. [92, 93]

As far as the Markov treatments are concerned, the latter depend strongly on the particular problem under investigation, and therefore the resulting set of kinetic equations describes a specific subsystem of interest, e.g., a gas of N electrons or excitons, a single carrier, etc. Moreover, as originally pointed out by Spohn and co-workers, [94] kinetic approaches based on the conventional Markov limit may lead to the violation of the positive-definite character of the density-matrix operator, and therefore to unphysical results; in particular, they clearly pointed out that the choice of the adiabatic decoupling strategy is definitely not unique, and only one among the available possibilities, developed in the pioneering work by Davies [80], could be shown to preserve positivity: it was the case of a “small” subsystem of interest interacting with a thermal environment, and selected through a partial-trace reduction. Unfortunately, this theory was restricted to finite-dimensional subsystems only (i.e., N -level atoms), and to the particular projection scheme of the partial trace.

It is in order to overcome this serious limitation in the study of solid-state systems that the alternative Markov procedure recalled in Chap. 3 has been proposed in [1]; the latter in fact (i) in the discrete-spectrum case coincides with the Davies model just recalled, (ii) in the semiclassical limit (see below) reduces to the well-known Fermi’s golden rule, and (iii) describes a genuine Lindblad evolution also in the continuous-spectrum case, thus providing a reliable and robust treatment of energy-dissipation and decoherence processes in semiconductor quantum devices.

In this chapter we will both express the single-particle density matrix $\hat{\rho}$ in terms of the global $\hat{\rho}$ and furnish the single-particle scattering-induced

dynamics arising from the global evolution introduced in Eq. (3.20), which takes care of both single- (e.g., carrier-phonon, see Eq. (1.4)) and double- (e.g. carrier-carrier, see Eq. (1.10)) carrier scattering mechanism. In addition, we will also consider the single-particle scattering dynamics arising from conventional (e.g., nonLindblad) Markov limits: in this way, in Chap. 12 a comparison between the two single-particle dynamics will show how only the Lindblad-generated dynamics is able to guarantee the positivity of the density matrix. The low-density limits of the scattering superoperators $\bar{\Gamma}(\hat{\rho})$ obtained both from conventional and alternative Markov approximations will be shown to be linear in $\hat{\rho}$, as the $\Gamma(\hat{\rho})$ of Eq. (5.8), for the case of carrier-phonon interaction mechanism (see Eqs. (11.43) and (11.44)). Finally, the positivity and linearity in $\hat{\rho}$ of the superoperator $\Gamma(\hat{\rho})$ descending from the novel Markov approximation will permit in Chaps. 14 and 15 a detailed analysis of some genuine scattering-induced quantum effects like the scattering-induced nonlocality or diffusion speedup.

11.2 The many-electron density matrix

In order to properly define a single-particle density matrix $\hat{\rho}$ able to furnish statical averages of generic one-electron observables \hat{G} in the form of Eq. (11.3), a couple of reduction are necessary. The first one has the role of restricting the degrees of freedom of the system under consideration to the electronic ones only: this is typically done by averaging out the quasiparticle degrees of freedom (in our case the phonons). This suggest the introduction of a many-electron density matrix $\hat{\rho}_c$ defined as the trace over the non-relevant quasiparticle degrees of freedom, labeled by subscript qp , of the global density matrix $\hat{\rho}$,

$$\hat{\rho}_c = \text{Tr} [\hat{\rho}]_{qp} \quad . \quad (11.7)$$

The trace introduced in Eq. (11.7) is in general complicated; however, a strong simplification comes if one assumes both that the electronic and the quasiparticle subsystems are uncorrelated,

$$\hat{\rho} = \hat{\rho}_c \otimes \hat{\rho}_{qp} \quad , \quad (11.8)$$

where $\hat{\rho}_{qp}$ denotes the many quasiparticle density matrix, and that the latter is assumed to be in thermal equilibrium,

$$\hat{\rho}_{qp} \equiv \hat{\rho}_{qp}^\circ, \quad (11.9)$$

where $\hat{\rho}_{qp}^\circ$ fulfills

$$\begin{aligned} \text{tr} \left[\hat{b}_{\mathbf{q}} \hat{\rho}_{qp}^\circ \right]_{qp} &= \text{tr} \left[\hat{b}_{\mathbf{q}}^\dagger \hat{\rho}_{qp}^\circ \right]_{qp} = 0 \quad , \\ \text{tr} \left[\hat{b}_{\mathbf{q}}^\dagger \hat{b}_{\mathbf{q}'} \hat{\rho}_{qp}^\circ \right]_{qp} &= N_{\mathbf{q}} \delta_{\mathbf{q}, \mathbf{q}'} \quad , \\ \text{tr} \left[\hat{b}_{\mathbf{q}} \hat{b}_{\mathbf{q}'} \hat{\rho}_{qp}^\circ \right]_{qp} &= \text{tr} \left[\hat{b}_{\mathbf{q}}^\dagger \hat{b}_{\mathbf{q}'}^\dagger \hat{\rho}_{qp}^\circ \right]_{qp} = 0 \quad , \end{aligned} \quad (11.10)$$

where $N_{\mathbf{q}}$ is the Bose-Einstein distribution.

Recalling that the global density-matrix operator $\hat{\rho}$ fulfill the dynamics given in Eq. (2.24), the Equation of motion of the many-electrons operator $\hat{\rho}_c$ may be written as

$$\frac{\partial \hat{\rho}_c}{\partial t} = \left. \frac{\partial \hat{\rho}_c}{\partial t} \right|_{\text{free}} + \left. \frac{\partial \hat{\rho}_c}{\partial t} \right|_{\text{scat}} \quad , \quad (11.11)$$

where the first term is given by

$$\left. \frac{\partial \hat{\rho}_c}{\partial t} \right|_{\text{free}} = \frac{1}{i\hbar} [\hat{H}^{\text{sp}}, \hat{\rho}_c] \quad , \quad (11.12)$$

where \hat{H}^{sp} has been given in Eq. (1.2) (apart from energy renormalizations which come also from the trace over the phononic degrees of freedom); $\left. \frac{\partial \hat{\rho}_c}{\partial t} \right|_{\text{free}}$ describes the free-evolution of $\hat{\rho}_c$. The second term in Eq. (11.11) depends on the models used to describe the scattering effects. In particular, applying the combined Eqs. (11.7), (11.9) and (11.10) to the scattering-induced Lindblad superoperator in Eq. (3.20) one obtains

(i) the carrier-phonon induced contribution $\left. \frac{\partial \hat{\rho}_c}{\partial t} \right|_{\text{scat=cph}}$ becomes

$$\begin{aligned} \left. \frac{\partial \hat{\rho}_c}{\partial t} \right|_{\text{cph}} &= \sum_{\mathbf{q}, \mathbf{q}'} \sum_{\alpha_1 \alpha_2 \alpha'_1 \alpha'_2} \hat{c}_{\alpha_1}^\dagger \hat{c}_{\alpha_2} \hat{c}_{\alpha'_1}^\dagger \hat{c}_{\alpha'_2} \times \\ &\times \left(\mathbf{A}_{\alpha_1 \alpha_2}^{\mathbf{q}+} \mathbf{A}_{\alpha'_1 \alpha'_2}^{\mathbf{q}' +*} \text{tr} \left[\hat{b}_{\mathbf{q}}^\dagger \hat{b}_{\mathbf{q}'}^\dagger \hat{\rho}_{qp}^\circ \right]_{qp} + \mathbf{A}_{\alpha_1 \alpha_2}^{\mathbf{q}-} \mathbf{A}_{\alpha'_1 \alpha'_2}^{\mathbf{q}' -*} \text{tr} \left[\hat{b}_{\mathbf{q}} \hat{b}_{\mathbf{q}'} \hat{\rho}_{qp}^\circ \right]_{qp} \right. \\ &\quad \left. + \mathbf{A}_{\alpha_1 \alpha_2}^{\mathbf{q}-} \mathbf{A}_{\alpha'_1 \alpha'_2}^{\mathbf{q}' +*} \text{tr} \left[\hat{b}_{\mathbf{q}} \hat{b}_{\mathbf{q}'}^\dagger \hat{\rho}_{qp}^\circ \right]_{qp} + \mathbf{A}_{\alpha_1 \alpha_2}^{\mathbf{q}+} \mathbf{A}_{\alpha'_1 \alpha'_2}^{\mathbf{q}' -*} \text{tr} \left[\hat{b}_{\mathbf{q}}^\dagger \hat{b}_{\mathbf{q}'}^\dagger \hat{\rho}_{qp}^\circ \right]_{qp} \right) \\ &= \sum_{\mathbf{q}, \pm} \left(\hat{\mathbf{A}}^{\mathbf{q}\pm} \hat{\rho}_c \hat{\mathbf{A}}^{\mathbf{q}\pm\dagger} - \frac{1}{2} \left\{ \hat{\rho}_c, \hat{\mathbf{A}}^{\mathbf{q}\pm\dagger} \hat{\mathbf{A}}^{\mathbf{q}\pm} \right\} \right) \quad , \end{aligned} \quad (11.13)$$

where

$$\begin{aligned}\hat{\mathbf{A}}_c^{\mathbf{q}\pm} &= \sqrt{N_{\mathbf{q}} + \frac{1}{2} \pm \frac{1}{2}} \sum_{\alpha_1 \alpha_2} \mathbf{A}_{\alpha_1 \alpha_2}^{\mathbf{q}\pm} \hat{c}_{\alpha_1}^\dagger \hat{c}_{\alpha_2} \\ &= \sum_{\alpha_1 \alpha_2} A_{\alpha_1 \alpha_2}^{\mathbf{q}\pm} \hat{c}_{\alpha_1}^\dagger \hat{c}_{\alpha_2}\end{aligned}\quad (11.14)$$

with the $\mathbf{A}_{\alpha_1' \alpha_2'}^{\mathbf{q}\pm}$ defined in Eq. (3.23);

(ii) introducing, for exposure purposes, the symbol $\hat{\mathbf{A}}_c^{\text{cc}}$ to indicate the same $\hat{\mathbf{A}}^{\text{cc}}$ defined in Eq. (3.22),

$$\hat{\mathbf{A}}_c^{\text{cc}} \equiv \hat{\mathcal{A}}^{\text{cc}} \quad , \quad (11.15)$$

the carrier-carrier induced contribution $\left. \frac{\partial \hat{\rho}_c}{\partial t} \right|_{\text{scat=cc}}$ becomes

$$\left. \frac{\partial \hat{\rho}_c}{\partial t} \right|_{\text{cc}} = \hat{\mathbf{A}}_c^{\text{cc}} \hat{\rho}_c \hat{\mathbf{A}}_c^{\text{cc}\dagger} - \frac{1}{2} \left\{ \hat{\rho}_c, \hat{\mathbf{A}}_c^{\text{cc}} \hat{\mathbf{A}}_c^{\text{cc}\dagger} \right\} \quad . \quad (11.16)$$

As a consequence, the scattering-induced dynamics for the global density matrix $\hat{\rho}$ in Eq. (3.20) provides the following Equation of motion for the many-electron density-matrix operator $\hat{\rho}_c$:

$$\left. \frac{\partial \hat{\rho}_c}{\partial t} \right|_{\text{scat}} = \sum_s \hat{\mathbf{A}}_c^s \hat{\rho}_c \hat{\mathbf{A}}_c^{s\dagger} - \frac{1}{2} \left\{ \hat{\rho}_c, \hat{\mathbf{A}}_c^{s\dagger} \hat{\mathbf{A}}_c^s \right\} \quad , \quad (11.17)$$

where the index s runs over the scattering-mechanisms (in particular, $s = \mathbf{q}, \pm$ or $s = \text{cc}$).

Applying the very same thermal assumptions (11.10) to the scattering superoperator provided by conventional Markov of Eq. (2.23), the scattering-induced dynamics for $\hat{\rho}_c$ is given by

$$\left. \frac{d \hat{\rho}_c}{dt} \right|_{\text{scat}} = \frac{1}{2} \sum_s \left(\hat{\mathbf{a}}_c^s \hat{\rho}_c \hat{\mathbf{b}}_c^{s\dagger} - \hat{\mathbf{a}}_c^{s\dagger} \hat{\mathbf{b}}_c^s \hat{\rho}_c \right) + \text{H.c.} \quad (11.18)$$

where s indicates once again the scattering mechanism and for the scattering-mechanisms here considered the operators $\hat{\mathbf{a}}_c^s$ and $\hat{\mathbf{b}}_c^s$ are given by

$$\begin{aligned}
 \hat{\mathbf{a}}_c^{\mathbf{q},\pm} &= \sum_{\alpha\alpha'} a_{\alpha\alpha'}^{\mathbf{q},\pm} \hat{c}_\alpha^\dagger \hat{c}_{\alpha'} \quad , \\
 \hat{\mathbf{b}}_c^{\mathbf{q},\pm} &= \sum_{\alpha\alpha'} b_{\alpha\alpha'}^{\mathbf{q},\pm} \hat{c}_\alpha^\dagger \hat{c}_{\alpha'} \quad , \\
 \hat{\mathbf{a}}_c^{\text{cc}} &= \sum_{\alpha\alpha'\bar{\alpha}\bar{\alpha}'} a_{\alpha\bar{\alpha}\alpha'\bar{\alpha}'}^{\text{cc}} \hat{c}_\alpha^\dagger \hat{c}_{\bar{\alpha}}^\dagger \hat{c}_{\bar{\alpha}'} \hat{c}_{\alpha'} \quad , \\
 \hat{\mathbf{b}}_c^{\text{cc}} &= \sum_{\alpha\alpha'\bar{\alpha}\bar{\alpha}'} b_{\alpha\bar{\alpha}\alpha'\bar{\alpha}'}^{\text{cc}} \hat{c}_\alpha^\dagger \hat{c}_{\bar{\alpha}}^\dagger \hat{c}_{\bar{\alpha}'} \hat{c}_{\alpha'} \quad ,
 \end{aligned} \tag{11.19}$$

with

$$\begin{aligned}
 a_{\alpha\alpha'}^{\mathbf{q},\pm} &= \frac{1}{\hbar} \sqrt{N_{\mathbf{q}} + \frac{1}{2} \pm \frac{1}{2}} g_{\alpha\alpha'}^{\mathbf{q},\pm} \quad , \\
 b_{\alpha\alpha'}^{\mathbf{q},\pm} &= \frac{2}{\hbar} \sqrt{N_{\mathbf{q}} + \frac{1}{2} \pm \frac{1}{2}} g_{\alpha\alpha'}^{\mathbf{q},\pm} \int_{t_0}^t dt' e^{-\frac{(\epsilon_\alpha - \epsilon_{\alpha'} \pm \epsilon_{\mathbf{q}})(t' - t_0)}{i\hbar}} \\
 &\approx 2\pi \sqrt{N_{\mathbf{q}} + \frac{1}{2} \pm \frac{1}{2}} g_{\alpha\alpha'}^{\mathbf{q},\pm} \delta(\epsilon_\alpha - \epsilon_{\alpha'} \pm \epsilon_{\mathbf{q}}) \quad , \\
 a_{\alpha\bar{\alpha}\alpha'\bar{\alpha}'}^{\text{cc}} &= \frac{1}{2\hbar} g_{\alpha\bar{\alpha}\alpha'\bar{\alpha}'} \quad , \\
 b_{\alpha\bar{\alpha}\alpha'\bar{\alpha}'}^{\text{cc}} &= \frac{1}{\hbar} g_{\alpha\bar{\alpha}\alpha'\bar{\alpha}'} \int_{t_0}^t dt' e^{-\frac{(\epsilon_\alpha + \epsilon_{\bar{\alpha}} - \epsilon_{\alpha'} - \epsilon_{\bar{\alpha}'})t'}{i\hbar}} \\
 &\approx 2\pi g_{\alpha\bar{\alpha}\alpha'\bar{\alpha}'} \delta(\epsilon_\alpha + \epsilon_{\bar{\alpha}} - \epsilon_{\alpha'} - \epsilon_{\bar{\alpha}'}) \quad ,
 \end{aligned} \tag{11.20}$$

where $g_{\alpha_1\alpha_2}^{\mathbf{q},\pm}$ and $g_{\alpha\bar{\alpha}\alpha'\bar{\alpha}'}$ are given in Eqs. (1.4) and (1.10) respectively; the coefficients $b_{\alpha\alpha'}^{\mathbf{q},\pm}$ and $b_{\alpha\bar{\alpha}\alpha'\bar{\alpha}'}^{\text{cc}}$ have been approximated in the completed-collision limit, e.g. $t_0 \rightarrow -\infty$ and omitting the energy renormalization contributions arising from the imaginary part of $\int_0^\infty dt'' e^{-\frac{(\epsilon_\alpha + \epsilon_{\bar{\alpha}} - \epsilon_{\alpha'} - \epsilon_{\bar{\alpha}'})t''}{i\hbar}}$, where $t'' = t' - t_0$.

11.3 The single-particle density matrix

Once the electronic reduction in Eq. (11.7) has been made, a further and last step is necessary in order to obtain $\hat{\rho}$ as in Eq. (11.2), e.g. the so-called

single-particle reduction,

$$\rho_{\alpha_1\alpha_2} = \text{Tr} \left[\hat{c}_{\alpha_2}^\dagger \hat{c}_{\alpha_1} \hat{\rho}_c \right] \quad . \quad (11.21)$$

The time derivative of the $\hat{\rho}_{\alpha_1\alpha_2}$ above defined is given by

$$\frac{d\rho_{\alpha_1\alpha_2}}{dt} = \text{Tr} \left[\hat{c}_{\alpha_2}^\dagger \hat{c}_{\alpha_1} \frac{d\hat{\rho}_c}{dt} \right] \quad , \quad (11.22)$$

and, thanks to the many-electron dynamics in Eq. (11.11), may be written as

$$\frac{d\rho_{\alpha_1\alpha_2}}{dt} = \left. \frac{d\rho_{\alpha_1\alpha_2}}{dt} \right|_{\text{sp}} + \left. \frac{d\rho_{\alpha_1\alpha_2}}{dt} \right|_{\text{scat}} \quad . \quad (11.23)$$

The first term in Eq. (11.23) evaluates the free-particle evolution, and is given by the first term of Eq. (5.8),

$$\frac{d\hat{\rho}}{dt} = \frac{1}{i\hbar} \left[\hat{H}^{\text{sp}}, \hat{\rho} \right] \quad , \quad (11.24)$$

where \hat{H}^{sp} has been defined in Eq. (5.9) while $\hat{\rho}$ may be written as

$$\hat{\rho} = \sum_{\alpha_1\alpha_2} \rho_{\alpha_1\alpha_2} |\alpha_1\rangle \langle \alpha_2| \quad : \quad (11.25)$$

since the states $|\alpha\rangle$ in Eq. (11.25) are usually chosen between the eigenstates of the single-particle Hamiltonian \hat{H}^{sp} , Eq. (11.24) may be written as

$$\left. \frac{d\rho_{\alpha_1\alpha_2}}{dt} \right|_{\text{sp}} = \frac{\epsilon_{\alpha_1} - \epsilon_{\alpha_2}}{i\hbar} \rho_{\alpha_1\alpha_2} \quad . \quad (11.26)$$

The evaluation of the second term in Eq. (11.23) depends both on the scattering mechanism considered (such as carrier-phonon or carrier-carrier) and on the model adopted to describe it. In section (2.2) we showed how their closed forms have been one of the main reason for the success of the Markov models. Analogously, we look for a closed form of (11.23): its nontrivial derivation, starting both from conventional Markov models in Eq. (2.23) and from the Lindblad dynamics of Eq. (3.20), will be the main argument of the next section.

11.4 Scattering-induced single-particle dynamics

Applying the single-particle reduction in Eq. (11.21) on the many-electron scattering-induced dynamics in Eqs. (11.17) and (11.18) one obtains

$$\begin{aligned}
 \left. \frac{d\rho_{\alpha_1\alpha_2}}{dt} \right|_{\text{scat}} &= \sum_s \text{tr} \left\{ \hat{c}_{\alpha_2}^\dagger \hat{c}_{\alpha_1} \left(\hat{\mathbf{A}}_c^s \hat{\rho}_c \hat{\mathbf{A}}_c^{s\dagger} - \frac{1}{2} \left\{ \hat{\mathbf{A}}_c^{s\dagger} \hat{\mathbf{A}}_c^s, \hat{\rho}_c \right\} \right) \right\} \\
 &= \frac{1}{2} \sum_s \text{tr} \left\{ \left[\hat{\mathbf{A}}_c^{s\dagger}, \hat{c}_{\alpha_2}^\dagger \hat{c}_{\alpha_1} \right] \hat{\mathbf{A}}_c^s \hat{\rho}_c \right\}_c \\
 &\quad + \frac{1}{2} \sum_s \text{tr} \left\{ \hat{\mathbf{A}}_c^{s\dagger} \left[\hat{c}_{\alpha_2}^\dagger \hat{c}_{\alpha_1}, \hat{\mathbf{A}}_c^s \right] \hat{\rho}_c \right\}_c \\
 &= \frac{1}{2} \sum_s \text{tr} \left\{ \left[\hat{\mathbf{A}}_c^{s\dagger}, \hat{c}_{\alpha_2}^\dagger \hat{c}_{\alpha_1} \right] \hat{\mathbf{A}}_c^s \hat{\rho}_c \right\}_c + \text{H.c.} \quad ,
 \end{aligned} \tag{11.27}$$

where H.c. denotes Hermitian conjugate, and

$$\begin{aligned}
 \left. \frac{d\rho_{\alpha_1\alpha_2}}{dt} \right|_{\text{scat}} &= \frac{1}{2} \sum_s \text{tr} \left\{ \hat{c}_{\alpha_2}^\dagger \hat{c}_{\alpha_1} \left(\hat{\mathbf{a}}_c^s \hat{\rho}_c \hat{\mathbf{b}}_c^{s\dagger} - \hat{\mathbf{a}}_c^{s\dagger} \hat{\mathbf{b}}_c^s \hat{\rho}_c + \text{H.c.} \right) \right\} \\
 &= \frac{1}{2} \sum_s \text{tr} \left\{ \left[\hat{\mathbf{a}}_c^{s\dagger}, \hat{c}_{\alpha_2}^\dagger \hat{c}_{\alpha_1} \right] \hat{\mathbf{b}}_c^s \hat{\rho}_c \right\}_c \\
 &\quad + \frac{1}{2} \sum_s \text{tr} \left\{ \hat{\mathbf{b}}_c^{s\dagger} \left[\hat{c}_{\alpha_2}^\dagger \hat{c}_{\alpha_1}, \hat{\mathbf{a}}_c^s \right] \hat{\rho}_c \right\}_c \quad ,
 \end{aligned} \tag{11.28}$$

respectively. Since the scattering-induced dynamics of $\hat{\rho}$ does not show crossed terms we may consider the carrier-phonon and carrier-carrier mechanisms one by one.

11.4.1 Carrier-phonon mechanism in the mean-field approximation

The operators $\hat{\mathbf{a}}_c^{\mathbf{q}\pm}$, $\hat{\mathbf{b}}_c^{\mathbf{q}\pm}$ and $\hat{\mathbf{A}}_c^{\mathbf{q}\pm}$ which generate the carrier-phonon superoperator in Eqs. (11.19) and (11.14) involve a couple of creation and annihilation operator \hat{c}_α^\dagger , \hat{c}_α . However, thanks to the fermionic commutation relation it is easy to notice that

$$\left[\hat{\mathbf{A}}_c^{\mathbf{q}\pm\dagger}, \hat{c}_{\alpha_2}^\dagger \hat{c}_{\alpha_1} \right] = \sum_{\alpha'} \left(A_{\alpha_2\alpha'}^{\mathbf{q}\pm*} \hat{c}_{\alpha'}^\dagger \hat{c}_{\alpha_1} - A_{\alpha'\alpha_1}^{\mathbf{q}\pm*} \hat{c}_{\alpha_2}^\dagger \hat{c}_{\alpha'} \right) . \tag{11.29}$$

Inserting Eq. (11.29) in the r.h.s. of Eq. (11.27) with $s = \mathbf{q}, \pm$, the latter may be rewritten as

$$\begin{aligned} \left. \frac{d\rho_{\alpha_1\alpha_2}}{dt} \right|_{\text{scat}} &= \frac{1}{2} \sum_{\mathbf{q}\pm} \left(\sum_{\alpha'\alpha'_1\alpha'_2} A_{\alpha_2\alpha'}^{\mathbf{q}\pm*} A_{\alpha'_1\alpha'_2}^{\mathbf{q}\pm} h_{\alpha'\alpha_1, \alpha'_1\alpha'_2} \right. \\ &\quad \left. - \sum_{\alpha'\alpha'_1\alpha'_2} A_{\alpha'\alpha_1}^{\mathbf{q}\pm*} A_{\alpha'_1\alpha'_2}^{\mathbf{q}\pm} h_{\alpha_2\alpha', \alpha'_1\alpha'_2} \right) + \text{H.c.} , \end{aligned} \quad (11.30)$$

where

$$h_{\alpha_3\alpha_4, \alpha'_3\alpha'_4} = \text{tr} \left\{ \hat{c}_{\alpha_3}^\dagger \hat{c}_{\alpha_4} \hat{c}_{\alpha'_3}^\dagger \hat{c}_{\alpha'_4} \hat{\rho}_c \right\}_c . \quad (11.31)$$

As anticipated, the crucial step in order to get a closed equation of motion for the single-particle density matrix consists of performing the well-known mean-field (or correlation-expansion) approximation [56, 95, 96],

$$h_{\alpha_3\alpha_4, \alpha'_3\alpha'_4} = \left(\delta_{\alpha_4\alpha'_3} - \rho_{\alpha_4\alpha'_3} \right) \rho_{\alpha'_4\alpha_3} . \quad (11.32)$$

Finally, inserting the Mean-Field Approximation (11.32) in Eq. (11.30), the (carrier-phonon) scattering-induced dynamics of the single-particle density-matrix element $\rho_{\alpha_1\alpha_2}$ is given by

$$\begin{aligned} \left. \frac{d\rho_{\alpha_1\alpha_2}}{dt} \right|_{\text{scat}} &= \frac{1}{2} \sum_{\mathbf{q}\pm} \sum_{\alpha'\alpha'_1\alpha'_2} (\delta_{\alpha_1\alpha'_1} - \rho_{\alpha_1\alpha'_1}) A_{\alpha'_1\alpha'_2}^{\mathbf{q}\pm} \rho_{\alpha'_2\alpha'} A_{\alpha'\alpha_2}^{\mathbf{q}\pm*} + \text{H.c.} \\ &\quad - \frac{1}{2} \sum_{\mathbf{q}\pm} \sum_{\alpha'\alpha'_1\alpha'_2} A_{\alpha_1\alpha'}^{\mathbf{q}\pm*} (\delta_{\alpha'\alpha'_1} - \rho_{\alpha'\alpha'_1}) A_{\alpha'_1\alpha'_2}^{\mathbf{q}\pm} \rho_{\alpha'_2\alpha_2} + \text{H.c.} + \\ &\quad + \frac{1}{2} \sum_{\mathbf{q}\pm} \sum_{\alpha'_1\alpha'_2} A_{\alpha'_1\alpha'_2}^{\mathbf{q}\pm} \rho_{\alpha'_2\alpha'_1} \sum_{\alpha'} (\rho_{\alpha_1\alpha'} A_{\alpha_2\alpha'}^{\mathbf{q}\pm*} - A_{\alpha'\alpha_1}^{\mathbf{q}\pm*} \rho_{\alpha'\alpha_2}) + \text{H.c.} : \end{aligned} \quad (11.33)$$

this equation may be seen as the matrix representation of the operator equation

$$\begin{aligned} \left. \frac{d\hat{\rho}}{dt} \right|_{\text{scat}} &= \frac{1}{2} \sum_{\mathbf{q}\pm} (\hat{\mathcal{I}} - \hat{\rho}) \hat{A}^{\mathbf{q}\pm} \hat{\rho} \hat{A}^{\mathbf{q}\pm\dagger} - \hat{A}^{\mathbf{q}\pm\dagger} (\hat{\mathcal{I}} - \hat{\rho}) \hat{A}^{\mathbf{q}\pm} \hat{\rho} + \text{H.c.} \\ &\quad + \frac{1}{2} \sum_{\mathbf{q}\pm} \text{Tr} \{ \hat{A}^{\mathbf{q}\pm\dagger} \hat{\rho} \} \left[\hat{A}^{\mathbf{q}\pm}, \hat{\rho} \right] + \text{H.c.} , \end{aligned} \quad (11.34)$$

where $\hat{\rho}$ has been defined in Eq. (11.25) and the single-particle operators and $\hat{A}^{\mathbf{q}\pm}$ may be written as

$$\hat{A}^{\mathbf{q}\pm} = \sum_{\alpha_1\alpha_2} |\alpha_1\rangle A_{\alpha_1\alpha_2}^{\mathbf{q}\pm} \langle\alpha_2| \quad . \quad (11.35)$$

Since the terms in the second line of Eq. (11.34) are all in the form of a commutator between the operator $\text{Tr}\{\hat{A}^{\mathbf{q}\pm\dagger}\hat{\rho}\}\hat{A}^{\mathbf{q}\pm}$ and the single-particle density-matrix operator $\hat{\rho}$ (or H.c.), they may be absorbed in the Liouville-von Neumann term. More in general, all the terms in the form of

$$A_{\alpha\alpha'}^{\mathbf{q}\pm} \rho_{\alpha'\alpha} \quad (11.36)$$

provide energy renormalizations, e.g. contributions to \hat{H}^{sp} in Eq. (11.5). However, since the latters do not contribute to the scattering induced superoperator in Eq. (11.6), they will be omitted from now on.

Summarizing, we have started from the many-body density-matrix operator $\hat{\rho}$ and its Eq. of motion (2.24) with scattering-induced contribution in Eq. (3.20); then, exploiting the reduction to the electronic subsystem, the single-particle reduction and the mean-field approximation in cascade we have found a closed equation of motion for the single-particle density matrix $\hat{\rho}$ in the form of Eq. (11.4), where the scattering superoperator $\bar{\Gamma}(\hat{\rho})$ may be rewritten either as

$$\left. \frac{d\hat{\rho}}{dt} \right|_{\text{scat}} \equiv \bar{\Gamma}(\hat{\rho}) = \frac{1}{2} \sum_{\mathbf{q}\pm} (\hat{\mathcal{I}} - \hat{\rho}) \hat{A}^{\mathbf{q}\pm} \hat{\rho} \hat{A}^{\mathbf{q}\pm\dagger} - \hat{A}^{\mathbf{q}\pm\dagger} (\hat{\mathcal{I}} - \hat{\rho}) \hat{A}^{\mathbf{q}\pm} \hat{\rho} + \text{H.c.} \quad (11.37)$$

where $\hat{\mathcal{I}}$ is the identity operator, or in components as

$$\begin{aligned} \left. \frac{d\rho_{\alpha_1\alpha_2}}{dt} \right|_{\text{scat}} = & \frac{1}{2} \sum_{\alpha'\alpha'_1\alpha'_2} \left((\delta_{\alpha_1\alpha'} - \rho_{\alpha_1\alpha'}) \mathcal{P}_{\alpha'\alpha_2,\alpha'_1\alpha'_2}^s \rho_{\alpha'_1\alpha'_2} \right. \\ & \left. - (\delta_{\alpha'\alpha'_1} - \rho_{\alpha'\alpha'_1}) \mathcal{P}_{\alpha'\alpha'_1,\alpha_1\alpha'_2}^{s*} \rho_{\alpha'_2\alpha_2} \right) + \text{H.c.} \end{aligned} \quad (11.38)$$

with generalized carrier-phonon scattering rates

$$\mathcal{P}_{\alpha_1\alpha_2,\alpha'_1\alpha'_2}^{s=\text{cph}} = \sum_{\mathbf{q}\pm} A_{\alpha_1\alpha'_1}^{\mathbf{q}\pm} A_{\alpha_2\alpha'_2}^{\mathbf{q}\pm*} \quad , \quad (11.39)$$

where $A_{\alpha\alpha'}^{\mathbf{q}\pm}$ have been defined in Eq. (11.20).

Analogously, applying the same procedure to the conventional Born-Markov equation in Eq. (11.18) and omitting any energy-renormalization contributions, the scattering-induced dynamics of $\hat{\rho}$ is given by

$$\left. \frac{d\hat{\rho}}{dt} \right|_{\text{scat}} \equiv \bar{\Gamma}(\hat{\rho}) = \frac{1}{2} \sum_{\mathbf{q}\pm} \left((\hat{\mathcal{I}} - \hat{\rho}) \hat{a}^{\mathbf{q}\pm} \hat{\rho} \hat{b}^{\mathbf{q}\pm\dagger} - \hat{a}^{\mathbf{q}\pm\dagger} (\hat{\mathcal{I}} - \hat{\rho}) \hat{b}^{\mathbf{q}\pm} \hat{\rho} \right) + \text{H.c.} \quad , \quad (11.40)$$

where the single-particle operators $\hat{a}^{\mathbf{q}\pm}$ and $\hat{b}^{\mathbf{q}\pm}$ are defined by

$$\hat{a}^{\mathbf{q}\pm} = \sum_{\alpha_1\alpha_2} a_{\alpha_1\alpha_2}^{\mathbf{q}\pm} |\alpha_1\rangle \langle\alpha_2| \quad , \quad \hat{b}^{\mathbf{q}\pm} = \sum_{\alpha_1\alpha_2} b_{\alpha_1\alpha_2}^{\mathbf{q}\pm} |\alpha_1\rangle \langle\alpha_2| \quad (11.41)$$

with coefficients $a_{\alpha_1\alpha_2}^{\mathbf{q}\pm}$ and $b_{\alpha_1\alpha_2}^{\mathbf{q}\pm}$ defined in Eq. (11.20); the scattering-induced dynamics in Eq. (11.40) may be written in components as Eq. (11.38) with scattering rates given by

$$\mathcal{P}_{\alpha_1\alpha_2,\alpha'_1\alpha'_2}^{s=\text{cph}} = \sum_{\mathbf{q}\pm} a_{\alpha_1\alpha'_1}^{\mathbf{q}\pm} b_{\alpha_2\alpha'_2}^{\mathbf{q}\pm*} \quad . \quad (11.42)$$

In both Eq. (11.37) and (11.40), the factors $(\hat{\mathcal{I}} - \hat{\rho})$ may be considered as a generalization of the Pauli factors $(1 - f_\alpha)$ present in conventional Boltzmann or Pauli Master Equation (1.19): in the low-density limit $(\hat{\mathcal{I}} - \hat{\rho}) \rightarrow \hat{\mathcal{I}}$ the nonlinear superoperators in Eqs. (11.37) and (11.40) become¹

$$\left. \frac{d\hat{\rho}}{dt} \right|_{\text{scat}} \equiv \Gamma(\hat{\rho}) = \sum_{\mathbf{q}\pm} \left(\hat{A}^{\mathbf{q}\pm} \hat{\rho} \hat{A}^{\mathbf{q}\pm\dagger} - \frac{1}{2} \{ \hat{\rho}, \hat{A}^{\mathbf{q}\pm\dagger} \hat{A}^{\mathbf{q}\pm} \} \right) \quad (11.43)$$

and

$$\left. \frac{d\hat{\rho}}{dt} \right|_{\text{scat}} \equiv \Gamma(\hat{\rho}) = \frac{1}{2} \sum_{\mathbf{q}\pm} \left(\hat{a}^{\mathbf{q}\pm} \hat{\rho} \hat{b}^{\mathbf{q}\pm\dagger} - \hat{a}^{\mathbf{q}\pm\dagger} \hat{b}^{\mathbf{q}\pm} \hat{\rho} \right) + \text{H.c.} \quad (11.44)$$

¹We stress that, strictly speaking, in the low-density limit the single-particle density-matrix formalism becomes highly questionable, since in this regime electron-hole Coulomb-correlation dominates. It follows that the use of the Lindblad scattering superoperator in (11.43) is well justified in semiconductor bulk and nanostructured materials characterized by carrier densities sufficiently high to neglect excitonic effects, and sufficiently low to neglect the above non-linear Pauli contributions; as a matter of fact, such requirements are often fulfilled by new-generation semiconductor quantum devices.

respectively. As anticipated, the low-density limit of the nonlinear scattering superoperator $\bar{\Gamma}(\hat{\rho})$ of Eqs. (11.37) and (11.40) becomes linear, as the operator $\Gamma(\hat{\rho})$ in Eq. (5.8). The comparison between the scattering-induced dynamics in Eqs. (11.43) and (11.44) shows how only the former is of Lindblad type, e.g. in the form

$$\left. \frac{d\hat{\rho}}{dt} \right|_{\text{scat}} \equiv \Gamma(\hat{\rho}) = \sum_s \left(\hat{A}^s \hat{\rho} \hat{A}^{s\dagger} - \frac{1}{2} \{ \hat{\rho}, \hat{A}^{s\dagger} \hat{A}^s \} \right), \quad (11.45)$$

thus being able to guarantee the complete-positivity of the electronic subsystems. As we will show in Chap 12, this difference between conventional and novel Markov approximations has tremendous effects also at high carrier densities, where neither of the two superoperators in Eqs. (11.37) and (11.40) furnish a Lindblad dynamics; nevertheless, the former is able to guarantee the positivity of $\hat{\rho}$, contrary to the latter.

11.4.2 The Carrier-Carrier mechanism in the mean-field approximation

The many-electrons dynamics induced by the carrier-carrier mechanism is given by Eq. (11.27) with $\hat{\mathbf{A}}^s = \hat{\mathbf{A}}_c^{\text{cc}}$, where the latter have been defined in Eqs. (11.15), (3.22). Inserting the equality (see Eq. (11.29) for comparison with the carrier-quasiparticle case)

$$\begin{aligned} \left[\hat{\mathbf{A}}_c^{\text{cc}\dagger}, \hat{c}_{\alpha_2}^\dagger \hat{c}_{\alpha_1} \right] &= \sum_{\alpha \bar{\alpha} \alpha'} \mathcal{A}_{\alpha' \alpha_2, \alpha \bar{\alpha}}^{\text{cc}*} \hat{c}_\alpha^\dagger \hat{c}_{\bar{\alpha}}^\dagger \hat{c}_{\alpha_1} \hat{c}_{\alpha'} \\ &- \sum_{\bar{\alpha} \alpha' \bar{\alpha}'} \mathcal{A}_{\alpha' \bar{\alpha}', \alpha_1 \bar{\alpha}}^{\text{cc}*} \hat{c}_{\alpha_2}^\dagger \hat{c}_{\bar{\alpha}}^\dagger \hat{c}_{\bar{\alpha}'} \hat{c}_{\alpha'} \end{aligned} \quad (11.46)$$

in the r.h.s. of Eq. (11.27), the latter becomes

$$\begin{aligned} \left. \frac{d\rho_{\alpha_1\alpha_2}}{dt} \right|_{\text{scat}} = & \left(\frac{1}{4} \sum_{\substack{\bar{\alpha}\bar{\alpha}' \\ \alpha'_1\alpha'_2\alpha'_3\alpha'_4}} \mathcal{A}_{\alpha'\alpha_2,\alpha\bar{\alpha}}^{\text{cc}*} \mathcal{A}_{\alpha'_1\alpha'_2\alpha'_3\alpha'_4}^{\text{cc}} k_{\alpha\bar{\alpha}\alpha_1\alpha',\alpha'_1\alpha'_2\alpha'_4\alpha'_3} \right. \\ & \left. - \frac{1}{4} \sum_{\substack{\bar{\alpha}\alpha' \\ \alpha'_1\alpha'_2\alpha'_3\alpha'_4}} \mathcal{A}_{\alpha'\bar{\alpha}',\alpha_1\bar{\alpha}}^{\text{cc}*} \mathcal{A}_{\alpha'_1\alpha'_2\alpha'_3\alpha'_4}^{\text{cc}} k_{\alpha_2\bar{\alpha}\bar{\alpha}',\alpha',\alpha'_1\alpha'_2\alpha'_4\alpha'_3} \right) + \text{H.c.} , \end{aligned} \quad (11.47)$$

where k is the four-particle correlation function

$$k_{\alpha_5\alpha_6\alpha_7\alpha_8,\alpha'_5\alpha'_6\alpha'_7\alpha'_8} = \text{tr} \left\{ \hat{c}_{\alpha_5}^\dagger \hat{c}_{\alpha_6}^\dagger \hat{c}_{\alpha_7} \hat{c}_{\alpha_8} \hat{c}_{\alpha'_5}^\dagger \hat{c}_{\alpha'_6}^\dagger \hat{c}_{\alpha'_7} \hat{c}_{\alpha'_8} \hat{\rho}_c \right\}_c ; \quad (11.48)$$

the latter may be mean-field approximated (see Eq. (11.32) for comparison) as

$$\begin{aligned} k_{\alpha_5\alpha_6\alpha_7\alpha_8,\alpha'_5\alpha'_6\alpha'_7\alpha'_8} = & \left(\rho_{\alpha'_7\alpha_6} \rho_{\alpha'_8\alpha_5} - \rho_{\alpha'_8\alpha_6} \rho_{\alpha'_7\alpha_5} \right) \times \\ & \times \left[\left(\delta_{\alpha_8\alpha'_5} - \rho_{\alpha_8\alpha'_5} \right) \left(\delta_{\alpha_7\alpha'_6} - \rho_{\alpha_7\alpha'_6} \right) \right. \\ & \left. - \left(\delta_{\alpha_7\alpha'_5} - \rho_{\alpha_7\alpha'_5} \right) \left(\delta_{\alpha_8\alpha'_6} - \rho_{\alpha_8\alpha'_6} \right) \right] . \end{aligned} \quad (11.49)$$

Inserting Eq. (11.49) in Eq. (11.47) and omitting self-contracting terms, e.g. contributions proportional to structures in the form of (see Eq. (11.36) for comparisons)

$$\mathcal{A}_{\alpha\alpha'\bar{\alpha}\bar{\alpha}'}^{\text{cc}} \rho_{\bar{\alpha}''\alpha''} \quad , \text{ with } \bar{\alpha}'' = \bar{\alpha}, \bar{\alpha}', \text{ and } \alpha'' = \alpha, \alpha' \quad (11.50)$$

(or H. c.), which once-again give rise to renormalization effects, the carrier-carrier induced dynamics on the single-particle density-matrix elements $\rho_{\alpha_1\alpha_2}$ may be written as in Eq. (11.38) with generalized scattering-rates

$$\mathcal{P}_{\alpha_1\alpha_2,\alpha'_1\alpha'_2}^{\text{s=cc}} = 2 \sum_{\bar{\alpha}_1\bar{\alpha}_2,\bar{\alpha}'_1\bar{\alpha}'_2} (\delta_{\bar{\alpha}_2\bar{\alpha}_1} - \rho_{\bar{\alpha}_2\bar{\alpha}_1}) \mathcal{A}_{\alpha_1\bar{\alpha}_1,\alpha'_1\bar{\alpha}'_1}^{\text{cc}} \mathcal{A}_{\alpha_2\bar{\alpha}_2,\alpha'_2\bar{\alpha}'_2}^{\text{cc}*} \rho_{\bar{\alpha}'_1\bar{\alpha}'_2} . \quad (11.51)$$

It is worth stressing that, differently from the generalized carrier-phonon rates in (11.39), the generalized carrier-carrier rates in (11.51) are themselves a function of the single-particle density matrix; this is a clear fingerprint of the two-body nature of the carrier-carrier interaction which

prohibits a direct operator interpretation such as in Eq. (11.37). It is straightforward to show that the conventional Markov approximation of Eq. (11.18) with $\hat{\mathbf{a}}_c^{\text{cc}}$ and $\hat{\mathbf{b}}_c^{\text{cc}}$ given in Eqs. (11.19) leads to the (carrier-carrier) scattering-induced dynamics in Eq. (11.38) with generalized scattering-rates

$$\mathcal{P}_{\alpha_1\alpha_2,\alpha'_1\alpha'_2}^{s=\text{cc}} = 2 \sum_{\bar{\alpha}_1\bar{\alpha}_2,\bar{\alpha}'_1\bar{\alpha}'_2} (\delta_{\bar{\alpha}_2\bar{\alpha}_1} - \rho_{\bar{\alpha}_2\bar{\alpha}_1}) a_{\alpha_1\bar{\alpha}_1,\alpha'_1\bar{\alpha}'_1}^{\text{cc}} b_{\alpha_2\bar{\alpha}_2,\alpha'_2\bar{\alpha}'_2}^{\text{cc}*} \rho_{\bar{\alpha}'_1\bar{\alpha}'_2}, \quad (11.52)$$

where the coefficients $a_{\alpha_1\bar{\alpha}_1,\alpha'_1\bar{\alpha}'_1}^{\text{cc}}$ and $b_{\alpha_2\bar{\alpha}_2,\alpha'_2\bar{\alpha}'_2}^{\text{cc}}$ have been defined in Eq. (11.20).

A closer inspection of Eqs. (11.38) and (11.51) or (11.52) confirms the two-body nature of the carrier-carrier interaction. Indeed, differently from the carrier-phonon scattering, in this case the density-matrix equation describes the time evolution of a so-called “main carrier”, whose density-matrix elements are labelled by α indices, interacting with a so-called “partner carrier” with density-matrix elements labelled by the overlined indices $\bar{\alpha}$ —this will be particularly evident within the diagonal limit introduced in Chap 13, see Eqs. (13.2) and (13.4).

11.4.3 In- vs Out-Scattering contributions

The scattering-induced dynamics in Eqs. (11.38) as well as their low-density limits in Eqs. (11.43) and (11.44) may be rewritten as the difference between so-called *in-* and *out-scattering* terms

$$\left. \frac{d\rho_{\alpha_1\alpha_2}}{dt} \right|_{\text{scat}} = F_{\alpha_1\alpha_2}^{\text{in}} - F_{\alpha_1\alpha_2}^{\text{out}}, \quad (11.53)$$

where $F_{\alpha_1\alpha_2}^{\text{in/out}}$ are defined in terms of the generalized scattering rates of, depending on the scattering mechanism and of the model used to describe them, Eqs. (11.39), (11.42), (11.51) and (11.52), and

- (i) in the case of the superoperators $\bar{\Gamma}(\hat{\rho})$ of Eqs. (11.37) and (11.40) they are nonlinear functions of the single-particle density matrix,

$$F_{\alpha_1\alpha_2}^{\text{in}} = \sum_s \sum_{\alpha'\alpha'_1\alpha'_2} (\delta_{\alpha_1\alpha'} - \rho_{\alpha_1\alpha'}) \mathcal{P}_{\alpha'\alpha_2,\alpha'_1\alpha'_2}^s \rho_{\alpha'_1\alpha'_2} \quad (11.54)$$

and

$$F_{\alpha_1\alpha_2}^{\text{out}} = \frac{1}{2} \sum_s \sum_{\alpha'_1\alpha'_2} (\delta_{\alpha'_1\alpha'} - \rho_{\alpha'_1\alpha'}) \mathcal{P}_{\alpha'_1\alpha',\alpha_1\alpha'_2}^{s*} \rho_{\alpha'_2\alpha_2} + \text{H.c.} \quad ; \quad (11.55)$$

(ii) in the case of the superoperators $\Gamma(\hat{\rho})$ of Eqs. (11.43) and (11.44) they are linear functions of the single-particle density matrix,

$$F_{\alpha_1\alpha_2}^{\text{in}} = \sum_s \sum_{\alpha'_1\alpha'_2} \mathcal{P}_{\alpha_1\alpha_2,\alpha'_1\alpha'_2}^s \rho_{\alpha'_1\alpha'_2} \quad (11.56)$$

and

$$F_{\alpha_1\alpha_2}^{\text{out}} = \frac{1}{2} \sum_s \sum_{\alpha'_1\alpha'_2} \mathcal{P}_{\alpha'_1\alpha'_1,\alpha_1\alpha'_2}^{s*} \rho_{\alpha'_2\alpha_2} + \text{H.c.} \quad . \quad (11.57)$$

The in/out nature of the scattering-induced dynamics has some interesting features, in fact

- (i) as we will show in Chap. 13, their diagonal limit reproduces the in/out scattering-dynamics provided by the Pauli master Equations in (1.19) and (1.18), while in a more correct semiclassical limit (exploited by means of the Wigner function) it recovers the Boltzmann collision term of Eq. (1.14), which displays in/out contributions as well;
- (ii) as it will be shown in Chap. 14, the separation in Eq. (11.53) has a key role in the phenomenon of quantum nonlocality.

11.5 Single-particle description of Spatially Open System

In what follows we extend the proposed single-particle treatment to quantum systems with spatially open boundaries, namely to the case of a quantum device electrically connected to one or more external carrier reservoirs. To this end, in analogy to the system factorization between electronic and phononic degrees of freedom in (11.8), we shall describe the global carrier system (device plus reservoirs) as the product of a device density-matrix operator times a quasiequilibrium density-matrix operator $\hat{\rho}_r^\circ$ corresponding to one or more carrier reservoirs:

$$\hat{\rho}_c = \hat{\rho}_d \otimes \hat{\rho}_r^\circ \quad . \quad (11.58)$$

The quantum-mechanical coupling between device and external reservoirs ($s \equiv \text{dr}$) may conveniently be described via the following interaction Hamiltonian

$$\hat{\mathbf{H}}^{\text{dr}} = \sum_{\alpha\beta} \left(\gamma_{\alpha\beta} \hat{c}_{\alpha}^{\dagger} \hat{\xi}_{\beta} + \gamma_{\alpha\beta}^{*} \hat{\xi}_{\beta}^{\dagger} \hat{c}_{\alpha} \right) , \quad (11.59)$$

where $\hat{c}_{\alpha}^{\dagger}$ (\hat{c}_{α}) are now creation (destruction) operators acting on the device single-particle states α , while $\hat{\xi}_{\beta}^{\dagger}$ ($\hat{\xi}_{\beta}$) denote creation (destruction) operators acting on the reservoir single-particle states β . Here, the first contribution describes carrier injection ($\beta \rightarrow \alpha$) via the destruction of a carrier in state β and the creation of a carrier in state α , while the second one describes carrier loss ($\alpha \rightarrow \beta$) via the inverse process. Moreover, the physical properties of the device-reservoir interaction Hamiltonian in (11.59) are dictated by the explicit form of the coupling matrix elements $\gamma_{\alpha\beta}$; the latter, in general, are given by a properly weighted spatial overlap between device and reservoir single-particle wavefunctions.

Following the general prescription in (3.21), the Lindblad operator corresponding to the device-reservoir interaction Hamiltonian (11.59) depends on the carrier coordinates only, and is always of the form

$$\hat{\mathbf{A}}_c^{\text{dr}} = \sum_{\alpha\beta} \left(A_{\alpha\beta}^{\text{dr}} \hat{c}_{\alpha}^{\dagger} \hat{\xi}_{\beta} + A_{\alpha\beta}^{\text{dr}*} \hat{\xi}_{\beta}^{\dagger} \hat{c}_{\alpha} \right) . \quad (11.60)$$

The evaluation of the single-particle dynamics induced by the above device-reservoir coupling may be performed following the very same steps of the corresponding carrier-phonon and carrier-carrier treatments previously considered. In particular, it is easy to realize that the single-particle contribution in Eq. (11.27) due to device-reservoir coupling involves average values of two device plus two reservoir creation/destruction operators. More specifically, in view of the device-reservoir factorization in (11.58) as well as of the typical quasiequilibrium nature of the reservoirs, one obtains

$$\text{tr} \left\{ \hat{c}_{\alpha_2}^{\dagger} \hat{c}_{\alpha_1} \hat{\xi}_{\beta_2}^{\dagger} \hat{\xi}_{\beta_1} \hat{\rho}_c \right\} = \rho_{\alpha_1\alpha_2} \rho_{\beta_1\beta_2}^{\circ} , \quad (11.61)$$

where $\rho_{\alpha_1\alpha_2}$ is the single-particle density matrix of the device and

$$\rho_{\beta_1\beta_2}^{\circ} = f_{\beta_1}^{\circ} \delta_{\beta_1\beta_2} \quad (11.62)$$

is the (diagonal) single-particle density matrix of the quasiequilibrium carrier reservoirs.

Employing the device-reservoir factorization result in (11.61), a straightforward calculation shows that the contribution to the system evolution due to the device-reservoir coupling Hamiltonian (11.59) is

$$\left. \frac{d\rho_{\alpha_1\alpha_2}}{dt} \right|_{\text{dr}} = \frac{1}{2} \sum_{\beta} \left(\mathcal{P}_{\alpha_1\alpha_2,\beta\beta}^{\text{dr}} f_{\beta}^{\circ} - \sum_{\alpha'} \mathcal{P}_{\alpha_1\alpha',\beta\beta}^{\text{dr}} \rho_{\alpha'\alpha_2} \right) + \text{H.c.} \quad (11.63)$$

with generalized scattering rates

$$\mathcal{P}_{\alpha_1\alpha_2,\beta_1\beta_2}^{\text{dr}} = A_{\alpha_1\beta_1}^{\text{dr}} A_{\alpha_2\beta_2}^{\text{dr}*} . \quad (11.64)$$

In the semiclassical limit (see Eq. (13.1)), the above device-reservoir scattering superoperator reduces to the relaxation-time model

$$\left. \frac{df_{\alpha}}{dt} \right|_{\text{dr}} = - \sum_{\beta} P_{\alpha\beta}^{\text{dr}} (f_{\alpha} - f_{\beta}^{\circ}) \quad (11.65)$$

with device-reservoir scattering rates

$$P_{\alpha\beta}^{\text{dr}} = \mathcal{P}_{\alpha\alpha,\beta\beta}^{\text{dr}} = \left| A_{\alpha\beta}^{\text{dr}} \right|^2 . \quad (11.66)$$

It is worth stressing that the above semiclassical equation, usually referred to as the injection-loss model, has been widely employed in the semiclassical modeling of optoelectronic semiconductor devices. [97]

In order to gain more insight on the structure of the density-matrix equation (11.63), the latter may conveniently be rewritten in a compact operatorial form; more specifically, recalling the definition of the single-particle density-matrix operator in (11.25) and introducing the device-reservoir coupling operators

$$\hat{A}_{\beta} = \sum_{\alpha} |\alpha\rangle A_{\alpha\beta}^{\text{dr}} \langle\beta| \quad (11.67)$$

as well as the reservoir density-matrix operator

$$\hat{\rho}^{\circ} = \sum_{\beta} |\beta\rangle f_{\beta}^{\circ} \langle\beta| , \quad (11.68)$$

one gets:

$$\left. \frac{d\hat{\rho}}{dt} \right|_{\text{scat}} = \sum_{\beta} \left(\hat{A}_{\beta} \hat{\rho}^{\circ} \hat{A}_{\beta}^{\dagger} - \frac{1}{2} \{ \hat{A}_{\beta} \hat{A}_{\beta}^{\dagger}, \hat{\rho} \} \right) . \quad (11.69)$$

Equation (11.69) should be compared to the Lindblad superoperator in Eq.(11.37) describing energy exchange with the phononic excitations. On the one end, the device-reservoir superoperator (11.69) is inhomogeneous, due to the presence of the density-matrix operator $\hat{\rho}^\circ$ of the external reservoirs. This implies that the trace of the device density matrix $\hat{\rho}$ is not conserved, as expected in a system that can exchange particles with the reservoirs.

The analysis presented so far can be regarded as a formal derivation of the Lindblad-like device-reservoir scattering superoperator recently proposed in Ref. [77], where the reservoir states are plane waves ($|\beta\rangle = |k\rangle$) and the device single-particle states are the scattering states of the confinement potential profile ($|\alpha\rangle = |\alpha_k\rangle$).

Chapter 12

Study of the positivity

Primary goal of this section is to face the most important issue related to the proposed kinetic treatment: the positivity analysis of the nonlinear density-matrix equation in (11.38). Indeed, if the single-particle density matrix describes a physical state, its eigenvalues are necessarily positive-definite and not greater than one (Pauli exclusion principle); in order to preserve such physical nature, it is imperative that the scattering-induced time evolution preserves the values of the density-matrix eigenvalues within the interval $[0, 1]$.

To this aim, let us start considering the case of carrier-phonon interaction previously discussed, whose nonlinear equation in (11.38) (equipped with the generalized rates in (11.39)) may also be easily rewritten in a more compact way via the one-electron operators respectively in Eqs. (11.25) and (11.35) as in Eq. (11.37). Importantly, due to the quantum-mechanical Pauli factors $(\hat{\mathcal{I}} - \hat{\rho})$, the scattering superoperator in Eq. (11.37) is nonlinear in $\hat{\rho}$ and non-Lindblad.¹ Only in the low-density limit, i.e. $\hat{\mathcal{I}} - \hat{\rho} \rightarrow \hat{\mathcal{I}}$, the nonlinear equation in Eq. (11.37) reduces to the Lindblad superoperator in Eq. (11.43) and the positive-definite character of $\hat{\rho}$ is thereby ensured; as already stressed, this is not verified for the conventional Markov approximation in Eq. (11.40), whose low-density limit in Eq. (11.44) is not

¹Indeed, at any time t Eq. (11.37) can always be locally linearized [25] treating the two Pauli factors $(\hat{\mathcal{I}} - \hat{\rho})$ as input parameters; however, the resulting (time-dependent) linear superoperator is definitely non-Lindblad.

in a Lindblad form. At finite or high densities, no straightforward conclusion can be drawn about the positive-definite character of the generic time-dependent solution $\hat{\rho}(t)$.

Nevertheless, we show now that the proposed nonlinear single-particle equation in (11.38) does preserve the positive-definite character of $\hat{\rho}$. In order to prove that, let us describe the single-particle density matrix $\rho_{\alpha_1\alpha_2}$ via the corresponding operator $\hat{\rho}$ in (11.25); at any time t it is possible to define its instantaneous (i.e., time-dependent) eigenvalues Λ_λ and eigenvectors $|\lambda\rangle$ according to

$$\hat{\rho}|\lambda\rangle = \Lambda_\lambda|\lambda\rangle, \quad (12.1)$$

which implies that

$$\Lambda_\lambda = \langle\lambda|\hat{\rho}|\lambda\rangle. \quad (12.2)$$

The eigenvalues Λ_λ in (12.1) of a single-particle density matrix $\hat{\rho}$ describing a physical state are necessarily positive-definite and not greater than one (Pauli exclusion principle). In order to preserve such positive-definite nature, it is imperative that the scattering-induced time evolution maintains the values of the eigenvalues within the physical interval $[0, 1]$; this can be verified by studying the time derivative of the generic eigenvalue in (12.2), namely:

$$\frac{d\Lambda_\lambda}{dt} = \frac{d\langle\lambda|}{dt}\hat{\rho}|\lambda\rangle + \langle\lambda|\frac{d\hat{\rho}}{dt}|\lambda\rangle + \langle\lambda|\hat{\rho}\frac{d|\lambda\rangle}{dt}. \quad (12.3)$$

In view of the completeness of the basis set $\{|\lambda\rangle\}$, the time derivative in (12.3) can also be written as:

$$\begin{aligned} \frac{d\Lambda_\lambda}{dt} &= \sum_{\lambda'} \frac{d\langle\lambda|}{dt}|\lambda'\rangle\langle\lambda'|\hat{\rho}|\lambda\rangle \\ &+ \langle\lambda|\frac{d\hat{\rho}}{dt}|\lambda\rangle \\ &+ \sum_{\lambda'} \langle\lambda|\hat{\rho}|\lambda'\rangle\langle\lambda'|\frac{d|\lambda\rangle}{dt}. \end{aligned} \quad (12.4)$$

Recalling that

$$\langle\lambda|\hat{\rho}|\lambda'\rangle = \Lambda_\lambda\delta_{\lambda\lambda'}, \quad (12.5)$$

the result in (12.4) reduces to

$$\frac{d\Lambda_\lambda}{dt} = \Lambda_\lambda \frac{d\langle\lambda|}{dt}|\lambda\rangle + \langle\lambda|\frac{d\hat{\rho}}{dt}|\lambda\rangle + \Lambda_\lambda \langle\lambda|\frac{d|\lambda\rangle}{dt}. \quad (12.6)$$

Taking into account that

$$\frac{d\langle\lambda|}{dt}|\lambda\rangle + \langle\lambda|\frac{d|\lambda\rangle}{dt} = \frac{d\langle\lambda|\lambda\rangle}{dt} = 0 , \quad (12.7)$$

the first and third term in (12.6) cancel out exactly, and one finally concludes that

$$\frac{d\Lambda_\lambda}{dt} = \langle\lambda|\frac{d\hat{\rho}}{dt}|\lambda\rangle = \frac{d\rho_{\lambda\lambda}}{dt} . \quad (12.8)$$

This shows that the time variation of the eigenvalues Λ_λ coincides with the time variation of the diagonal elements $\rho_{\lambda\lambda}$ of the operator $\hat{\rho}$ within the instantaneous eigenbasis $\{|\lambda\rangle\}$.

In order to evaluate the above time derivative, the crucial step is to analyze the explicit form of the proposed single-particle scattering superoperator written in the density-matrix eigenbasis of Eq. (12.1). Taking into account that the generic density-matrix equation (11.38) is basis-independent, by replacing the original single-particle basis $\{|\alpha\rangle\}$ with the density-matrix eigenbasis $\{|\lambda\rangle\}$ and making use of Eq. (12.5), its diagonal elements turn out to be:

$$\frac{d\rho_{\lambda\lambda}}{dt} = \sum_{\lambda'} [(1 - \Lambda_\lambda)P_{\lambda\lambda'}^s\Lambda_{\lambda'} - (1 - \Lambda_{\lambda'})P_{\lambda'\lambda}^s\Lambda_\lambda] , \quad (12.9)$$

where

$$P_{\lambda\lambda'}^s = \mathcal{P}_{\lambda\lambda,\lambda'\lambda'}^s \quad (12.10)$$

are positive-definite quantities given by the diagonal elements of the generalized scattering rates (see Eqs. (11.39) and (11.51)) written in our instantaneous density-matrix eigenbasis. By inserting this last result into Eq. (12.8), one finally gets

$$\frac{d\Lambda_\lambda}{dt} = \sum_{\lambda'} [(1 - \Lambda_\lambda)P_{\lambda\lambda'}^s\Lambda_{\lambda'} - (1 - \Lambda_{\lambda'})P_{\lambda'\lambda}^s\Lambda_\lambda] . \quad (12.11)$$

This last result is highly non-trivial: it states that, in spite of the partially coherent nature of the carrier dynamics in (11.38), the time evolution of the eigenvalues Λ_λ is governed by a non-linear Boltzmann-type equation, formally identical to the semiclassical result in (13.2).

We are now in the position to state that the physical interval $[0, 1]$ is the only possible variation range of our eigenvalues Λ_λ . To this end, one can show that, when the latter approach the extremal values, 0 or 1, their

time derivatives do not allow them to exit the interval. Indeed, a closer inspection of the Boltzmann-like equation in (12.11) shows that:

- (i) if one of the eigenvalues Λ_λ is equal to zero, the corresponding time derivative in (12.11) is always non-negative;
- (ii) if one of the eigenvalues Λ_λ is equal to one, its time derivative in (12.11) is always non-positive.

This leads us to the important conclusion that, for both carrier-phonon and carrier-carrier scattering, the proposed nonlinear single-particle equation (11.38) preserves the positive-definite character of the single-particle density matrix.

We finally stress that the above positivity analysis is based on the fact that the scattering rates in (12.10) are positive-definite quantities. This property, which applies to the proposed single-particle equation (obtained starting from the scattering superoperator in (3.20)), is generally not fulfilled by conventional Markov models. In particular, for the case of carrier-phonon scattering, the nonlinear equation (11.40) is not intrinsically positive-definite, as confirmed by the fact that in the low-density limit the latter reduces to the non-Lindblad form of Eq. (11.44). Since the generalized scattering rates corresponding to the above non-Lindblad superoperator are given in Eq. (11.42), within the eigenbasis $\{|\lambda\rangle\}$ their diagonal elements (see Eqs. (11.42) and (12.10))

$$P_{\lambda\lambda'}^{\text{cph}} = \mathcal{P}_{\lambda\lambda,\lambda'\lambda'}^{\text{s=cph}} = \sum_{\mathbf{q}^\pm} a_{\lambda\lambda'}^{\mathbf{q}^\pm} b_{\lambda\lambda'}^{\mathbf{q}^{\pm*}} \quad (12.12)$$

are not necessarily positive-definite. This is the reason why, starting from a non-Lindblad many-body scattering model, the system dynamics may exit the physical eigenvalue region, giving rise to positivity violations also in the low-density limit. [1, 98]

To emphasize this point, in Fig. 12.1 we report the time evolution of the density-matrix eigenvalues for a subset of simulated experiments in the simple case of a two-level system. The evolutions in both panel are governed by Eq. (11.23), where the eigenergies in Eq. (11.26) are randomly generated (with uniform distribution) between 0 and $\hbar\omega_0$ (ω_0 denoting the typical single-particle energy scale in units of \hbar), and the explicit form of the last

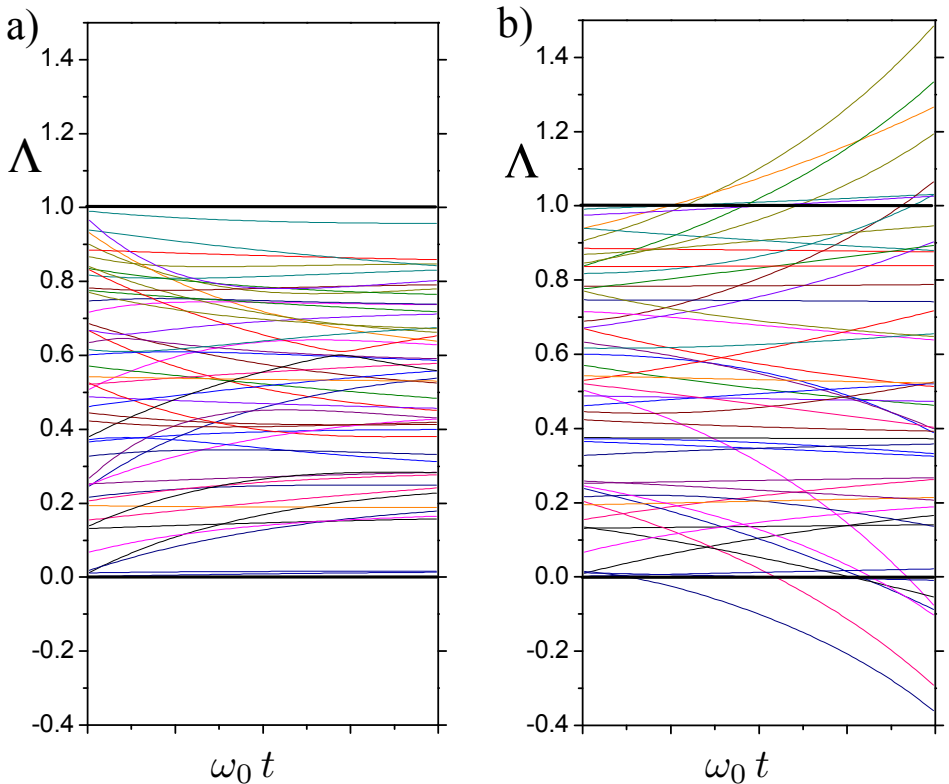


Figure 12.1. Density-matrix eigenvalues as a function of time for a subset of 25 randomly generated evolutions corresponding to a simple two-level system in the presence of carrier-phonon interaction. Comparison between the proposed single-particle model in (11.37) (panel a) and the conventional model in (11.40) (panel b) (see text).

term is given by the non-linear scattering superoperator in (11.38) with generalized carrier-phonon scattering rates of the form

$$\mathcal{P}_{\alpha_1\alpha_2,\alpha'_1\alpha'_2}^{s=\text{cph}} = A_{\alpha_1\alpha'_1} B_{\alpha_2\alpha'_2}^* , \quad (12.13)$$

where $A_{\alpha_1\alpha_2}$ and $B_{\alpha_1\alpha_2}$ are random complex numbers, whose modulus and phase are uniformly generated between 0 and $\sqrt{\omega_0}$ and 0 and 2π , respectively. In particular, while for mimicking conventional Markov models the two carrier-phonon operators A and B are generated independently (see

Eq. (11.42)), in simulating the proposed scattering superoperator we take $A_{\alpha_1\alpha_2} = B_{\alpha_1\alpha_2}$ (see Eq. (11.39)).

Our simulated experiments are based on a numerical solution of the density-matrix equation (11.23), starting each simulated experiment from a randomly selected single-particle density matrix $\rho_{\alpha_1\alpha_2}(t=0) = P_{\alpha_1}\delta_{\alpha_1\alpha_2}$, where P_α are randomly generated (with uniform distribution) between 0 and 1; more specifically, the free single-particle rotation in (11.26) has been treated exactly, while the scattering-induced dynamics has been evaluated via a standard time-step integration scheme. [25]

As one can see, while for the proposed nonlinear equation in (11.37) all the eigenvalue trajectories fall within the physical interval $[0, 1]$ (see panel a)), for the nonlinear equation in (11.40) a significant number of simulated eigenvalue trajectories exit the physical interval (panel b)).

Similarly, thanks to its Lindblad-like structure also the open-system dynamics in Eq. (11.69) guarantees the positivity; in fact, the latter may be written in components in terms of the eigenbasis $\{\lambda\}$ of the device density-matrix operator $\hat{\rho}$ (keeping unchanged the reservoir basis $\{\beta\}$) as

$$\left. \frac{d\Lambda_\lambda}{dt} \right|_{\text{scat}} = \sum_{\beta} (f_{\beta}^{\circ} - \Lambda_\lambda) \|A_{\lambda\beta}^{\text{dr}}\|^2 \quad , \quad (12.14)$$

with

$$A_{\lambda\beta}^{\text{dr}} = \sum_{\alpha} u_{\lambda\alpha}^* A_{\alpha\beta}^{\text{dr}} \quad , \quad (12.15)$$

where $u_{\lambda\alpha}$ are the elements of the unitary matrix which is responsible for the change of basis $\{\alpha\} \rightarrow \{\lambda\}$, e.g.

$$|\lambda\rangle = \sum_{\alpha} u_{\lambda\alpha} |\alpha\rangle \quad . \quad (12.16)$$

A closer inspection of the injection-loss equation in (12.14) shows that:

- (i) if one of the eigenvalues Λ_λ is equal to zero, the factor $f_{\beta}^{\circ} - \Lambda_\lambda$ is always non-negative for every reservoir state $|\beta\rangle$ (and hence the corresponding time derivative in (12.11));
- (ii) if one of the eigenvalues Λ_λ is equal to one, the factor $f_{\beta}^{\circ} - \Lambda_\lambda$ is always non-positive for every reservoir state $|\beta\rangle$ (and hence the corresponding time derivative in (12.11)).

As a consequence, due to its Lindblad-like structure the proposed linear single-particle equation (11.38) description of open-systems preserves the positive-definite character of the single-particle density matrix.

Chapter 13

The Semiclassical limit

Extending the scattering-free discussion of Sec 6.2 and Eq. (6.31), we are now ready to complete the link between the semiclassical or Boltzmann theory of Eq. (1.12) and the single-particle density-matrix formalism (see Eq. (11.6)). As discussed in the fundamental solid-state text-book by Ashcroft and Mermin, [21] a general and rigorous (i.e. quantum-mechanical) derivation of the standard semiclassical charge-transport theory constitutes a formidable task. The simplest approach to this tedious problem —usually referred to as the “diagonal limit”— is to neglect all non-diagonal density matrix elements, which implies to assume a single-particle density matrix of the form [25]

$$\rho_{\alpha_1\alpha_2} = f_{\alpha_1} \delta_{\alpha_1\alpha_2} \quad . \quad (13.1)$$

From a physical point of view, this amounts to assume that the impact of various energy dissipation versus decoherence phenomena is so strong to suppress at any time all inter-state ($\alpha_1 \neq \alpha_2$) quantum-mechanical phase coherence. By inserting the diagonal-limit prescription (13.1) into Eq. (11.38), the latter assumes the expected nonlinear Boltzmann-type or Pauli Master Equation form (see Eq. (1.19))

$$\left. \frac{df_\alpha}{dt} \right|_{\text{scat}} = \sum_{s=\text{cph,cc}} \sum_{\alpha'} ((1 - f_\alpha) P_{\alpha\alpha'}^s f_{\alpha'} - (1 - f_{\alpha'}) P_{\alpha'\alpha}^s f_\alpha) \quad (13.2)$$

with semiclassical carrier-phonon scattering rates

$$P_{\alpha\alpha'}^{s=\text{cp}} = \mathcal{P}_{\alpha\alpha,\alpha'\alpha'}^{s=\text{cp}} = \sum_{\mathbf{q},\pm} \left| A_{\alpha\alpha'}^{\mathbf{q}\pm} \right|^2 \quad (13.3)$$

and semiclassical carrier-carrier scattering rates

$$P_{\alpha\alpha'}^{s=cc} = \mathcal{P}_{\alpha\alpha,\alpha'\alpha'}^{s=cc} = 2 \sum_{\bar{\alpha}\bar{\alpha}'} (1 - f_{\bar{\alpha}}) \left| \mathcal{A}_{\alpha\bar{\alpha},\alpha'\bar{\alpha}'}^{cc} \right|^2 f_{\bar{\alpha}'} . \quad (13.4)$$

The above semiclassical limit shows once again that the nonlinearity factors $(\delta_{\alpha_1\alpha_2} - \rho_{\alpha_1\alpha_2})$ in Eqs. (11.51) and (11.42) can be regarded as the quantum-mechanical generalization of the Pauli factors $(1 - f_{\alpha})$ of the conventional Boltzmann theory (see also Sec. 1.3).

Indeed, the Boltzmann-like equation in (13.2) can be regarded as the formal justification and starting point of a wide variety of Monte Carlo simulations of charge transport in semiconductor nanostructures, whose main microscopic ingredients are the carrier wavefunctions $\psi_{\alpha}(\mathbf{r})$ as well as the corresponding scattering rates $P_{\alpha\alpha'}$ obtained via the Fermi's golden rule.

In spite of the success of such Boltzmann-like treatment applied to the study of the steady-state electro-optical response of semiconductor nanodevices, [99–110] the latter is not able to describe the time-dependent evolution of the spatial carrier density. This can be easily understood by defining the spatial charge density $n(\mathbf{r})$ in terms of the single-particle density matrix $\hat{\rho}$ (rather than using the Wigner function as in Eq. (5.6)) as

$$n(\mathbf{r}) = \sum_{\alpha_1\alpha_2} \psi_{\alpha_1}(\mathbf{r}) \rho_{\alpha_1\alpha_2} \psi_{\alpha_2}^*(\mathbf{r}) \quad ; \quad (13.5)$$

within the diagonal approximation of Eq. (13.1) the latter reduces to

$$n(\mathbf{r}) = \sum_{\alpha} |\psi_{\alpha}(\mathbf{r})|^2 f_{\alpha} . \quad (13.6)$$

This tells us that for the particular case of a bulk system —the one considered in the conventional Boltzmann theory— the single-particle basis states $|\alpha\rangle$ are momentum eigenstates, whose probability density $|\psi_{\alpha}(\mathbf{r})|^2$ is space-independent. It follows that for a bulk system the carrier density $n(\mathbf{r})$ corresponding to the above diagonal-limit picture is space-independent as well.

The obvious conclusion is that the diagonal-approximation scheme just recalled does not allow one to recover the space-dependent Boltzmann theory. Nevertheless, as already stressed, a number of simulation strategies [69, 85, 86, 99–110] based on such diagonal-approximation paradigm came out to

be quite successful in describing the steady-state electro-optical response of various semiconductor nanomaterials and devices; this is particularly true in the presence of a strong energy dissipation and decoherence, since in this case the latter dominate over scattering-free carrier diffusion (not properly described within the diagonal-approximation picture).

In order to perform a derivation of the conventional Boltzmann transport equation, it is thus vital to replace the above diagonal-approximation scheme with a genuine space-dependent description of the problem; this may be conveniently performed once again via the Wigner picture, completing the scattering-free discussion of Sec. 6.2 with the semiclassical limit of the many-particle contributions, while we will omit the treatments of the device-reservoir interactions of Eq. (11.69) (which has been omitted also in Eq. (1.12), where the normalization of the distribution $\int d\mathbf{r}d\mathbf{v}f(\mathbf{r}, \mathbf{v})$ was constant in time)¹. In particular, we start from the low-density superoperator (11.45), whose corresponding matrix elements can be conveniently expressed as in Eq. (11.53) with in and out contribution given in Eqs. (11.56) and (11.57). Next, we consider the Wigner function defined in Eq. (5.1) and its equation of motion (5.12) with superoperator Γ defined in Eq. (11.45).

In order to discuss the so-called semiclassical limit, which will prove to recover the Boltzmann transport equation, we consider the (formal) limit for $\hbar \rightarrow 0$ of the Wigner transport theory. As far as the single-particle contribution in Eq. (6.6) is concerned, this limit has already been discussed in Sec. (6.2) in terms of the well-known Moyal brackets, [64] which for $\hbar \rightarrow 0$ reduce to the usual diffusion-plus-drift terms of the Boltzmann theory (see Eq. (1.14) in Sec. (1.3)).

The most difficult task of the semiclassical limit is to show that for $\hbar \rightarrow 0$ the (spatially non-local) scattering superoperator in (5.14) reduces to the (spatially local) collision term of the Boltzmann theory. In order

¹As a consequence, the limitations of the inflowing boundary-conditions analyzed in Secs. (7.2) and (9.3) do not apply to the Wigner-function analysis presented in this Chapter, since the latter refers to an infinitely extended system and not to a quantum device with open spatial boundaries.

to complete this task, the first step is to rewrite the Wigner scattering superoperator in (5.16) with $\Gamma(\hat{\rho})$ of Eq. (11.45) within the momentum representation. More specifically, denoting with

$$A^s(\mathbf{p}_1, \mathbf{p}_2) = \langle \mathbf{p}_1 | \hat{A}^s | \mathbf{p}_2 \rangle \quad (13.7)$$

the (continuous) matrix elements of the Lindblad operators in (11.45) and taking into account that

$$\langle \mathbf{p}_1 | \hat{W}(\mathbf{r}, \mathbf{p}) | \mathbf{p}_2 \rangle = e^{\frac{(\mathbf{p}_1 - \mathbf{p}_2) \cdot \mathbf{r}}{i\hbar}} \delta\left(\frac{\mathbf{p}_1 + \mathbf{p}_2}{2} - \mathbf{p}\right), \quad (13.8)$$

the explicit form of the scattering superoperator in (5.16) with $\Gamma(\hat{\rho})$ of Eq. (11.45) comes out to be

$$\begin{aligned} \Gamma(\mathbf{r}, \mathbf{p}; \mathbf{r}', \mathbf{p}') &= \left(\frac{2}{\pi\hbar}\right)^3 \sum_s \int d\mathbf{p}_1 d\mathbf{p}_2 e^{\frac{2(\mathbf{p}_1 - \mathbf{p}_2 + \mathbf{p}' - \mathbf{p}) \cdot \mathbf{r}}{i\hbar}} e^{-\frac{2(\mathbf{p}_2 - \mathbf{p}') \cdot (\mathbf{r}' - \mathbf{r})}{i\hbar}} \times \\ &\quad \times A^s(2\mathbf{p} - \mathbf{p}_1, 2\mathbf{p}' - \mathbf{p}_2) A^{s*}(\mathbf{p}_1, \mathbf{p}_2) \\ &- \left(\frac{2}{\pi\hbar}\right)^3 \sum_s \Re \left\{ \int d\mathbf{p}_1 d\mathbf{p}_2 e^{\frac{2(\mathbf{p}' - \mathbf{p}) \cdot \mathbf{r}}{i\hbar}} e^{-\frac{2(\mathbf{p}_1 - \mathbf{p}') \cdot (\mathbf{r}' - \mathbf{r})}{i\hbar}} \times \right. \\ &\quad \left. \times A^{s*}(\mathbf{p}_2, 2\mathbf{p} - \mathbf{p}_1) A^s(\mathbf{p}_2, 2\mathbf{p}' - \mathbf{p}_1) \right\}. \end{aligned} \quad (13.9)$$

By inserting the above result into Eq. (5.14), one gets:

$$\begin{aligned} \left. \frac{\partial f^W(\mathbf{r}, \mathbf{p})}{\partial t} \right|_{\text{scat}} &= \left(\frac{2}{\pi\hbar}\right)^3 \sum_s \int d\mathbf{r}' d\mathbf{p}' d\mathbf{p}_1 d\mathbf{p}_2 e^{\frac{2(\mathbf{p}_1 - \mathbf{p}_2 + \mathbf{p}' - \mathbf{p}) \cdot \mathbf{r}}{i\hbar}} e^{-\frac{2(\mathbf{p}_2 - \mathbf{p}') \cdot (\mathbf{r}' - \mathbf{r})}{i\hbar}} \times \\ &\quad \times A^s(2\mathbf{p} - \mathbf{p}_1, 2\mathbf{p}' - \mathbf{p}_2) A^{s*}(\mathbf{p}_1, \mathbf{p}_2) f^W(\mathbf{r}', \mathbf{p}') \\ &- \left(\frac{2}{\pi\hbar}\right)^3 \sum_s \Re \left\{ \int d\mathbf{r}' d\mathbf{p}' d\mathbf{p}_1 d\mathbf{p}_2 e^{\frac{2(\mathbf{p}' - \mathbf{p}) \cdot \mathbf{r}}{i\hbar}} e^{-\frac{2(\mathbf{p}_1 - \mathbf{p}') \cdot (\mathbf{r}' - \mathbf{r})}{i\hbar}} \times \right. \\ &\quad \left. \times A^{s*}(\mathbf{p}_2, 2\mathbf{p} - \mathbf{p}_1) A^s(\mathbf{p}_2, 2\mathbf{p}' - \mathbf{p}_1) f^W(\mathbf{r}', \mathbf{p}') \right\}. \end{aligned} \quad (13.10)$$

Let us now analyze the semiclassical limit of the above quantum-mechanical scattering superoperator. From a physical point of view, in the limit $\hbar \rightarrow 0$ the various phase factors entering Eq. (13.10) will display infinitely fast oscillations, which allows one to evaluate some of the above coordinate and

momentum integrals via a sort of adiabatic-decoupling procedure. As far as the coordinate \mathbf{r}' is concerned, for any regular function $F(\mathbf{r})$ we have:

$$\lim_{\hbar \rightarrow 0} \int d\mathbf{r}' e^{\frac{\mathbf{p}'' \cdot (\mathbf{r}' - \mathbf{r})}{i\hbar}} F(\mathbf{r}') = (2\pi\hbar)^3 \delta(\mathbf{p}'') F(\mathbf{r}) . \quad (13.11)$$

By employing this general property, in the semiclassical limit ($\hbar \rightarrow 0$) the scattering superoperator in (13.10) simplifies to:

$$\begin{aligned} \left. \frac{\partial f^W(\mathbf{r}, \mathbf{p})}{\partial t} \right|_{\text{scat}} &= 8 \sum_s \int d\mathbf{p}' d\mathbf{p}_1 e^{\frac{2(\mathbf{p}_1 - \mathbf{p}) \cdot \mathbf{r}}{i\hbar}} A^s(2\mathbf{p} - \mathbf{p}_1, \mathbf{p}') A^{s*}(\mathbf{p}_1, \mathbf{p}') f^W(\mathbf{r}, \mathbf{p}') \\ &\quad - 8 \sum_s \Re \left\{ \int d\mathbf{p}' d\mathbf{p}_2 e^{\frac{2(\mathbf{p}' - \mathbf{p}) \cdot \mathbf{r}}{i\hbar}} A^{s*}(\mathbf{p}_2, 2\mathbf{p} - \mathbf{p}') A^s(\mathbf{p}_2, \mathbf{p}') f^W(\mathbf{r}, \mathbf{p}') \right\} . \end{aligned} \quad (13.12)$$

In addition to the spatial adiabatic decoupling in (13.11), in the semiclassical limit it is also possible to show that for any regular function $G(\mathbf{r}, \mathbf{p})$:

$$\lim_{\hbar \rightarrow 0} \int d\mathbf{p}'' e^{\frac{(\mathbf{p}'' - \mathbf{p}) \cdot \mathbf{r}}{i\hbar}} G(\mathbf{r}, \mathbf{p}'') = \frac{(2\pi\hbar)^3}{\Omega} G(\mathbf{r}, \mathbf{p}) . \quad (13.13)$$

Here Ω denotes a proper crystal normalization volume; indeed, in order to derive this result it is crucial to perform a sort of spatial coarse graining, i.e., a spatial average of the function G over a volume Ω much larger than the typical carrier coherence length and much smaller than the macroscopic spatial variations of our material. By employing the general property in (13.13) the scattering superoperator in (13.12) reduces to:

$$\begin{aligned} \left. \frac{\partial f^W(\mathbf{r}, \mathbf{p})}{\partial t} \right|_{\text{scat}} &= \frac{(2\pi\hbar)^3}{\Omega} \sum_s \int d\mathbf{p}' \times \\ &\quad \times \left[|A^s(\mathbf{p}, \mathbf{p}')|^2 f^W(\mathbf{r}, \mathbf{p}') - |A^s(\mathbf{p}', \mathbf{p})|^2 f^W(\mathbf{r}, \mathbf{p}) \right] . \end{aligned} \quad (13.14)$$

This is exactly the Boltzmann collision term of the semiclassical theory we were looking for; indeed, the latter can be written in a more compact form according to Eq. (1.14), where

$$P(\mathbf{p}, \mathbf{p}') = \sum_s P^s(\mathbf{p}, \mathbf{p}') \quad (13.15)$$

and

$$P^s(\mathbf{p}, \mathbf{p}') = \frac{(2\pi\hbar)^3}{\Omega} |A^s(\mathbf{p}, \mathbf{p}')|^2 . \quad (13.16)$$

This shows that the scattering rates of the Boltzmann transport theory can be easily expressed in terms of the matrix elements of the various Lindblad operators.

In order to establish a direct link with the conventional Fermi's-golden-rule prescription, let us finally move from the continuous momentum representation employed so far to its discrete version corresponding to the crystal normalization volume Ω ; more precisely, employing the usual continuous-versus-discrete prescription, the scattering rates in (13.16) can also be written as

$$P_{\mathbf{p}, \mathbf{p}'}^s = \left| A_{\mathbf{p}, \mathbf{p}'}^s \right|^2 , \quad (13.17)$$

in total agreement with the low-density limit, e.g. $(1 - f_\alpha) \rightarrow 1$, of diagonal-approximation result in (13.4).

Chapter 14

Quantum nonlocality

The goal of this chapter is to provide a rigorous treatment of scattering nonlocality, e.g. a non-null scattering-induced charge-density variation,

$$\left. \frac{\partial n(\mathbf{r})}{\partial t} \right|_{\text{scat}} \neq 0 \quad , \quad (14.1)$$

where $n(\mathbf{r})$ has been defined in terms of $\hat{\rho}$ in Eq. (13.5). It is important to stress that such a phenomenon is a genuine quantum-mechanical feature: in fact, as already stressed in Sec. (1.3), the semiclassical Boltzmann-Equation (1.14) does not provide a scattering-induced charge-density variation (see Eq. (1.17)).

Thanks to Eq. (11.4) the time variation of $n(\mathbf{r})$ given in Eq. (13.5) may be written as

$$\frac{\partial n(\mathbf{r})}{\partial t} = \left. \frac{\partial n(\mathbf{r})}{\partial t} \right|_{\text{sp}} + \left. \frac{\partial n(\mathbf{r})}{\partial t} \right|_{\text{scat}} \quad . \quad (14.2)$$

Here as in the following we will explore the low-density limit, where the single-particle density-matrix equation of motion is given by (5.8) and hence the terms in the r.h.s. of Eq. (14.2) are given by

$$\left. \frac{\partial n(\mathbf{r})}{\partial t} \right|_{\text{sp}} = \frac{1}{i\hbar} \sum_{\alpha_1 \alpha_2} \psi_{\alpha_1}(\mathbf{r})(\epsilon_{\alpha_1} - \epsilon_{\alpha_2}) \rho_{\alpha_1 \alpha_2} \psi_{\alpha_2}^*(\mathbf{r}) \quad (14.3)$$

and

$$\left. \frac{\partial n(\mathbf{r})}{\partial t} \right|_{\text{scat}} = \sum_{\alpha_1 \alpha_2} \psi_{\alpha_1}(\mathbf{r}) \Gamma(\hat{\rho})_{\alpha_1 \alpha_2} \psi_{\alpha_2}^*(\mathbf{r}) \quad . \quad (14.4)$$

In order to show the genuine quantum nonlocality we will concentrate on the linear operator $\Gamma(\hat{\rho})$ given in Eq. (11.43), while we will disregard the one in Eq. (11.44) due to the fact that it does not preserve the positivity. However, we will compare the results with those coming from another widely employed model for describing the dissipation and decoherence in semiconductors, the Relaxation Time Approximation (RTA): as we will show in the following, the latter displays some unphysical features, contrary to the Lindblad superoperator.

14.1 Physical model and simulation strategy

As prototypical physical system we shall consider an effective one-dimensional GaN-based nanostructure, whose main energy-dissipation and decoherence mechanism is carrier-LO phonon scattering. The latter will be described via the low-density Lindblad scattering superoperator in (11.43) with $s = q, \pm$ and $\hat{A}^{q,\pm}$ given in Eq. (11.35) after replacing the three-dimensional wavevector \mathbf{q} with the one-dimensional index q .

It is imperative to stress that the choice of considering a simple one-dimensional model is by no means dictated by computational limits; indeed, opposite to more refined quantum-kinetic approaches, the proposed simulation strategy may be easily applied to realistic nanostructures within a fully three-dimensional description, as recently realized in Ref. [77]. We just decided to adopt a one-dimensional system in order to facilitate the analysis of scattering-induced spatial nonlocality, and to better elucidate its physical origin and magnitude.

For the case of a one-dimensional system with coordinate z and momentum p , the space (see Eq. (13.5)) and momentum charge distributions are simply given by

$$n(z) = \sum_{\alpha_1 \alpha_2} \psi_{\alpha_1}(z) \rho_{\alpha_1 \alpha_2} \psi_{\alpha_2}^*(z) \quad (14.5)$$

and

$$n(p) = \sum_{\alpha_1 \alpha_2} \tilde{\psi}_{\alpha_1}(p) \rho_{\alpha_1 \alpha_2} \tilde{\psi}_{\alpha_2}^*(p), \quad (14.6)$$

where $\tilde{\psi}_{\alpha}(p) \equiv \langle p | \alpha \rangle$ denotes the Fourier transform of $\psi_{\alpha}(z)$.

Combining the prescription in (14.5) with the density-matrix equation

(5.10), the total time evolution of the spatial carrier density $n(z)$ is described via the one-dimensional versions ($\mathbf{r} \rightarrow z$) of Eqs. (14.2)-(14.4). As already pointed out in Chap. 13, for the relevant case of the Lindblad superoperator in (11.53) the corresponding time evolution can be expressed as the difference of two terms, which in the semiclassical limit reduce to the in- minus out-scattering structure of the conventional Boltzmann theory (see Eq. (1.14)). This suggests to write the one-dimensional version of Eq. (14.4) as

$$\left. \frac{\partial n(z)}{\partial t} \right|_{\text{scat}} = F^{\text{in}}(z) - F^{\text{out}}(z) \quad (14.7)$$

with

$$F^{\text{in/out}}(z) = \sum_{\alpha_1 \alpha_2} \psi_{\alpha_1}(z) F_{\alpha_1 \alpha_2}^{\text{in/out}} \psi_{\alpha_2}^*(z). \quad (14.8)$$

Our simulation strategy is based on a numerical solution of the density-matrix equation in (5.10); this is realized via a fixed-time-step discretization [25] based on an exact integration of the single-particle dynamics. More specifically, the single-particle states α of the structure under examination are described via the usual envelope-function picture (see Sec. 1.1) within the standard effective-mass approximation, [111] in terms of a plane-wave expansion. [25]

In order to mimic the main features of a realistic GaN-based material, the following parameters have been employed: effective mass $m^* = 0.2m_o$ (m_o denoting the free-electron one) and LO-phonon energy $\epsilon_{\text{LO}} = 80$ meV; moreover, the amplitude of the carrier-phonon matrix elements in Eq. (1.4) are chosen such to reproduce an average bulk carrier-LO phonon scattering rate $\tau_{\text{LO}} = 25$ fs.

For all the simulated experiments presented below we have chosen as initial condition a single-particle density matrix $\bar{\rho}_{\alpha_1 \alpha_2}$ corresponding to a gaussian carrier distribution both in space and momentum, namely

$$\bar{n}(z) \propto \frac{e^{-\frac{z^2}{2\bar{\Delta}_z}}}{\sqrt{2\pi} \bar{\Delta}_z}, \quad \bar{n}(p) \propto \frac{e^{-\frac{p^2}{2\bar{\Delta}_p}}}{\sqrt{2\pi} \bar{\Delta}_p}, \quad (14.9)$$

where $\bar{\Delta}_z$ describes the degree of spatial localization of our initial state, and $\bar{\Delta}_p = \sqrt{m^* k_B T}$ describes the thermal fluctuations of our carrier gas.

It is easy to show that such initial condition corresponds to a one-dimensional Wigner function

$$\bar{f}^W(z, p) \propto \hbar \frac{e^{-\frac{z^2}{2\bar{\Delta}_z^2}} e^{-\frac{p^2}{2\bar{\Delta}_p^2}}}{\sqrt{2\pi} \bar{\Delta}_z \bar{\Delta}_p}, \quad (14.10)$$

and therefore to an initial density matrix

$$\bar{\rho}_{\alpha_1\alpha_2} \propto \frac{1}{2\pi} \int dz dp W_{\alpha_1\alpha_2}(z, p) \frac{e^{-\frac{z^2}{2\bar{\Delta}_z^2}} e^{-\frac{p^2}{2\bar{\Delta}_p^2}}}{\sqrt{2\pi} \bar{\Delta}_z \bar{\Delta}_p}, \quad (14.11)$$

where $W_{\alpha_1\alpha_2}(z, p)$ are the one-dimensional analogues of $W_{\alpha_1\alpha_2}(\mathbf{r}, \mathbf{p})$ defined in Eq. (5.19).¹

Primary goal of our simulated experiments is to investigate the non-local character of the Lindblad-like scattering superoperator in (11.53), and to compare it with other scattering models. The simplest parameter-free form of the scattering term entering our density-matrix equation (5.10) is given by the following RTA model: [77]

$$\left. \frac{d\rho_{\alpha_1\alpha_2}}{dt} \right|_{\text{scat}} = -\frac{\Gamma_{\alpha_1} + \Gamma_{\alpha_2}}{2} (\rho_{\alpha_1\alpha_2} - \rho_{\alpha_1\alpha_2}^\circ). \quad (14.12)$$

Here $\rho_{\alpha_1\alpha_2}^\circ = f_{\alpha_1}^\circ \delta_{\alpha_1\alpha_2}$ is the equilibrium density matrix dictated by the host material, and

$$\Gamma_\alpha = \sum_s \sum_{\alpha'} P_{\alpha'\alpha}^s \quad (14.13)$$

is the *total scattering rate* (i.e., summed over all final states α' and relevant interaction mechanisms s) corresponding to the microscopic transition probabilities $P_{\alpha'\alpha}^s$ of the semiclassical transport theory given by the standard Fermi's golden rule. [112] Within such relaxation-time paradigm, the

¹We stress that the (mixed-state) density matrix in (14.11) is not always physical; indeed, it is possible to show that the uncertainty principle imposes the following restriction: $\bar{\Delta}_z \geq \frac{\hbar}{2\bar{\Delta}_p}$. Recalling that $\bar{\Delta}_p = \sqrt{m^* k_B T}$, it follows that at room temperature and for the GaN parameters previously recalled, one gets: $\bar{\Delta}_z \geq \frac{\hbar}{2\sqrt{m^* k_B T}} \simeq 2 \text{ nm}$.

diagonal contributions ($\alpha_1 = \alpha_2$) describe population transfer (and thus energy dissipation) toward the equilibrium carrier distribution $f_{\alpha_1}^o$ according to the relaxation rate Γ_{α_1} , whereas the off-diagonal contributions ($\alpha_1 \neq \alpha_2$) describe a decay of the inter-state polarizations according to the decoherence rate $(\Gamma_{\alpha_1} + \Gamma_{\alpha_2})/2$.

In spite of its simple form and straightforward physical interpretation, the structure of the relaxation-time term (14.12) is intrinsically different from the in- minus out-structure of the Boltzmann collision term as well as of the Lindblad superoperator in (11.53), and for this reason it may lead to a significant overestimation of decoherence processes (see below).

14.2 Scattering nonlocality in homogeneous GaN systems

Our first set of room-temperature simulated experiments corresponds to an effective (one-dimensional) homogeneous GaN system (i.e., no confinement potential profile along the z direction).

Let us start our analysis by investigating the carrier-LO phonon scattering nonlocality induced by the Lindblad superoperator in (11.53). Figure 14.1 shows the scattering-induced time derivative of the spatial carrier density (see Eq. (14.7)) as a function of the relative coordinate $z/\bar{\Delta}_z$ for three different values of the localization parameter $\bar{\Delta}_z$. As we can see, in the presence of an initial nanometric confinement (solid and dashed curves) the phonon-induced time variation is significantly different from zero; the latter displays a negative peak —corresponding to a sort of replica of the initial distribution— and, more importantly, a positive contribution extending over a much larger range. This is exactly the signature of scattering-induced spatial nonlocality we were looking for. By significantly increasing the value of $\bar{\Delta}_z$ (dash-dotted curve), the magnitude and relative spatial extension of such nonlocality effects is strongly reduced, thus confirming that in the semiclassical limit $\bar{\Delta}_z \rightarrow \infty$ the scattering-induced time variation tends to zero, as predicted by the conventional Boltzmann theory (see Sec. 1.3).

In order to better understand the physical origin and relative magnitude of the positive versus negative regions in Fig. 14.1, let us examine separately the impact of in- and out-scattering terms (see Eq. (14.7)). Figure 14.2

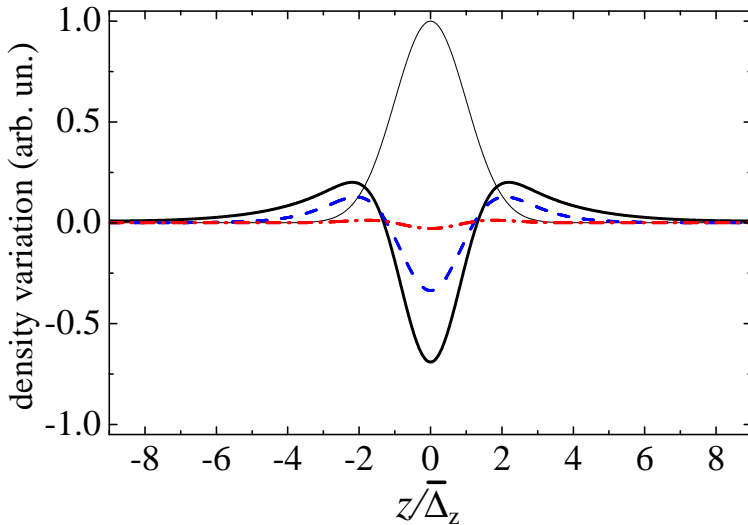


Figure 14.1. Room-temperature carrier-LO phonon scattering nonlocality induced by the Lindblad superoperator in Eq. (11.53) in a homogeneous GaN system: scattering-induced time derivative of the spatial carrier density (see Eq. (14.7)) as a function of the relative coordinate $z/\bar{\Delta}_z$ for three different values of the localization parameter: $\bar{\Delta}_z = 5$ nm (solid curve), $\bar{\Delta}_z = 10$ nm (dashed curve), and $\bar{\Delta}_z = 50$ nm (dash-dotted curve), together with the initial spatial density profile in Eq. (14.9) (thin solid curve) (see text).

shows in- (panel a) and out-scattering contributions (panel b) corresponding to the time derivatives of the spatial carrier density (see Eq. (14.7)) reported in Fig. 14.1. As we can see, in the presence of an initial nanometric confinement (solid and dashed curves) the in-scattering contribution (panel a) is significantly larger than the initial distribution profile (see thin solid curve in Fig. 14.1) while, in contrast, the out-scattering contribution (panel b) comes out to be more localized. It is exactly such different spatial extension of in- and out-scattering contributions that gives rise to the density-variation profiles in Fig. 14.1; in particular, the significant delocalization of the in-scattering contribution (compared to the out-scattering

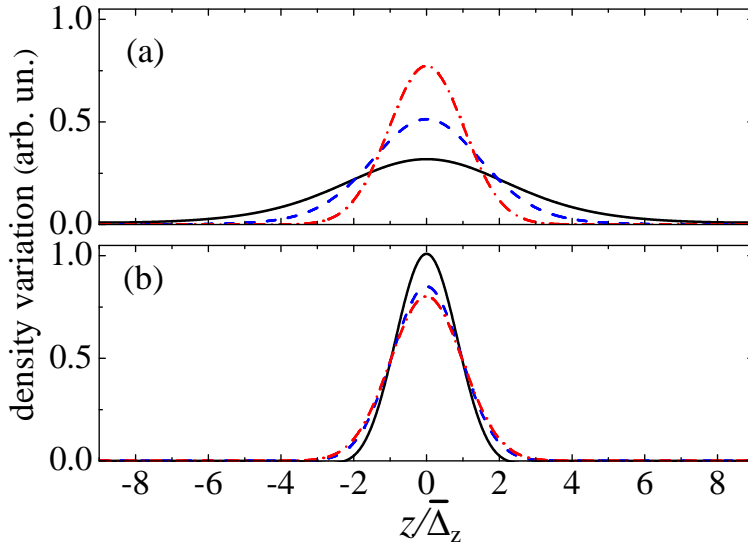


Figure 14.2. Room-temperature carrier-LO phonon scattering nonlocality induced by the Lindblad superoperator in Eq. (11.53) in a homogeneous GaN system: in- (panel a) and out-scattering contributions (panel b) corresponding to the time derivatives of the spatial carrier density (see Eq. (14.7)) reported in Fig. 14.1 (see text).

one) is responsible (i) of the negative central peak, and (ii) of the two positive external regions.² By significantly increasing the value of $\overline{\Delta}_z$ (dash-dotted curves), in- and out-scattering contributions tend to coincide, which implies that their difference tends to vanish, in total agreement with the corresponding result in Fig. 14.1 (dash-dotted curve). This clearly shows that the local character of the Boltzmann theory (see Eq. (1.17)) originates from an exact cancellation between in- and out-scattering contributions, which takes place in the semiclassical limit (i.e., $\overline{\Delta}_z \rightarrow \infty$) only.

Based on the numerical results presented so far, it is easy to conclude that the impact of scattering nonlocality is intimately related to the different

²It is worth stressing that, in view of the trace-preserving character of the Lindblad superoperator (11.43), the total carrier density (i.e., integrated over the spatial coordinate z) is preserved; this implies that the positive and negative regions in Fig. 14.1 should cancel each other out.

spatial extension of in- and out-scattering contributions. In order to better quantify the phenomenon under examination, it is useful to introduce the effective nonlocality parameter

$$\eta^{\text{in/out}} = \frac{1}{\bar{\Delta}_z} \sqrt{\frac{\int z^2 |F^{\text{in/out}}(z)| dz}{\int |F^{\text{in/out}}(z)| dz}}. \quad (14.14)$$

According to its definition, this dimensionless parameter can be regarded as the standard deviation of the spatial density variation $F^{\text{in/out}}(z)$ (see Eq. (14.7)) in units of $\bar{\Delta}_z$. It follows that when the shape of the density variation $F^{\text{in/out}}(z)$ tends to the initial Gaussian profile (see dash-dotted curves in Fig. 14.2), the nonlocality parameter $\eta^{\text{in/out}}$ in (14.14) tends to one; moreover, for charge variations wider than the initial distribution (see solid and dashed curves in Fig. 14.2a) the nonlocality parameter is expected to be greater than one, while for charge variations sharper than the initial distribution (see solid and dashed curves in Fig. 14.2b) the latter is expected to be smaller than one.

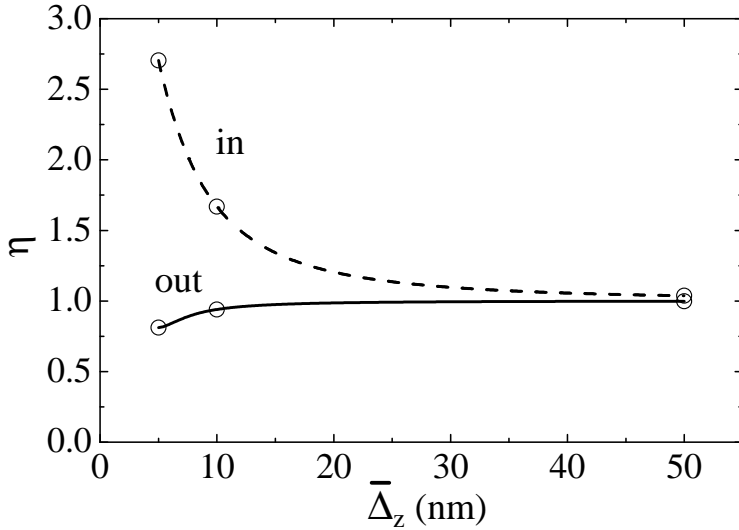


Figure 14.3. Nonlocality parameter in Eq. (14.14) as a function of $\bar{\Delta}_z$ for both in- and out-scattering contributions. Here, the 5 nm, 10 nm, and 50 nm values (see symbols) correspond to the in- and out-scattering profiles of Fig. 14.2 (see text).

This scenario is fully confirmed by the numerical results reported in Fig. 14.3, where the nonlocality parameter in (14.14) is plotted as a function of $\bar{\Delta}_z$ for both in- and out-scattering contributions (here, the two curves have been obtained repeating our numerical calculation for a large set of $\bar{\Delta}_z$ values). As we can see, in the presence of a strong spatial confinement ($\bar{\Delta}_z = 5$ nm) (see solid curves in Fig. 14.2) the nonlocality parameter of the in-scattering term is definitely greater than one, while for the out-scattering term the latter is significantly smaller than one. By increasing the value of $\bar{\Delta}_z$, the difference between in- and out-parameters is progressively reduced, and for $\bar{\Delta}_z = 50$ nm (see dash-dotted curves in Fig. 14.2) their value is already very close to unity.

The homogeneous-GaN simulated experiments presented so far allows one to draw two basic conclusions: (i) in the presence of a nanometric spatial confinement one deals with a significant carrier-phonon scattering nonlocality (see solid curve in Fig. 14.1); (ii) opposite to other simplified scattering models (see below), the Lindblad superoperator of Eq. (11.43) is able to properly reproduce the semiclassical-limit behavior (see dash-dotted curve in Fig. 14.1), thus recovering the local character of the Boltzmann collision term.

At this point it is crucial to compare the action of the Lindblad scattering superoperator (11.53) (see Fig. 14.1) with that of simplified dissipation models, and in particular with the conventional relaxation-time approximation. Figure 14.4 shows the scattering-induced time derivative of the spatial carrier density corresponding to the relaxation-time model in (14.12) as a function of the relative coordinate $z/\bar{\Delta}_z$ for the same three values of the localization parameter $\bar{\Delta}_z$ considered in Fig. 14.1. As we can see, also for the case of the relaxation-time model one deals with significant nonlocality effects. However, comparing Fig. 14.4 with Fig. 14.1, it is easy to recognize strong differences between the Lindblad treatment and the relaxation-time approximation: opposite to the Lindblad-superoperator results of Fig. 14.1, here the shape and amplitude of the charge-density variation is not strongly influenced by the value of $\bar{\Delta}_z$; more importantly, while in Fig. 14.1 the positive regions are spatially localized (i.e., they display a maximum and then vanish at large distances), here the charge variation tends to a constant and $\bar{\Delta}_z$ -independent value. This constitutes an unambiguous proof of the intrinsic limitations of the relaxation-time approximation; indeed, opposite to the Lindblad-superoperator treatment, the latter (i) comes out to be

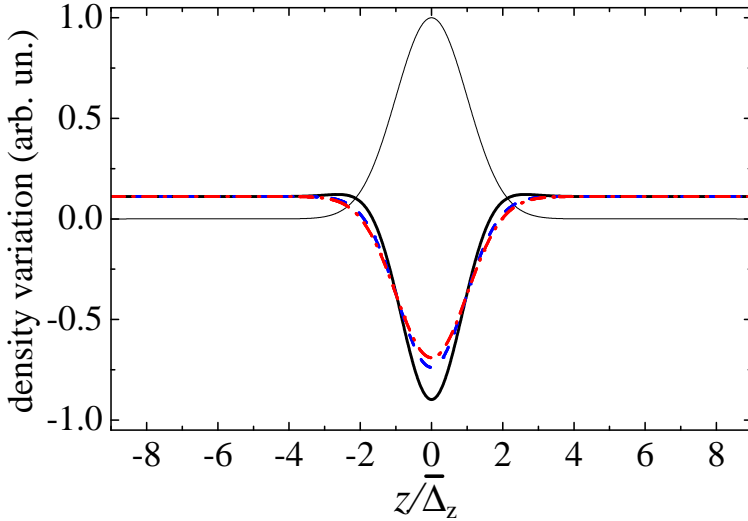


Figure 14.4. Same as in Fig. 14.1 but for the relaxation-time model in Eq. (14.12) (see text).

totally non-local (as confirmed by its nearly constant values at large coordinate values),³ and (ii) in the semiclassical limit ($\bar{\Delta}_z \rightarrow \infty$) it is intrinsically unable to reproduce the local character of the Boltzmann collision term.

As we shall see, the totally non-local character of the relaxation-time model may give rise to a strong overestimation of the scattering-induced quantum diffusion (see Figs. 15.2 and 15.3 in the next chapter).

³Indeed, for the relaxation-time model in (14.12) it is not possible to introduce a nonlocality parameter (see Eq. (14.14)), since the spatial standard deviation of the charge-density variation in Fig. 14.4 is always infinite.

Chapter 15

Dissipation-induced quantum diffusion

15.1 Quantum diffusion in homogeneous GaN systems

So far our focus has been devoted to the investigation of the spatial nonlocality induced by carrier-LO phonon coupling; a somehow similar analysis has been made in [23] for acoustic phonons in GaAs. However, in order to establish how such scattering-induced charge redistribution will affect the overall diffusion process, it is imperative to perform a time-dependent analysis including single-particle as well as scattering dynamics as in Eq. (14.2). Figure 15.1 displays the sub-picosecond time evolution of the spatial carrier density corresponding to the initial mixed state in (14.11) with $\overline{\Delta}_z = 10$ nm, obtained in the absence of carrier-phonon coupling (upper panel), via the Lindblad scattering superoperator in (11.53) (central panel), and via the relaxation-time model in (14.12) (lower panel). As we can see, compared to the scattering-free case (upper panel), both Lindblad and relaxation-time treatments give rise to a speedup of the diffusion process, and the effect is more pronounced in the relaxation-time case (lower panel).

Such ultrafast diffusion dynamics is the result of a highly non-trivial interplay between single-particle and scattering contributions; indeed, it is well known that also in the presence of a spatially local (i.e., Boltzmann) scattering model (for which the contribution in (14.7) is always equal to

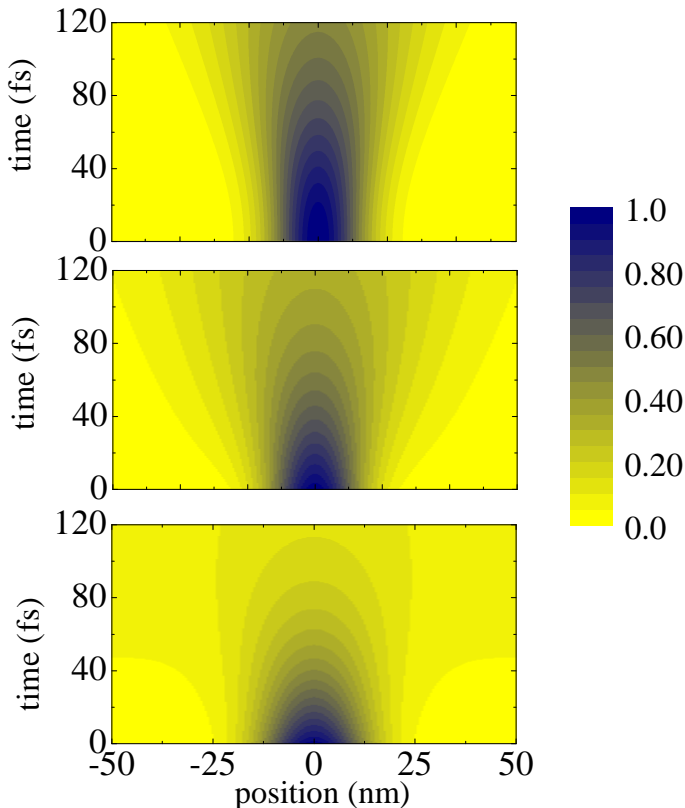


Figure 15.1. Room-temperature quantum-diffusion dynamics in a homogeneous GaN system obtained in the absence of carrier-phonon coupling (upper panel), via the Lindblad scattering superoperator in Eq. (11.53) (central panel), and via the relaxation-time model in Eq. (14.12) (lower panel): sub-picosecond time evolution of the spatial carrier density corresponding to the initial mixed state in Eq. (14.11) with $\overline{\Delta}_z = 10$ nm (see text).

zero) any scattering-induced carrier redistribution tends to speedup the diffusion process. [21] In order to better evaluate the genuine diffusion contribution due to scattering nonlocality, it is then crucial to start our simulated experiments from a thermalized carrier distribution; this has been realized adopting the initial state in (14.11); indeed, for a parabolic-band homogeneous system (as the one considered here) in the absence of scattering nonlocality, the time evolution of the spatial carrier density is described by

the following (time-dependent) Gaussian distribution (see upper panel in Fig. 15.1)

$$n(z, t) \propto \frac{e^{-\frac{z^2}{2\Delta_z^2(t)}}}{\sqrt{2\pi}\Delta_z(t)} \quad (15.1)$$

with

$$\Delta_z(t) = \bar{\Delta}_z \sqrt{1 + \frac{t^2}{\tau_d^2}}, \quad (15.2)$$

where

$$\tau_d = \frac{m^* \bar{\Delta}_z}{\bar{\Delta}_p} \quad (15.3)$$

describes the typical time scale of the scattering-free diffusion process (for the case of Fig. 15.1 this is about 70 fs).

The physical origin and relative magnitude of the diffusion speedup reported in Fig. 15.1 can be easily understood in terms of the scattering-induced nonlocality previously investigated. Indeed, for both the Lindblad (Fig. 14.1) and the relaxation-time model (Fig. 14.4), carrier-phonon scattering induces a progressive charge transfer from the initial peak toward outer regions, which results in an overall spatial broadening. As already pointed out, the impact of such scattering-induced diffusion is expected to be particularly pronounced in the case of the relaxation-time model, since the latter is totally non-local (see Fig. 14.4). Such highly non physical behavior gives rise to an increased dissipation and decoherence dynamics, which in turn results in the significant overestimation of the diffusion process reported in the lower panel of Fig. 15.1.

To quantify the amount of extra diffusion reported in Fig. 15.1, let us introduce the effective carrier distribution width

$$\lambda = \sqrt{\frac{\int z^2 n(z) dz}{\int n(z) dz}}. \quad (15.4)$$

Figure 15.2 shows the time evolution of the above effective distribution width λ . Here, the local-scattering result $\lambda = \Delta_z(t)$ (solid curve) is compared to the corresponding results obtained adopting as scattering models the Lindblad superoperator (11.53) (dashed curve) as well as the relaxation-time model (14.12) (dash-dotted curve). As expected, the relaxation-time

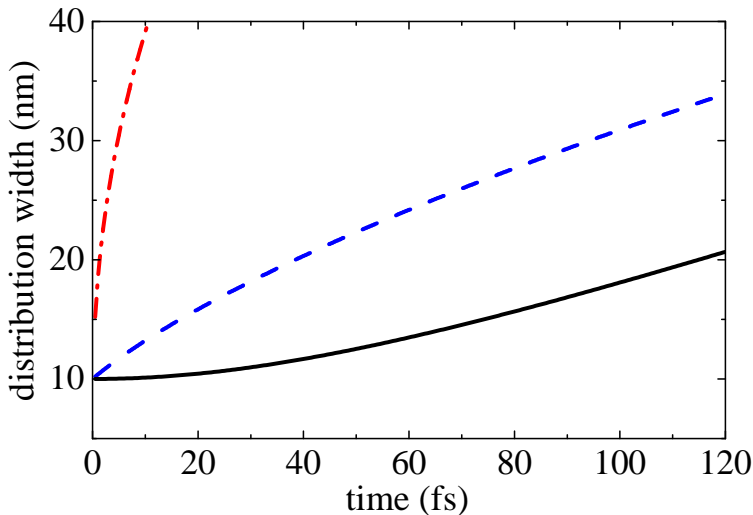


Figure 15.2. Effective spatial-distribution width λ in Eq. (15.4) as a function of time. Here, the local-scattering result (see Eq. (15.1)) (solid curve) is compared to the corresponding results obtained adopting as scattering models the Lindblad superoperator in Eq. (11.53) (dashed curve) as well as the relaxation-time model in Eq. (14.12) (dash-dotted curve) (see text).

model gives rise to a strong overestimation of the diffusion process (see dash-dotted curve) compared to the Lindblad-superoperator treatment (dashed curve).

As anticipated, the relaxation-time model in (14.12) does not exhibit the well established in- minus out-scattering structure of the Boltzmann collision term as well as of the Lindblad superoperator in (11.53); it follows that within such simplified model the decay of the inter-state phase coherence (also referred to as inter-state polarization) is not dictated by a balance between in- and out-contributions, but is determined by out-scattering contributions only, leading to an overestimation of electronic decoherence. In order to elucidate this crucial point, let us start by analyzing the explicit form of Eq. (5.10) for the case of the relaxation-time model in (14.12). By denoting with

$$\rho_{\alpha_1\alpha_2}^i(t) = \rho_{\alpha_1\alpha_2}(t) e^{-\frac{(\epsilon_{\alpha_1} - \epsilon_{\alpha_2})t}{i\hbar}} \quad (15.5)$$

the single-particle density matrix written in the interaction picture (see Eq.

(2.10)), the time evolution of its non-diagonal ($\alpha_1 \neq \alpha_2$) elements is given by

$$\frac{d\rho_{\alpha_1\alpha_2}^i}{dt} = -\frac{\Gamma_{\alpha_1} + \Gamma_{\alpha_2}}{2} \rho_{\alpha_1\alpha_2}^i, \quad (15.6)$$

which shows that, in addition to the free rotation in (15.5), the inter-state polarization decays according to the decoherence rate $(\Gamma_{\alpha_1} + \Gamma_{\alpha_2})/2$. In contrast, by inserting into Eq. (5.10) the explicit form of the Lindblad superoperator (11.53), it is easy to get

$$\begin{aligned} \frac{d\rho_{\alpha_1\alpha_2}^i}{dt} &= (\mathcal{L}_{\alpha_1\alpha_2, \alpha_1\alpha_2} + \mathcal{L}_{\alpha_2\alpha_1, \alpha_2\alpha_1}) \rho_{\alpha_1\alpha_2}^i \\ &+ \sum_{\alpha'_1\alpha'_2 \neq \alpha_1\alpha_2} \left(e^{\frac{(\epsilon_{\alpha'_1} - \epsilon_{\alpha'_2} - \epsilon_{\alpha_1} + \epsilon_{\alpha_2})t}{i\hbar}} \mathcal{L}_{\alpha_1\alpha_2, \alpha'_1\alpha'_2} \rho_{\alpha'_1\alpha'_2}^i + \text{H.c.} \right) \end{aligned} \quad (15.7)$$

with

$$\mathcal{L}_{\alpha_1\alpha_2, \alpha'_1\alpha'_2} = \frac{1}{2} \sum_s \left(\mathcal{P}_{\alpha_1\alpha_2, \alpha'_1\alpha'_2}^s - \delta_{\alpha_2\alpha'_2} \sum_{\alpha'} \mathcal{P}_{\alpha'\alpha', \alpha_1\alpha_1}^{s*} \right). \quad (15.8)$$

In the presence of strongly nonelastic interaction processes, the overall impact of the second term in (15.7) is strongly reduced thanks to the fast temporal oscillations of the various free-rotation phase factors; moreover, taking into account that in such nonelastic-interaction limit $\mathcal{P}_{\alpha\alpha', \alpha\alpha'}^s \rightarrow 0$, one gets

$$\mathcal{L}_{\alpha\alpha', \alpha\alpha'} \rightarrow -\Gamma_{\alpha}/2, \quad (15.9)$$

which implies that in this limit the Lindblad-model equation in (15.7) reduces to the relaxation-time one in (15.6). In contrast, in the presence of quasielastic processes one deals with a significant cancellation between in- and out-scattering contributions, not accounted for by the relaxation-time equation (15.6). It is worth stressing that such intrinsic limitation of relaxation-time models has been already recognized in the analysis of ultrafast phenomena in photoexcited semiconductors [56], showing that the latter becomes particularly severe for the case of quasielastic processes. [113]

To confirm this physical interpretation, we have repeated the simulated experiments presented so far artificially reducing the GaN LO-phonon energy by a factor 4 (from 80 to 20 meV), such to mimic the quasielastic-process limit. The time evolution of the effective distribution width λ corresponding to these new simulations is reported in Fig. 15.3. As expected,

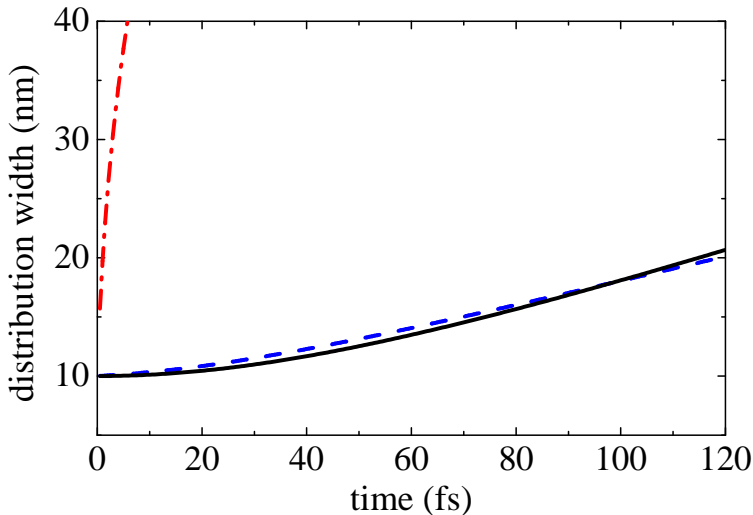


Figure 15.3. Same as in Fig. 15.2 but for a reduced value of the LO-phonon energy ($\epsilon_{\text{LO}} = 20$ meV) (see text).

compared to the results reported in Fig. 15.2, the decoherence overestimation produced by the relaxation-time model (dash-dotted curve) is still increased, while the diffusion speedup induced by the Lindblad superoperator (dashed curve) is strongly reduced. Indeed, in spite of the fact that the LO-phonon energy is still significantly different from zero, the effect of phonon scattering is already negligible. This is a clear indication that in the presence of genuine quasi elastic processes like, e.g., carrier-acoustic phonons or carrier-carrier scattering (i) the relaxation-time model is definitely inadequate, and (ii) quantum diffusion due to scattering nonlocality is expected to play a minor role.

15.2 Scattering-induced suppression of the coherent oscillations in superlattices

As a final set of simulated experiments aimed at showing the power and flexibility of the proposed density-matrix approach, we have extended the homogeneous-system analysis presented so far to the case of a periodic nanostructure. Figure 15.4 displays the sub-picosecond time evolution of

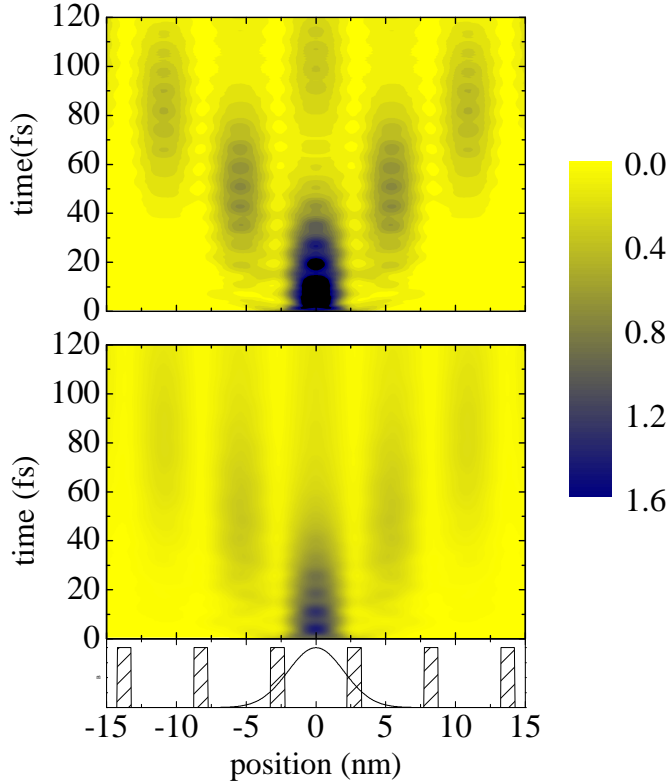


Figure 15.4. Room-temperature quantum-diffusion dynamics in a GaN-based superlattice (lower panel) (band offset of 0.3 eV and well and barrier widths of 4.5 and 1 nm) obtained in the absence of carrier-phonon coupling (upper panel) and via the Lindblad scattering superoperator in Eq. (11.53) (central panel): sub-picosecond time evolution of the spatial carrier density corresponding to the initial mixed state in Eq. (14.11) with $\bar{\Delta}_z = 2$ nm (see text).

the spatial carrier density in a GaN-based superlattice (see lower panel) corresponding to the initial mixed state in (14.11) with $\bar{\Delta}_z = 2$ nm, obtained in the scattering-free case (upper panel) and employing the Lindblad scattering superoperator in (11.53) (central panel). Compared to the corresponding homogeneous-system results of Fig. 15.1, here the superlattice structure (see lower panel) gives rise to a non-trivial interplay between the

spatial quantum confinement dictated by the nanostructure potential profile and the scattering-induced diffusion, resulting in a superlattice-induced modulation of the density profile.

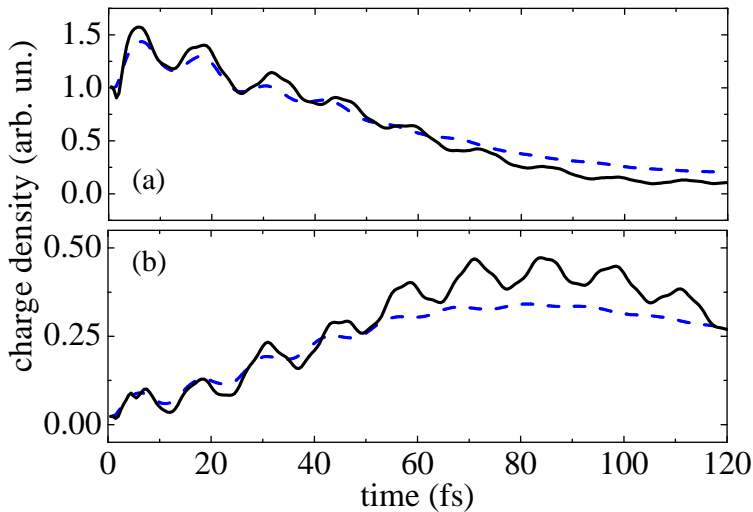


Figure 15.5. Time evolution of the carrier population in the central well of the superlattice (panel a) as well as in the two adjacent wells (panel b) corresponding to the scattering-free simulation (solid curves (upper panel in Fig. 15.4)) and to the Lindblad-scattering simulation (dashed curves (central panel in Fig. 15.4)) (see text).

In the absence of carrier-phonon scattering (upper panel) one deals with coherent charge oscillations originating from the diffusion dynamics of the initial packet through the superlattice structure. In particular, it is easy to recognize the typical signature of inter-well coherent tunneling, a peculiar phenomenon in coupled quantum-well structures. [100] To better elucidate this crucial feature, in Fig. 15.5 we have reported the time evolution of the carrier population in the central well of the superlattice (panel a) as well as in the two adjacent wells (panel b). As we can see, in the scattering-free case (solid curves corresponding to the upper-panel result of Fig. 15.4) one deals with a significant charge transfer from the central well toward the adjacent ones and vice versa, the so-called coherent-tunneling dynamics. However, compared to simple two-well systems, here the situation is by far more complicated: once a fraction of the central-well charge has reached the

adjacent wells, part of it will be transferred back to the central well, but also to the external nearest-neighbor ones; this process will progressively extend to an increasing number of wells, giving rise to the quantum-mechanical diffusion process displayed in the upper panel of Fig. 15.4.

In the presence of carrier-LO phonon scattering (see central panel in Fig. 15.4 and dashed-curves in Fig. 15.5), the fully coherent dynamics just described is strongly suppressed; indeed, the significant temporal oscillations in Fig. 15.5 are strongly reduced, giving rise at long times to a classical-like diffusion scenario typical of a so-called incoherent-tunneling dynamics. [100]

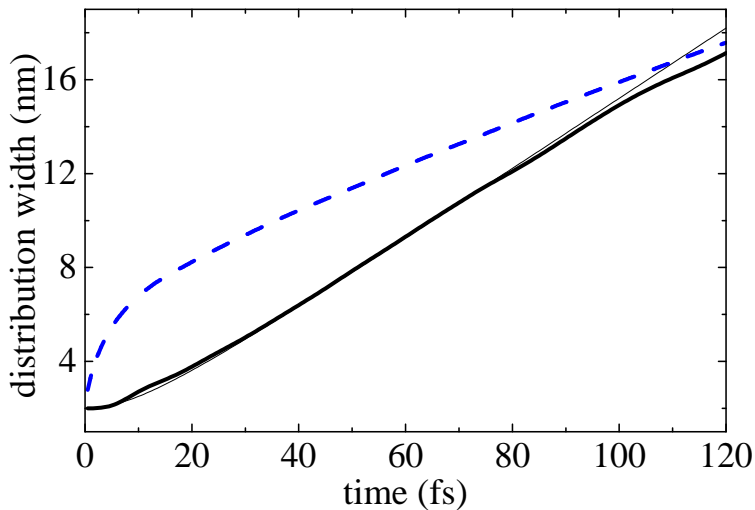


Figure 15.6. Effective spatial-distribution width λ in Eq. (15.4) as a function of time. Here, the local-scattering homogeneous result in Eq. (15.1) (thin solid curve) is compared to the scattering-free superlattice result (solid curve corresponding to the upper-panel result of Fig. 15.4) as well as to the Lindblad-scattering superlattice result (dashed curve corresponding to the central-panel result of Fig. 15.4) (see text).

Finally, it is important to point out that in the presence of energy dissipation the interplay between single-particle phase coherence (dictated by the superlattice potential profile) and phonon-induced decoherence (dictated by the Lindblad scattering superoperator) is highly non trivial. This is clearly shown in Fig. 15.6, where we report the effective spatial-distribution

width λ in (15.4) corresponding to the two simulated experiments of Fig. 15.4 as well as to the scattering-free homogeneous result of Fig. 15.1.

As we can see, at short times (less than 100 fs) the scattering-free diffusion dynamics within the superlattice structure (solid curve) does not differ significantly from the corresponding homogeneous result (thin solid curve). In contrast, the presence of carrier-LO phonon scattering (dashed curve) gives rise to a significant diffusion speedup (compared to the scattering-free result (solid curve)); at longer times the non-local action of the scattering superoperator vanishes, and at the end of the simulation the spatial broadening induced by the Lindblad superoperator comes out to be similar to the scattering-free one. Such non-trivial behavior can be explained as follows: at short times the strong spatial localization of the initial distribution induces a significant diffusion speedup due to carrier-phonon nonlocality effects; at longer times such scattering-induced nonlocality is strongly reduced, and, at the same time, energy dissipation tends to destroy inter-state phase coherence, thus limiting the diffusion process compared to the scattering-free case.

Generally speaking, we finally stress that the ability of investigating such space dependent phenomena originating from the complex interplay between single-particle quantum coherence and phonon-induced energy dissipation versus decoherence —definitely not possible via Boltzmann-like Monte Carlo simulation schemes— constitutes a distinguished feature of the proposed quantum mechanical treatment.

Chapter 16

Summary and Conclusion

In Chaps. (11) and (12), following the already published papers [78, 114] and exploiting the Lindblad scattering superoperator coming from the alternative Markov limit recalled in Chap. 3, we have applied in cascade the electronic reduction and the mean-field approximation to the many-body dynamics, obtaining in this way a closed equation of motion for the electronic single-particle density matrix, in the presence of carrier-phonon as well as carrier-carrier scattering mechanisms. While in the low-density limit the equation exhibits a Lindblad form —like for the many-electron density matrix— at finite carrier concentrations the resulting time evolution for the single-particle density matrix turns out to be non-linear and non-Lindblad.

We have proven (see Eq. (12.11)) that, despite the lack of a Lindblad form, the mean-field approximation does preserve the positive-definite character of the single-particle density matrix, an essential prerequisite of any reliable and robust kinetic treatment of semiconductor quantum devices. This result is in striking contrast with the case of mean-field approximation applied to conventional (non-Lindblad) Markov approaches (see Eq. (11.18)), where the corresponding single-particle equations may lead to positivity violations and thus to unphysical results.

The proposed single-particle formulation has then been extended to the case of quantum systems with spatial open boundaries; such microscopic treatment can be regarded as a formal derivation of a recently proposed density-matrix treatment [77] based on a Lindblad-like system-reservoir scattering superoperator.

In Chaps. (13), (14) and (15), we have provided, following the published papers [23, 115–117], a rigorous treatment of scattering-induced spatial non-locality in homogeneous as well as in nanostructured materials.

On the one end, starting from the conventional density-matrix formalism and employing as ideal instrument for the study of the semiclassical limit the well-known Wigner-function picture, we have performed a fully quantum-mechanical derivation of the space-dependent Boltzmann collision term.

On the other end, we have analyzed the validity limits of such semiclassical approximation scheme, pointing out, in particular, regimes where scattering-nonlocality effects may play a relevant role; to this end we have supplemented our analytical investigation with a relevant set of simulated experiments (already published in [116]).

Our numerical investigation of ultrafast space-dependent phenomena in homogeneous GaN systems allows one to draw the following conclusions.

In the presence of carrier localization on the nanometric space scale (see Fig. 14.1) within the proposed Lindblad treatment one deals with significant phonon-induced nonlocality effects; our analysis has shown that such non-local character is the result of a different spatial localization of in- and out-scattering contributions (see Figs. 14.2 and 14.3); these nonlocality effects will progressively vanish as the carrier delocalization increases, thus recovering, as expected, the local character of the Boltzmann collision term.

A detailed comparison of the proposed Lindblad scattering model (see Fig. 14.1) with the conventional relaxation-time approximation (see Fig. 14.4), has shown that the latter (i) leads to a significant overestimation of phonon-induced decoherence as well as scattering nonlocality, and (ii) is intrinsically unable to reproduce the local character of the Boltzmann collision term.

Thanks to our time-dependent simulations, we have shown that in homogeneous GaN systems one deals with a relevant competition between free-particle diffusion and phonon-induced non-local effects, giving rise to a global diffusion speedup (see Fig. 15.1); once again, a comparison between the proposed Lindblad treatment and the relaxation-time model has clearly shown that the latter leads to a significant overestimation of such diffusion speedup (see Fig. 15.2), and that this limitation is particularly severe for the case of quasielastic dissipation processes (see Fig. 15.3).

Moving from homogeneous systems to periodically modulated nanostructures, the interpretation of the diffusion process in the presence of phonon-induced dissipation is by far more complicated. Indeed, compared

to the homogeneous-system results (see Fig. 15.1), the presence of the superlattice structure (see Figs. 15.4 and 15.5) gives rise to a non-trivial interplay between the spatial quantum confinement dictated by the nanostructure potential profile and the scattering-induced diffusion, resulting in a superlattice-induced modulation of the density profile.

Let us finally stress that in the presence of particularly strong interaction mechanisms as well as of extremely short electromagnetic excitations, the application of the Markov limit becomes questionable; [56, 96] however, for a wide range of nanodevices and operation conditions the proposed Markov treatment is expected to well reproduce the sub-picosecond dynamics induced by a large variety of single-particle scattering mechanisms.

Bibliography

- [1] D. Taj, R. C. Iotti, and F. Rossi, “Microscopic modeling of energy relaxation and decoherence in quantum optoelectronic devices at the nanoscale,” *Eur. Phys. J. B*, vol. 72, pp. 305–322, 2009.
- [2] D. Taj, L. Genovese, and F. Rossi, “Quantum-transport simulations with the wigner-function formalism: Failure of conventional boundary-condition schemes,” *Europhys. Lett.*, vol. 74, pp. 1060–1066, 2006.
- [3] R. P. Feynman, “There’s plenty of room at the bottom,” *Engineering and science*, vol. 23, no. 5, pp. 22–36, 1960.
- [4] N. Taniguchi, “Mathematical properties of quantum evolution equations,” in *Proceedings of the International Conference on Production Engineering: Tokyo, 1974* (I. C. on Production Engineering, I. I. for Production Engineering Research, and N. seiki gakkai, eds.), pp. 45–109, Japan Society of Precision Engineering, 1974.
- [5] J. Bardeen and W. H. Brattain, “The transistor, a semi-conductor triode,” *Phys. Rev.*, vol. 74, pp. 230–231, Jul 1948.
- [6] W. Shockley, “The theory of p-n junctions in semiconductors and p-n junction transistors,” *Bell System Technical Journal*, vol. 28, no. 3, pp. 435–489, 1949.
- [7] M. Riordan and L. Hoddeson, *Crystal fire: The birth of the information age*. WW Norton & Company, 1997.
- [8] G. Teal, “Some recent developments in silicon and germanium materials and devices,” in *National IRE Conf., (Dayton, OH)*, pp. 551–559, 1954.
- [9] G. E. Moore *et al.*, “Progress in digital integrated electronics,” *IEDM Tech. Digest*, vol. 11, 1975.

- [10] J. Wu, Y.-L. Shen, K. Reinhardt, H. Szu, and B. Dong, “A nanotechnology enhancement to moore’s law,” *Applied Computational Intelligence and Soft Computing*, vol. 2013, p. 2, 2013.
- [11] A. Seabaugh, “The tunneling transistor,” *Spectrum, IEEE*, vol. 50, pp. 35–62, October 2013.
- [12] R. N. Hall, G. E. Fenner, J. D. Kingsley, T. J. Soltys, and R. O. Carlson, “Coherent light emission from gaas junctions,” *Phys. Rev. Lett.*, vol. 9, pp. 366–368, Nov 1962.
- [13] J. V. Neumann, A. W. Taub, and A. H. Taub, *The Collected Works of John Von Neumann: 6-Volume Set*. Reader’s Digest Young Families, 1963.
- [14] Z. I. Alferov and R. Kazarinov, “Semiconductor laser with electric pumping,” *Inventor’s certificate*, vol. 181737, 1963.
- [15] H. Kroemer, “Solid state radiation emitters,” Mar. 14 1967. US Patent 3,309,553.
- [16] L. Esaki, “New phenomenon in narrow germanium $p - n$ junctions,” *Phys. Rev.*, vol. 109, pp. 603–604, Jan 1958.
- [17] L. Esaki, “Long journey into tunneling,” *Rev. Mod. Phys.*, vol. 46, pp. 237–244, Apr 1974.
- [18] Z. I. Alferov, “Nobel lecture: The double heterostructure concept and its applications in physics, electronics, and technology,” *Rev. Mod. Phys.*, vol. 73, pp. 767–782, Oct 2001.
- [19] R. F. Kazarinov and R. A. Suris, “Possibility of the amplification of electromagnetic waves in a semiconductor with a superlattice,” *Sov. Phys. Semicond.*, vol. 5, p. 707, 1971.
- [20] J. Faist, F. Capasso, D. L. Sivco, C. Sirtori, A. L. Hutchinson, and A. Y. Cho, “Quantum cascade laser,” *Science*, vol. 264, no. 5158, pp. 553–556, 1994.
- [21] N. Ashcroft and N. Mermin, *Solid State Physics*. Cengage Learning India Private Limited, 2011.
- [22] P. Yu and M. Cardona, *Fundamentals of Semiconductors: Physics And Materials Properties*. No. v. 3 in Advanced texts in physics, Springer, 2005.
- [23] R. Rosati and F. Rossi, “Microscopic modeling of scattering quantum non-locality in semiconductor nanostructures,” *Appl. Phys. Lett.*, vol. 103, p. 113105, SEP 9 2013.

- [24] L. Boltzmann, *Lectures on Gas Theory*. Dover Books on Physics, Dover Publications, 2012.
- [25] F. Rossi, *Theory of Semiconductor Quantum Devices: Microscopic Modeling and Simulation Strategies*. Springer, 2011.
- [26] R. Alicki, “General theory and applications to unstable particles,” in *Quantum Dynamical Semigroups and Applications*, pp. 1–46, Springer, 2007.
- [27] G. Lindblad, “Generators of quantum dynamical semigroups,” *Commun. Math. Phys.*, vol. 48, no. 2, pp. 119–130, 1976.
- [28] H. Breuer and F. Petruccione, *The Theory of Open Quantum Systems*. OUP Oxford, 2007.
- [29] V. Gorini, A. Kossakowski, and E. C. G. Sudarshan, “Completely positive dynamical semigroups of n-level systems,” *Journal of Mathematical Physics*, vol. 17, no. 5, pp. 821–825, 1976.
- [30] W. R. Frensley, “Boundary-conditions for open quantum-systems driven far from equilibrium,” *Rev. Mod. Phys.*, vol. 62, pp. 745–791, JUL 1990.
- [31] A. Arnold, “Mathematical properties of quantum evolution equations,” in *Quantum Transport: Modelling, Analysis and Asymptotics* (G. Allaire, N. Ben-Abdallah, and G. Frosali, eds.), Lecture Notes in Mathematics / C.I.M.E. Foundation Subseries, pp. 45–109, Springer, 2008.
- [32] M. Toda, N. Saito, R. Kubo, and N. Saito, *Statistical Physics I: Equilibrium Statistical Mechanics*. Springer Series in Solid-State Sciences, Springer Berlin Heidelberg, 1998.
- [33] W. R. Frensley, “Transient response of a tunneling device obtained from the wigner function,” *Phys. Rev. Lett.*, vol. 57, pp. 2853–2856, Dec 1986.
- [34] W. R. Frensley, “Wigner-function model of a resonant-tunneling semiconductor device,” *Phys. Rev. B*, vol. 36, pp. 1570–1580, Jul 1987.
- [35] A. M. Krivan, N. C. Kluksdahl, and D. K. Ferry, “Scattering states and distribution functions for microstructures,” *Phys. Rev. B*, vol. 36, pp. 5953–5959, Oct 1987.
- [36] N. C. Kluksdahl, A. M. Krivan, D. K. Ferry, and C. Ringhofer, “Self-consistent study of the resonant-tunneling diode,” *Phys. Rev. B*, vol. 39, pp. 7720–7735, Apr 1989.

- [37] F. A. Buot and K. L. Jensen, "Lattice weyl-wigner formulation of exact many-body quantum-transport theory and applications to novel solid-state quantum-based devices," *Phys. Rev. B*, vol. 42, pp. 9429–9457, Nov 1990.
- [38] D. R. Miller and D. P. Neikirk, "Simulation of intervalley mixing in double-barrier diodes using the lattice wigner function," *Applied Physics Letters*, vol. 58, no. 24, pp. 2803–2805, 1991.
- [39] M. J. McLennan, Y. Lee, and S. Datta, "Voltage drop in mesoscopic systems: A numerical study using a quantum kinetic equation," *Phys. Rev. B*, vol. 43, pp. 13846–13884, Jun 1991.
- [40] H. C. Tso and N. J. M. Horing, "Wigner-function formulation of non-linear electron-hole transport in a quantum well and analysis of the linear transient and steady state," *Phys. Rev. B*, vol. 44, pp. 11358–11380, Nov 1991.
- [41] D. K. Ferry and J.-R. Zhou, "Form of the quantum potential for use in hydrodynamic equations for semiconductor device modeling," *Phys. Rev. B*, vol. 48, pp. 7944–7950, Sep 1993.
- [42] K. K. Gullapalli, D. R. Miller, and D. P. Neikirk, "Simulation of quantum transport in memory-switching double-barrier quantum-well diodes," *Phys. Rev. B*, vol. 49, pp. 2622–2628, Jan 1994.
- [43] C. L. Fernando and W. R. Frensley, "Intrinsic high-frequency characteristics of tunneling heterostructure devices," *Phys. Rev. B*, vol. 52, pp. 5092–5104, Aug 1995.
- [44] K.-Y. Kim and B. Lee, "Wigner-function formulation in anisotropic semiconductor quantum wells," *Phys. Rev. B*, vol. 64, p. 115304, Aug 2001.
- [45] M. Nedjalkov, H. Kosina, S. Selberherr, C. Ringhofer, and D. K. Ferry, "Unified particle approach to wigner-boltzmann transport in small semiconductor devices," *Phys. Rev. B*, vol. 70, p. 115319, Sep 2004.
- [46] M. Nedjalkov, D. Vasileska, D. K. Ferry, C. Jacoboni, C. Ringhofer, I. Dimov, and V. Palankovski, "Wigner transport models of the electron-phonon kinetics in quantum wires," *Phys. Rev. B*, vol. 74, p. 035311, Jul 2006.
- [47] D. Querlioz, J. Saint-Martin, A. Bournel, and P. Dollfus, "Wigner monte carlo simulation of phonon-induced electron decoherence in semiconductor nanodevices," *Phys. Rev. B*, vol. 78, p. 165306, Oct 2008.

- [48] O. Morandi, “Multiband wigner-function formalism applied to the zener band transition in a semiconductor,” *Phys. Rev. B*, vol. 80, p. 024301, Jul 2009.
- [49] D. Querlioz, J. Saint-Martin, and P. Dollfus, “Implementation of the wigner-boltzmann transport equation within particle monte carlo simulation,” *Journal of Computational Electronics*, vol. 9, no. 3-4, pp. 224–231, 2010.
- [50] P. D. Yoder, M. Grupen, and R. Smith, “Demonstration of intrinsic tristability in double-barrier resonant tunneling diodes with the wigner transport equation,” *Electron Devices, IEEE Transactions on*, vol. 57, pp. 3265–3274, Dec 2010.
- [51] A. Savio and A. Poncet, “Study of the wigner function at the device boundaries in one-dimensional single- and double-barrier structures,” *J. Appl. Phys.*, vol. 109, p. 033713, FEB 1 2011.
- [52] M. Trovato and L. Reggiani, “Quantum maximum-entropy principle for closed quantum hydrodynamic transport within a wigner function formalism,” *Phys. Rev. E*, vol. 84, p. 061147, Dec 2011.
- [53] F. Rossi, A. Di Carlo, and P. Lugli, “Microscopic theory of quantum-transport phenomena in mesoscopic systems: A monte carlo approach,” *Phys. Rev. Lett.*, vol. 80, pp. 3348–3351, 1998.
- [54] R. Proietti Zaccaria and F. Rossi, “On the problem of generalizing the semiconductor bloch equation from a closed to an open system,” *Phys. Rev. B*, vol. 67, p. 113311, 2003.
- [55] M. Pascoli, P. Bordone, R. Brunetti, and C. Jacoboni, “Wigner paths for electrons interacting with phonons,” *Phys. Rev. B*, vol. 58, pp. 3503–3506, Aug 1998.
- [56] F. Rossi and T. Kuhn, “Theory of ultrafast phenomena in photoexcited semiconductors,” *Rev. Mod. Phys.*, vol. 74, pp. 895–950, 2002.
- [57] R. Rosati, F. Dolcini, R. C. Iotti, and F. Rossi, “Wigner-function formalism applied to semiconductor quantum devices: Failure of the conventional boundary condition scheme,” *Phys. Rev. B*, vol. 88, p. 035401, 2013.
- [58] M. Hillery, R. O’Connell, M. Scully, and E. Wigner, “Distribution functions in physics: Fundamentals,” *Physics Reports*, vol. 106, no. 3, pp. 121 – 167, 1984.
- [59] R. Glauber, “Optical coherence and photon statistics,” in *Quantum Optics and Electronics*, vol. 1, p. 63, 1965.

- [60] E. C. G. Sudarshan, "Equivalence of semiclassical and quantum mechanical descriptions of statistical light beams," *Phys. Rev. Lett.*, vol. 10, pp. 277–279, Apr 1963.
- [61] P. D. Drummond, C. W. Gardiner, and D. F. Walls, "Quasiprobability methods for nonlinear chemical and optical systems," *Phys. Rev. A*, vol. 24, pp. 914–926, Aug 1981.
- [62] K. Husimi, "Some formal properties of the density matrix," in *Proc. Phys. Math. Soc. Jpn*, vol. 22, p. 123, 1940.
- [63] R. Feynman and A. Hibbs, *Quantum mechanics and path integrals*. International series in pure and applied physics, McGraw-Hill, 1965.
- [64] J. E. Moyal and M. S. Bartlett, "Quantum mechanics as a statistical theory," *Math. Proc. Cambridge Phil. Soc.*, vol. 45, pp. 99–124, 1949.
- [65] H. J. Groenewold, "On the principles of elementary quantum mechanics," *Physica*, vol. 12, pp. 405–460, Oct. 1946.
- [66] L. D. Landau, E. M. Lifshits, J. Sykes, and J. Bell, *Course of theoretical physics: Mechanics*. Pergamon Press, 1960.
- [67] S. Datta, *Electronic Transport in Mesoscopic Systems*. Cambridge Studies in Semiconductor Physics and Microelectronic Engineering, Cambridge University Press, 1997.
- [68] L. Barletti and P. F. Zweifel, "Parity-decomposition method for the stationary wigner equation with inflow boundary conditions," *Transport Theory and Statistical Physics*, vol. 30, no. 4-6, pp. 507–520, 2001.
- [69] R. Gebauer and R. Car, "Current in open quantum systems," *Phys. Rev. Lett.*, vol. 93, p. 160404, OCT 15 2004.
- [70] O. Hess and T. Kuhn, "Maxwell-bloch equations for spatially inhomogeneous semiconductor lasers .1. theoretical formulation," *Phys. Rev. A*, vol. 54, pp. 3347–3359, OCT 1996.
- [71] L. Demeio, P. Bordone, and C. Jacoboni, "Multiband, non-parabolic wigner-function approach to electron transport in semiconductors," *Transport Theor. Stat.*, vol. 34, no. 7, pp. 499–522, 2005.
- [72] H. Jiang and W. Cai, "Effect of boundary treatments on quantum transport current in the green's function and wigner distribution methods for a nano-scale dg-mosfet," *Journal of Computational Physics*, vol. 229, no. 12, pp. 4461–4475, 2010.
- [73] H. Jiang, W. Cai, and R. Tsu, "Accuracy of the frensley inflow boundary condition for wigner equations in simulating resonant tunneling

- diodes,” *Journal of Computational Physics*, vol. 230, no. 5, pp. 2031–2044, 2011.
- [74] L. Kadanoff and G. Baym, *Quantum statistical mechanics: Green’s function methods in equilibrium and nonequilibrium problems*. Frontiers in physics, W.A. Benjamin, 1962.
- [75] H. Haug and A. Jauho, *Quantum Kinetics in Transport and Optics of Semiconductors*. Springer, 2007.
- [76] S. Datta, “Nanoscale device modeling: the green’s function method,” *Superlattice. Microst.*, vol. 28, pp. 253–278, OCT 2000.
- [77] F. Dolcini, R. C. Iotti, and F. Rossi, “Interplay between energy dissipation and reservoir-induced thermalization in nonequilibrium quantum nanodevices,” *Phys. Rev. B*, vol. 88, p. 115421, SEP 16 2013.
- [78] R. Rosati, R. C. Iotti, F. Dolcini, and F. Rossi, “Derivation of nonlinear single-particle equations via many-body lindblad superoperators: A density-matrix approach,” *Phys. Rev. B*, vol. 90, p. 125140, Sep 2014.
- [79] M. Scully and S. Zubairy, *Quantum Optics*. Cambridge University Press, 1997.
- [80] E. Davies, *Quantum theory of open systems*. Academic Press, 1976.
- [81] H. Haug and S. Koch, *Quantum Theory of the Optical and Electronic Properties of Semiconductors*. World Scientific, 2004.
- [82] L. Van Hove, “Statistical mechanics: A survey of recent lines of investigation,” *Rev. Mod. Phys.*, vol. 29, pp. 200–204, Apr 1957.
- [83] W. Kohn and J. M. Luttinger, “Quantum theory of electrical transport phenomena,” *Phys. Rev.*, vol. 108, pp. 590–611, Nov 1957.
- [84] R. Zwanzig, “Memory effects in irreversible thermodynamics,” *Phys. Rev.*, vol. 124, pp. 983–992, Nov 1961.
- [85] M. V. Fischetti, “Master-equation approach to the study of electronic transport in small semiconductor devices,” *Phys. Rev. B*, vol. 59, pp. 4901–4917, Feb 1999.
- [86] I. Knezevic, “Decoherence due to contacts in ballistic nanostructures,” *Phys. Rev. B*, vol. 77, p. 125301, Mar 2008.
- [87] M. Lindberg and S. W. Koch, “Effective bloch equations for semiconductors,” *Phys. Rev. B*, vol. 38, pp. 3342–3350, Aug 1988.
- [88] T. Kuhn and F. Rossi, “Analysis of coherent and incoherent phenomena in photoexcited semiconductors - a monte-carlo approach,” *Phys. Rev. Lett.*, vol. 69, pp. 977–980, 1992.

- [89] U. Hohenester and W. Pötz, “Density-matrix approach to nonequilibrium free-carrier screening in semiconductors,” *Phys. Rev. B*, vol. 56, pp. 13177–13189, Nov 1997.
- [90] H. Bi Sun and G. J. Milburn, “Quantum open-systems approach to current noise in resonant tunneling junctions,” *Phys. Rev. B*, vol. 59, pp. 10748–10756, Apr 1999.
- [91] C. Flindt, T. Novotný, and A.-P. Jauho, “Current noise in a vibrating quantum dot array,” *Phys. Rev. B*, vol. 70, p. 205334, Nov 2004.
- [92] D. B. Tran Thoai and H. Haug, “Band-edge quantum kinetics for coherent ultrashort-pulse spectroscopy in polar semiconductors,” *Phys. Rev. B*, vol. 47, pp. 3574–3581, Feb 1993.
- [93] J. Schilp, T. Kuhn, and G. Mahler, “Electron-phonon quantum kinetics in pulse-excited semiconductors: Memory and renormalization effects,” *Phys. Rev. B*, vol. 50, pp. 5435–5447, Aug 1994.
- [94] H. Spohn, “Kinetic equations from hamiltonian dynamics: Markovian limits,” *Rev. Mod. Phys.*, vol. 52, pp. 569–615, Jul 1980.
- [95] V. M. Axt and S. Mukamel, “Nonlinear optics of semiconductor and molecular nanostructures; a common perspective,” *Rev. Mod. Phys.*, vol. 70, pp. 145–174, JAN 1998.
- [96] V. M. Axt and T. Kuhn, “Femtosecond spectroscopy in semiconductors: a key to coherences, correlations and quantum kinetics,” *Rep. Prog. Phys.*, vol. 67, pp. 433–512, APR 2004.
- [97] R. C. Iotti and F. Rossi, “Microscopic theory of semiconductor-based optoelectronic devices,” *Rep. Prog. Phys.*, vol. 68, pp. 2533–2571, 2005.
- [98] R. C. Iotti, E. Ciancio, and F. Rossi, “Quantum transport theory for semiconductor nanostructures: A density-matrix formulation,” *Phys. Rev. B*, vol. 72, p. 125347, 2005.
- [99] M. Ryzhii and V. Ryzhii, “Monte carlo analysis of ultrafast electron transport in quantum well infrared photodetectors,” *Appl. Phys. Lett.*, vol. 72, pp. 842–844, FEB 16 1998.
- [100] R. C. Iotti and F. Rossi, “Nature of charge transport in quantum-cascade lasers,” *Phys. Rev. Lett.*, vol. 87, p. 146603, 2001.
- [101] R. Köhler, A. Tredicucci, F. Beltram, H. E. Beere, E. H. Linfield, A. G. Davies, D. A. Ritchie, R. C. Iotti, and F. Rossi, “Terahertz semiconductor-heterostructure laser,” *Nature*, vol. 417, pp. 156–159, 2002.

- [102] H. Callebaut, S. Kumar, B. S. Williams, Q. Hu, and J. L. Reno, "Importance of electron-impurity scattering for electron transport in terahertz quantum-cascade lasers," *Appl. Phys. Lett.*, vol. 84, pp. 645–647, FEB 2 2004.
- [103] J. T. Lu and J. C. Cao, "Coulomb scattering in the monte carlo simulation of terahertz quantum-cascade lasers," *Appl. Phys. Lett.*, vol. 89, p. 211115, NOV 20 2006.
- [104] E. Bellotti, K. Driscoll, T. D. Moustakas, and R. Paiella, "Monte carlo study of gan versus gaas terahertz quantum cascade structures," *Appl. Phys. Lett.*, vol. 92, p. 101112, MAR 10 2008.
- [105] C. Jirauschek, "Monte carlo study of carrier-light coupling in terahertz quantum cascade lasers," *Appl. Phys. Lett.*, vol. 96, p. 011103, JAN 4 2010.
- [106] A. Matyas, M. A. Belkin, P. Lugli, and C. Jirauschek, "Temperature performance analysis of terahertz quantum cascade lasers: Vertical versus diagonal designs," *Appl. Phys. Lett.*, vol. 96, p. 201110, MAY 17 2010.
- [107] R. C. Iotti, F. Rossi, M. S. Vitiello, G. Scamarcio, L. Mahler, and A. Tredicucci, "Impact of nonequilibrium phonons on the electron dynamics in terahertz quantum cascade lasers," *Appl. Phys. Lett.*, vol. 97, p. 033110, 2010.
- [108] M. S. Vitiello, R. C. Iotti, F. Rossi, L. Mahler, A. Tredicucci, H. E. Beere, D. A. Ritchie, Q. Hu, and G. Scamarcio, "Non-equilibrium longitudinal and transverse optical phonons in terahertz quantum cascade lasers," *Appl. Phys. Lett.*, vol. 100, p. 091101, 2012.
- [109] A. Matyas, P. Lugli, and C. Jirauschek, "Role of collisional broadening in monte carlo simulations of terahertz quantum cascade lasers," *Appl. Phys. Lett.*, vol. 102, p. 011101, JAN 7 2013.
- [110] R. C. Iotti and F. Rossi, "Coupled carrier-phonon nonequilibrium dynamics in terahertz quantum cascade lasers: a monte carlo analysis," *New J. Phys.*, vol. 15, p. 075027, JUL 26 2013.
- [111] G. Bastard, *Wave mechanics applied to semiconductor heterostructures*. Monographies de physique, Les Éditions de Physique, 1988.
- [112] C. Jacoboni and P. Lugli, *The Monte Carlo Method for Semiconductor Device Simulation*. Springer, 1989.
- [113] F. Rossi, S. Haas, and T. Kuhn, "Ultrafast relaxation of photoexcited carriers - the role of coherence in the generation process," *Phys. Rev.*

- Lett.*, vol. 72, pp. 152–155, 1994.
- [114] R. Rosati, R. Iotti, and F. Rossi, “Microscopic modeling of quantum devices at high carrier densities via lindblad-type scattering superoperators,” in *Computational Electronics (IWCE), 2014 International Workshop on*, pp. 1–3, June 2014.
- [115] R. Rosati and F. Rossi, “Quantum diffusion due to scattering nonlocality in nanoscale semiconductors,” *EPL*, vol. 105, no. 1, p. 17010, 2014.
- [116] R. Rosati and F. Rossi, “Scattering nonlocality in quantum charge transport: Application to semiconductor nanostructures,” *Phys. Rev. B*, vol. 89, p. 205415, MAY 14 2014.
- [117] R. Rosati and F. Rossi, “Phonon-induced quantum diffusion in semiconductors,” in *Computational Electronics (IWCE), 2014 International Workshop on*, pp. 1–4, June 2014.